BULETINUL ŞTIINŢIFIC

al

Universităţii „POLITEHNICA” din Timişoara, România

Seria MECANICĂ

SCIENTIFIC BULLETIN

of

the „POLITEHNICA” University of Timişoara, Romania

Transactions on MECHANICS

Tomul 54(68), Fascicola 4, 2009
ISSN 1224-6077

EDITURA POLITEHNICA

CONTENTS

SCIENTIFIC BULLETIN OF
THE „POLITEHNICA" UNIVERSITY OF TIMISOARA, ROMANIA
TRANSACTIONS ON MECHANICS
BULETINUL ŞTIINŢIFIC AL
UNIVERSITĂŢII „POLITEHNICA" DIN TIMIŞOARA, ROMÂNIA
SERIA MECANICĂ
Tom 54 (68) **ISSN 1224 - 6077** **Fasc. 4, 2009**

LOW BUDGET UPPER LIMB EXOSKELETON - MANUFACTURING AND TESTING

Dan Ioan STOIA*
Mechanical Engineering Faculty , Bv. Mihai Viteazu, No.1,
Timisoara 300222, Romania, dan.stoia@mec.upt.ro

Abstract. The paper presents the concept, manufacturing and testing of a force amplifier exoskeleton. The exoskeleton materializes two mechanical upper limbs and has the main function of amplifying the lifting force of the human arms. Using a simple design concept, the exoskeleton was manufacture in *low budget* conditions, resulting in a very good execution cost – performances ratio. The mechanical tests were performed in order to prove these performances.

Keywords: exoskeleton, force amplifier, kinematical parameters, low budget

1. Introduction

The paper proposes a biomechanical study on an exoskeleton designed and constructed to amplify the force of the human upper limb. One of the exoskeleton's construction concepts was to join together the mechanical and electrical systems in a *low budget* project.

There are many types of exoskeletons, and the issues that involve their concepts and constructions are very present in today's researches [1], [2], [3], [4].

An exoskeleton is a kind of man-machine system centered by human, designed as an external mechanical structure whose joints correspond to those of human body or limbs. It combines the human intelligence and the machine power so that it enhances the intelligence of the machine and the power of the human operator. As a result, the human operator can achieve what he is not capable of by himself [5], [6].

The studied parameters of the exoskeleton refer to: kinematical parameters of the mechanical arm (angular amplitudes and velocities); the lifting force generated by the mechanical system, additionally to the human arm force.

In order to determine these parameters, the following steps were followed: 3D modeling of the components and the assembly; mechanical strength calculations, choosing the optimal materials; exoskeleton building.

2. Materials and Methods

The components of the exoskeleton were modeled in SolidWorks CAD environment and assembled together by establishing the proper relations between the elements (figure 1). The 3D components are: one trapezoidal frame (1), two rigid arms (7), two actuators (6), spherical articulation of the mechanical shoulder (5), two cylindrical joins (4) and (3), the insertion points (IP) (2), and standard screws and nuts for elements connections.

In order to validate the model construction from both geometrical and strength point of views, the assembly was analyzed using Finite Element Method (FEM) in Cosmos Works environment.

Material properties of each component were taken into consideration. The structure of the exoskeleton was designed to be constructed from

aluminum square profiles, due to the good strength/specific weight ratio of these.

The *low budget* actuators used in the construction were borrowed from a satellite positioning system. These linear actuators are composed by a 12-20V DC electric motor, a gearbox reducer and a screw-nut couple for transforming the rotational movement in translation.

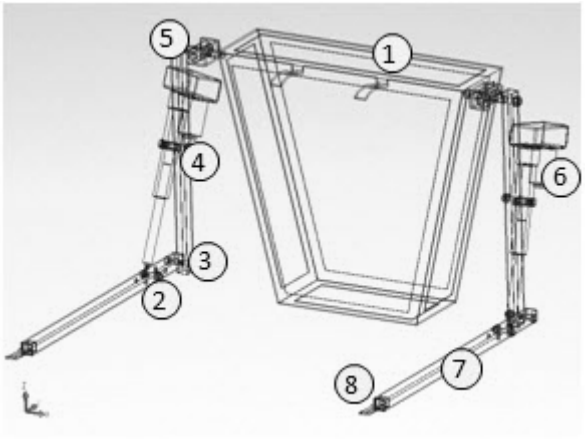

Figure 1 3D wireframe assembly of the exoskeleton

The cylindrical joints were materialized by cylindrical steel bolts fitted in cylindrical housings. In order to reduce the construction cost of the exoskeleton, standard assembling elements: screws, nuts and washers were used.

The electrical board and circuits are handmade build. In order to determine the biomechanical parameters of the exoskeleton, two tests were realized. The first test reveals the variation of the lifting force with the current of the electric motor and the actuator's points of insertion. The second test refers to the kinematical characteristics of the exoskeleton.

The tests were realized in both Motion Analysis and CIDUCOS Laboratories of the Politehnica University of Timisoara. The equipments used in tests were: Ultratest *i* testing stand for lifting force measurements and Zebris equipment for kinematical analyzes.

The mechanical testing system can be observed in the figure 2, were one of the arm of the exoskeleton was fixed between the machine's table and the loading cell.

The tests were done successive for the three possible actuator's positions of insertion (figure 3). Having the actuator placed in the first insertion position, the force was measured during the electrical excitation of the motor. In the same time, the DC power supply indicate us the current consumed by the motor, for a certain voltage (12 and 20V).

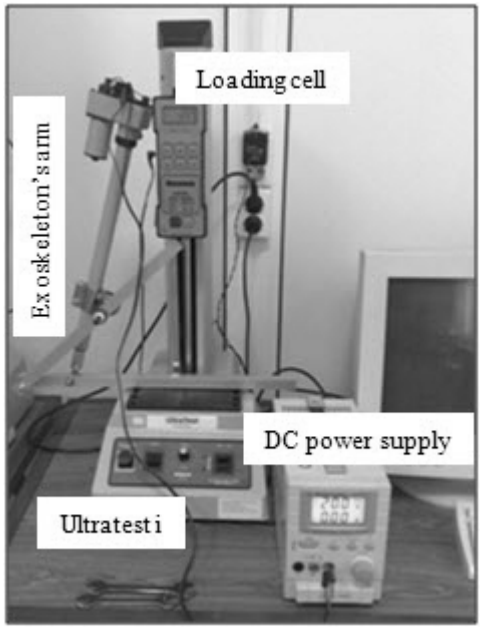

Figure 2 Mechanical testing system: Ultratest *i*, DC power supply, one exoskeleton arm

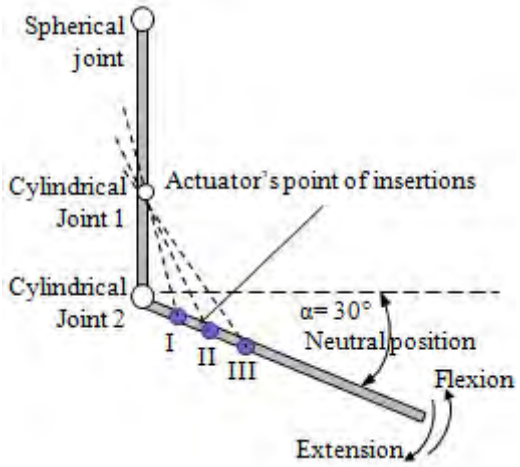

Figure 3 Functional sketch of the exoskeleton

In order to make the kinematical evaluation of the exoskeleton, Zebris ultrasound based system was used.

The two sets of markers (microphones) were attached on the exoskeleton's arm. One set was placed on the final effector, while the other one was placed on the upper extremity of the arm (near spherical joint).

The exoskeleton assembly was placed on front of the ultrasound emitter. Starting from the neutral position of the arm (figure 3), flexion and extension movements were recorded.

During the recording time, the angular variation in time (angular velocity) and angular acceleration of the arm were measured.

3. Results and Conclusions

As a first result, the lifting force of the robotic arm will be presented. By looking in the figure 4, we can observe the insertion points of the actuator. Accordingly to these points, we got six results of the lifting force.

For the first IP, two tests were performed: one for 12 volts supply of the motor and the other one for 20 V. As we expect to be, high voltage and high current lead to a maximum lifting force, which in this case is about 240 N (figure 4).

For the second IP (*II*), the results can be observed in the figure 5. Here, by decreasing the arm of the resistant moment, higher forces were recorded. A maximum force of 445 N was recorded for 20V supply, at a 1.1A.

The last experimental case (IP *III*) provides us best force result, 470 N, value achieved and constantly maintained at 20 volts supply. The electrical current in this case was 1.2 A (figure 6). In each experimental case, a linear tendency between force and current was manifested.

The result of the kinematical behavior of the exoskeleton was evidenced the angular amplitudes in flexion and extension of the arm, together with the angular velocities of the movement. For presentation, two diagrams were drawn: the range of mobility (figure 7) and the second one, the phase diagram of the velocity (figure 8).

The figure 7 presents the angular amplitudes in flexion and extension of the arm, accordingly to the neutral position (30° to horizontal). The negative angular values represent extension while positive values represent flexion. The maximum mobility is symmetrical relating to neutral position, the maximum angle in each case being 55 deg.

This mobility was adjusted to be symmetrical from the linear transmitting mechanism of the actuator, and the position of the cylindrical joint 1 (figure 3).

Figure 8 presents us the phase diagram of the angular velocity. Here, the velocity and angle are represented in phase.

The lack of constant angular velocity during the movement can be explained through the free vibrations occurred in the joints. Also, the movement between the arm and forearm were influenced the velocity reading.

We can note that the velocity is changing from 0 to 7.4 deg/sec, obtaining an average value of 3.74 deg/sec.

The angular velocity of the robotic arm can be increased by increasing the motor's voltage, while linear velocity of the end effector can be increased by using the first insertion point.

In order to make a compromise regarding the construction and the functionality of the exoskeleton, we dealt with the following variables: lifting force required; linear velocity desired for the movement; range of mobility of the forearm; power of the supply unit.

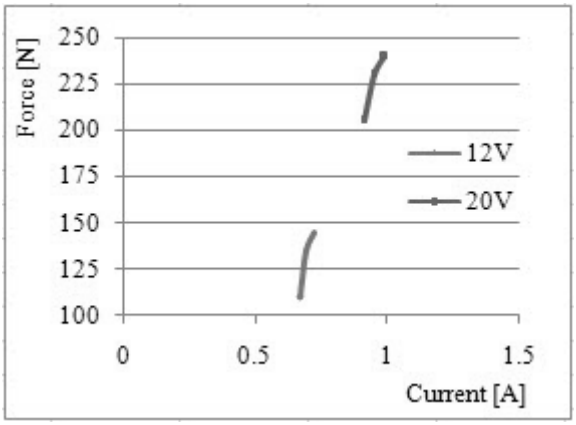

Figure 4 Force-current diagram for IP *I*

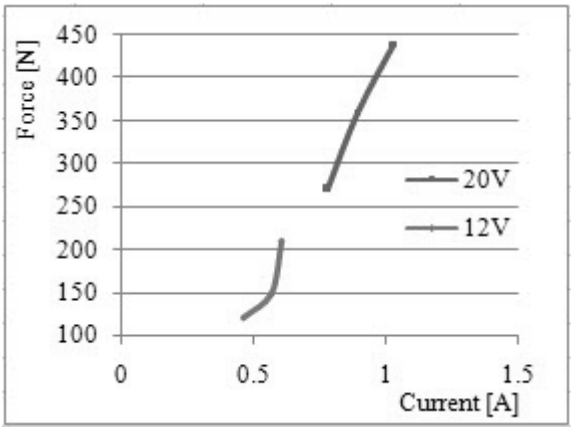

Figure 5 Force-current diagram for IP *II*

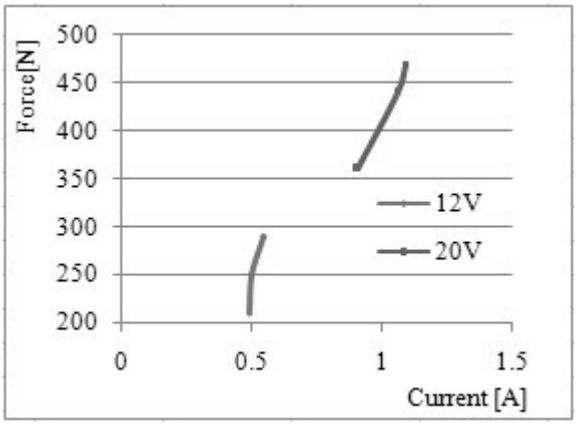

Figure 6 Force-current diagram for IP *III*

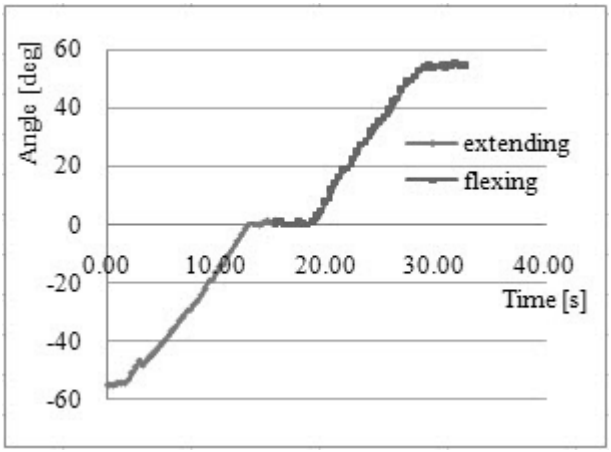

Figure 7 Range of mobility of the arm

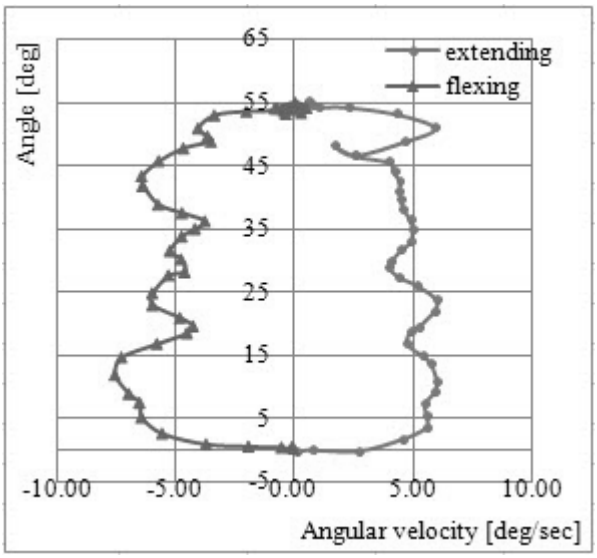

Figure 8 Phase diagram of the movement

By analyzing these variables, several functional limitations of the exoskeleton can be identified: High lifting force lead to a heavy power supply unit or batteries, increasing the overall size of the exoskeleton. Due to the kinematical limitations of the actuators, the construction reduces the angular range of movement of the person who's wearing this system; also, the velocity of the forearm is dramatically reduced.

Acknowledgement

This paper presents some results of the Diploma Project: *Proiectarea unui exoschelet realizabil cu buget redus*. The diploma project was realized in 2009 by the students Ulucian Ovidiu and Barbu Ramona, under coordination of dr.eng. Stoia Dan Ioan.

References

1. M. Brown, N. Tsagarakis, D.G. Caldwell, Exoskeletons for human force augmentation, Industrial Robot, An International Journal, vol.30, issue 6, pp.592 – 602, 2003, ISSN 0143-991X
2. C. Hirsh, T. Karloski, Design and implementation of mechanized exoskeletons in the armed forces, Ninth Annual Freshman Conference, University of Pittsburgh, Paper # 9047, Session B2, 2009, ISSN 10945296
3. K. Homma, T. Arai, Design of an upper limb assist system with parallel mechanism, IEEE ICRA, Nogoya, Japan, pp.1302- 1307, 1995
4. P. Shi, Y. Zhang, X. Yang, Lower Extremity Exoskeleton Control and Stability Analysis Based on Virtual Prototyping Technique, CSSE, vol. 1, International Conference on Computer Science and Software Engineering, pp.1131- 1134, 2008, ISBN 978-0-7695-3336-0
5. C. Yang, J. Zhang, Y. Chen, Y. Dong, Y. Zhang, A review of exoskeleton-type systems and their key technologies, Proceedings of the Institution of Mechanical Engineers, Journal of Mechanical Engineering Science, 2008, vol. 222, no. 8, pp.1599- 1603, ISSN 0954-4062
6. S. Yang, UC Berkeley researchers developing robotic exoskeleton that can enhance human strength and endurance, UC Berkeley, http://www.berkeley.edu/news/media/releases/2004/03/03_exo.shtml, Accessed: 2009-11-30.

FABRICAȚIA ŞI TESTAREA CU BUGET REDUS A EXOSCHELETULUI DE MEMBRU SUPERIOR

Rezumat

Lucrarea prezintă concepția, execuția şi testarea unui exoschelet amplificator de forță. Exoscheletul constă în două brațe mecanice şi are ca funcție principală amplificarea forței de ridicare a membrelor superioare. Utilizând concepte simple de proiectare, exoscheletul a fost fabricat cu costuri reduse, rezultând un raport bun între costurile de execuție şi performanțe.

Scientific reviewers: **Liviu BERETEU, "Politehnica" University of Timişoara, România**
Ion DUMITRU, "Politehnica" University of Timişoara, România

SCIENTIFIC BULLETIN OF
THE „POLITEHNICA" UNIVERSITY OF TIMISOARA, ROMANIA
TRANSACTIONS ON MECHANICS
BULETINUL ŞTIINŢIFIC AL
UNIVERSITĂŢII „POLITEHNICA" DIN TIMIŞOARA, ROMÂNIA
SERIA MECANICĂ
Tom 54 (68) **ISSN 1224 - 6077** **Fasc. 4, 2009**

DESIGN OF CUSTOMIZED HIP PROSTHESES

Mircea KREPELKA[*], Mirela TOTH-TAŞCĂU[*]
*Mechanical Engineering Faculty, Timişoara, Bv. Mihai Viteazu No 1, România,
e-mail: mk06deck@yahoo.com, mirela.toth-tascau@mec.upt.ro

Abstract. Studying the status of hip replacement operations in Romania, we found that the number of operations grows significantly every year. Following implant techniques and models, using medical imaging techniques and 3D reconstruction software we designed three different models of hip implants. The main objective of designing the implants was reducing the removal of healthy bone tissue required for classic total hip replacement. This paper presents CAD modeling techniques and the steps needed to establish the optimal form of implant, from a basic structure and ultimately leading to the virtual model of medical implant used in hip replacements. Models obtained will serve to achieve virtual functional assemblies (different types of prosthetic hip joints), which will be subject to numerical analysis and their practical achievement using unconventional technology of rapid prototyping manufacturing. CAD modeling of anatomical structures and prosthetic components was achieved using conventional techniques available in the CAD environment SolidEdge V19. The conventional modeling has pursued an exact transposition of the anatomical details of hip joint bone structure to obtain a 3D model of hip prosthesis, which faithfully copies any irregularities of the bone. This approach allows the implant surface to remain in constant contact with the bone surface, reducing the risk of loosening, providing stability.

Keywords: hip joint, implant stem, total hip replacement, hip resurfacing, CAD modelling

1. Introduction

The normal hip functions as a "ball and socket" joint. The femoral head (ball) articulates with the acetabulum (socket), allowing smooth range of motion in multiple plans.

During normal walking, the human hip joint undergoes cyclic loading that develop forces three to five times those of body weight on prosthetic components. In addition, during some particular movements, such as running or climbing, the hip joint is exposed to much greater forces (12 times those of body weight). Biomechanical analysis of these forces has challenged design engineers to develop the prosthetic components to maximize support of the implant throughout the walking cycle.

In general, implants are designed to closely approximate the function of the natural hip joint [4].

Total hip replacement (THR) or arthroplasty (THA) is one of the most successful orthopedic procedures performed today. For patients with hip pain due to a variety of conditions, THA can relieve pain, restore function, and improve quality of life. Total hip replacement, is a surgical procedure in which the hip joint is replaced by a prosthetic implant. Replacing the hip joint consists of replacing both the acetabulum and the femoral head.

A Total Hip Prosthesis (THP) is an artificial hip joint that replaces the patient hip joint and is composed of two components: the femoral (thighbone) component and the cup component. The acetabular component (or cup component) has a spherical shape being implanted into the acetabulum. The femoral component (or stem component) consists of a long metal stem, being placed into the marrow cavity of the

femoral bone. Generally, the femoral component consists of four parts:

- ball, a metal or ceramic ball component that replaces the removed femoral head and articulates with the cup;
- neck, a metallic part that connects the stem and the ball;
- collar, a disc between the neck and the stem that rests on the sawed off femoral bone; is used only for some models;
- stem, a metallic component that places the implant into the femur.

Each component of the hip prosthesis is designed and manufactured in various shapes and sizes to accommodate various body sizes and types. In some designs, the stem and ball are one piece; other designs are modular, allowing for additional customization in fit.

Thus, there are many models of total hip prostheses on the market and new models appear steadily allowing improvements in long term functionality of the prosthesis [2]. There are two main types of THP: mono-block construction and modular construction, each of them having its own advantages and disadvantages.

Modern Total Hip Arthroplasty (THA) systems are modular. This means that the femoral stem, head, acetabular shell and liner are separate pieces. This modularity allows for greater flexibility in customizing prosthesis sizing and fit. The acetabular part is usually a polyethylene liner with or without metal backing.

Fixation is with cement, spikes, screws or cementless with porous coating for bone in-growth. The femoral part is composed of a metal stem (chromium cobalt or titanium or titanium alloy) and a femoral head of metal or ceramic. Stem-fixation is also either with cement or cementless with porous coating for bone in-growth [6].

THP can be classified in different ways. The commonly used THP are [5]:

- *Conventional Total Hip prosthesis* - cemented cup and cemented stem, or polyethylene cup articulating against metallic ball component – is cheaper and technically more easy to fit into the skeleton;
- *Ceramic Total Hip prosthesis* - ceramic on ceramic/polyethylene total hips - ceramic cup articulates with the ceramic/polyethylene ball component; the cup of the ceramic total hip is composed of at least two layers: the inner layer - a ceramic cup proper that is in contact with the ceramic ball, and the outer layer - a metallic component that is in direct contact with the bone tissue of the hip socket;
- *Metal-on-metal Total Hip prosthesis* - both bearing surfaces (the ball and the cup component) made of metal. One important advantage of this type of THP is that it is allowed lubrication of the surfaces with "joint fluid". In addition, it is considered that metal-on-metal THP produces much less of the wear particles, and thus has much fewer failures.

As an alternative to total hip replacement is hip resurfacing. Hip resurfacing procedure places a metal cap on the femoral head instead of amputating it. Thus, there is no long stem placed into the femur. The potential advantages of hip resurfacing include less bone removal (bone preservation), a potentially lower number of hip dislocations due to a relatively larger femoral head size, and possibly easier revision surgery for a subsequent total hip replacement device because a surgeon will have more bone stock available to work with. The potential disadvantages of hip resurfacing are femoral neck fractures (rate of 0-4%), aseptic loosening, and metal wear [3].

Studying the status of hip replacement operations in Romania, we found that the number of operations grows significantly every year.

2. Design aspects

The design aspects (dimensions, radial clearance between the head and the metal socket must be kept as small as possible, surface roughness, etc.) and materials used to manufacture orthopedic implants are of great importance in joint replacements.

The paper proposes three distinct models of hip prosthesis: a resurfacing prosthesis, a short stem implant and a long stem implant based on a 3D joint reconstruction of a patient images accomplished with CT scans and Mimics and Magics software (figure 1).

2.1. Design of hip resurfacing

Hip resurfacing arthoplasty is a type of hip replacement that replaces the arthritic surface of the joint but removes far less bone than the traditional total hip replacement. Because the hip resurfacing removes less bone, it may be preferable for younger patients that are expected to need a second, or revision, hip replacement surgery as they grow older and wear out the original artificial hip replacement [1].

Steps performed in the design of the resurfacing implant were:

- Importing previously reconstructed femur and positioning it in the work plan.
- Increasing the area of interest (the proximal femur), choosing the symmetry axis of the

femoral neck and creating the drawing representing the negative of the desired shape after reaming the femoral head and cutting the femur 360º around the axis of symmetry. The result obtained is the new shape of the femoral head, conical and with a channel for introduction of the fixation pin of the implant, removing a small amount of bone (figure 2).

- Using sketches prior undertaken to cutting the femoral head we made the implant shape identical to the inner shape of the femur previously created. The conical interior of the implant provides an additional fixation (figure 3).

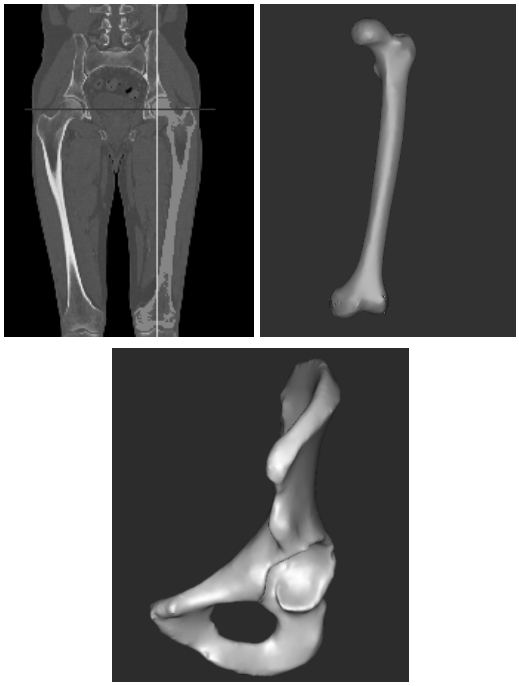

Figure 1. Stages of 3D hip joint reconstruction

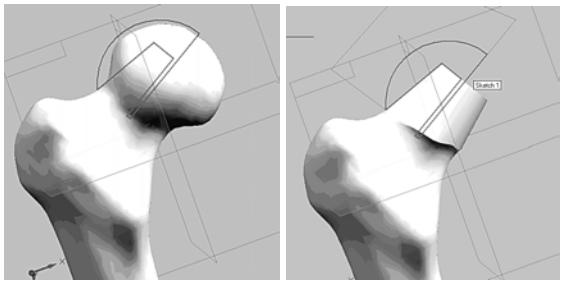

Figure 2. Reaming of the femoral head

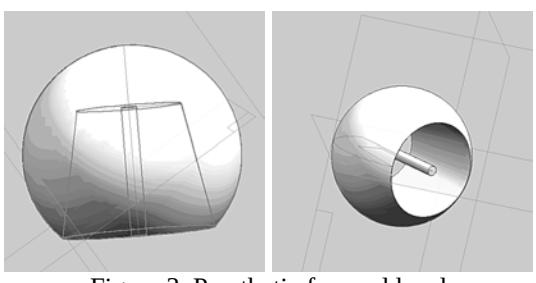

Figure 3. Prosthetic femoral head

- For a better view, we chosen different textures, colors and transparency from the range offered by the program or exclusively show contours. The assembly of the femur and resurfacing component is presented in figure 4.

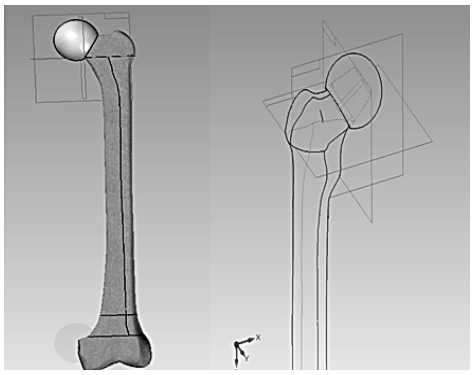

Figure 4. Femoral bone resurfacing - assembly

The designed resurfacing implant will be made of Ti-6AL-4V alloy with smooth and glossy outer surface.

2.2. Design of a short stem implant

The design of a short stem implant was started by importing the scanned femur in Solid Edge program and choosing the new implant size and position. Being a short implant, it is important that it fills the bone marrow canal of the femur as effectively as possible. The direct sketching on the femur helps to obtain the implant shape and the optimum angle for a normal geometry of the implant, eliminating the risk of dislocations, micro movements, inequality of limb.

The obtained shape of the implant stem is presented in figure 5.

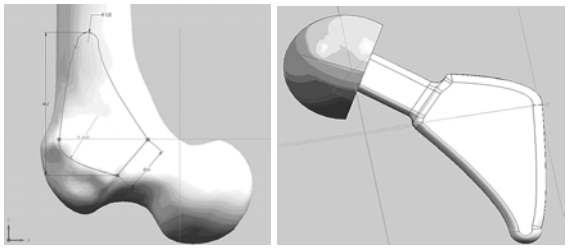

Figure 5. First shape of the implant stem

A series of angled grooves were created on the side surfaces enabling us to further increase the available surface area and bone in-growth minimising implant migration (figure 6).

The acetabular cup consists of two components: a metallic shell and an Ultra High Molecular Weight Polyethylene liner fixed into the shell which acts as a bearing surface due to its

low friction coefficient and also absorbs shocks (figure 7).

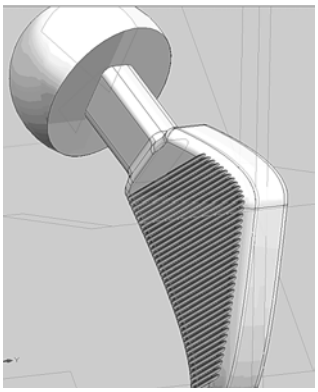

Figure 6. Groove pattern on the sides of the implant stem

The shell fits into the hip joint so there before it needs to copy the shape of the acetabular socket. The fixation is accomplished by using a porous low density Titanium alloy along a series of horizontal grooves on its exterior surface (figure 8).

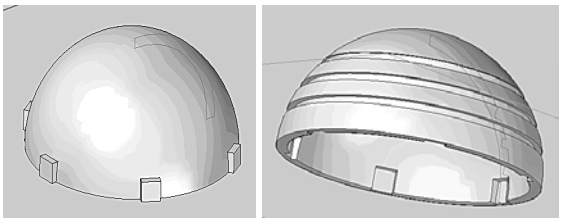

Figure 7. Acetabular components: shell and liner

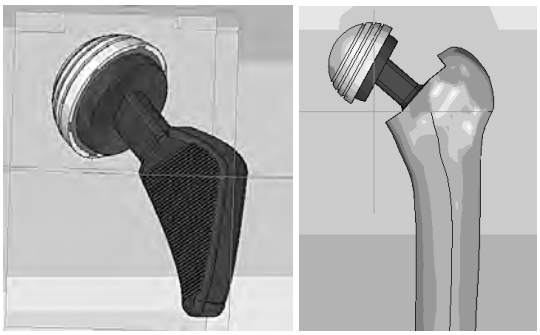

Figure 8. Assembled prosthesis and its position in the femoral bone

2.3. Design of a long stem implant

The third solution for a prosthetic hip is a long stem implant with ports for bone growth. Like the version with short stem, the implant materials are Ti-6AL-4V alloy and Ultra High Molecular Weight Polyethylene.

The curvature of the stem determines the implants final angle so it will match the geometry of the joint (figure 9).

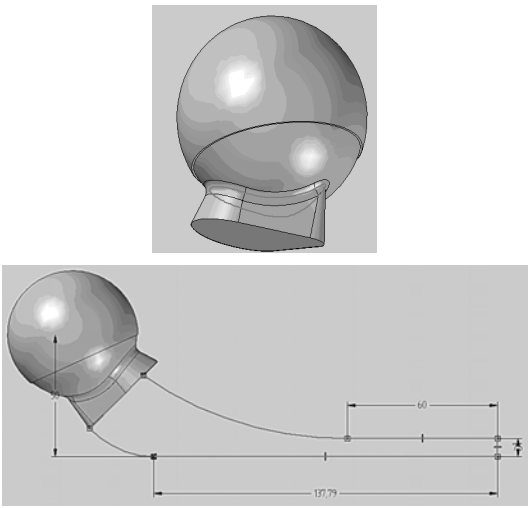

Figure 9. Choosing the angle and the length of the stem

Ports were made in the proximal part of the stem, where bone will grow on the surface of the porous Titanium alloy and also inside the ports performing and optimal fastening (figure 10).

The Polyethylene shell was designed with a lip that helps to prevent movement inside the shell (figure 11).

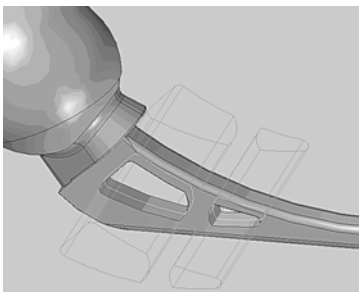

Figure 10. Ports in the proximal part of the stem

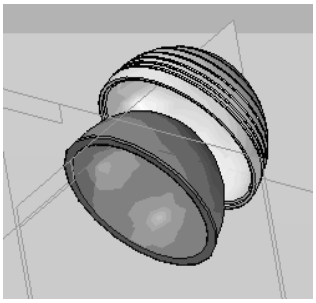

Figure 11. Acetabular cup

The assembly of the long stem implant - bone is presented in figure 12.

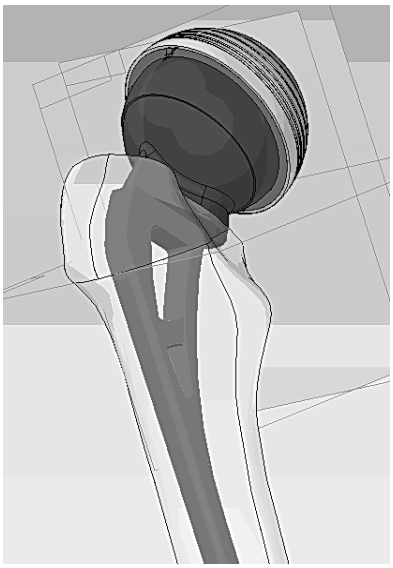

Figure 12. Bone-implant assembly

3. Comparative Analysis

In order to underline the advantages and disadvantages of the designed implants a comparative analysis has been performed. To make it easier to compare the three constructive solutions an overlapped representation of the femur-implant assemblies was created (figure 13).

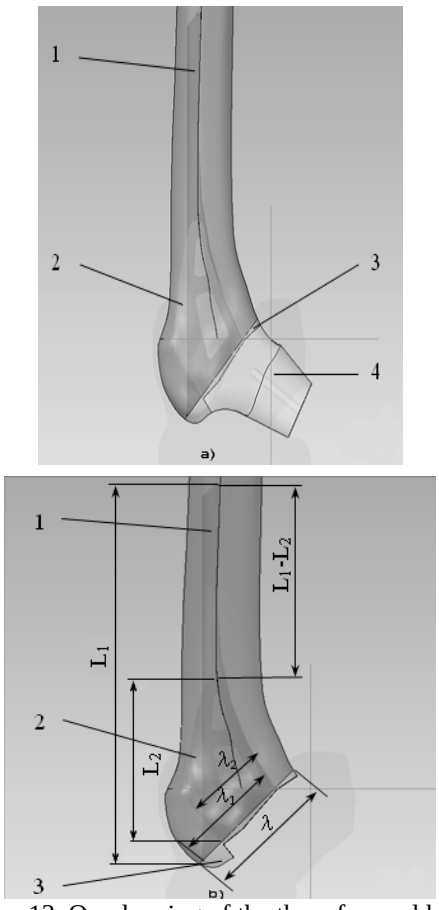

Figure 13. Overlapping of the three femoral bones

Thus, the notations used in figure 13 have the following meanings:

- 1 - gap required for the implantation of the long stem prosthesis;
- 2 - gap required for the implantation of the short stem prosthesis;
- 3 - portion of the bone saved when using the short stem design;
- 4 - portion of the femur bone saved if the resurfacing design;
- L_1 – length of the long femoral stem;
- L_2 - length of the short femoral stem;
- (L_1-L_2) - difference between penetration into marrow canal of the femur, the long and the short stem;
- λ_1- neck width of long stem;
- λ_2 - neck width of short stem;
- λ - width at the great trochanter base, in the area where cutting occurs.

In figure 13.a it can be seen the difference between the stems regarding the depth of penetration into the femur. Also, it can be seen that resurfacing the femoral head may preserve a significant portion of the patient's bone. In figure 13.b it can be seen the difference between short femoral stem and long femoral stem regarding the depth of penetration into the marrow canal of the femur, denoted by L_1-L_2. The width of the stem necks can be compared at the trochanter in the area where cutting occurs.

4. Conclusions

The comparative analysis of the three constructive solutions can highlight the following conclusions:

- As a first solution for the hip joint prosthesis, femoral head resurfacing must be considered, if the bone structure allows it. In this case it can be preserved a significant portion of the femoral head and not enter the marrow canal of the femur, thereby preserving its integrity;
- As a second solution for the hip joint prosthesis, the short stem implant may be considered, in which case the depth of penetration into the marrow canal and the cutting width are smaller;
- The third solution is the long stem implant, for which the depth of penetration into the femoral canal and the cutting width are larger.

Other considered solutions could be a partial prosthesis, which in turn can be short or long stem, which is recommended if the acetabular cavity is intact and healthy. The designed hip implants will be manufactured and validated by numerical analysis (Finite Element Method) and mechanical tests.

The developed research was performed based on the idea that improvements in design and manufacture of prostheses and surgical techniques will lead to a greater durability and improvements in patient activity.

References

1. H.C. Amstutz, Hip Resurfacing - Principles, Indications, Techniques and Results, Saunders, Elsevier Science Health Science Div, Philadelphia 2008, ISBN 978-1-4160-4724-7
2. Ch. Delaunay, The Charnley total hip replacement. The Gold Standard of primary hip replacement, 36 years on, Maîtrise Orthopédique. Le Journal Orthopédique sur le web, http://www.maitrise-orthop.com/corpusmaitri/orthopaedic/mo83_delaunay/delaunay_us.shtml, 2008
3. M.A. Mont et al. , Hip resurfacing arthroplasty. Journal of American Academy of Orthopedic Surgeons, 2006, 14(8), pp. 454-463, http://www.jaaos.org/, Accessed: 2009-11-15
4. J.S. Siopack, H.E. Jergesen, Total Hip Arthroplasty, Western Journal of Medicine 1995, vol. 162, pp. 243-249, http://www.ncbi.nlm.nih. gov/ pmc/articles/PMC1022709/ pdf/westjmed 00055-0049.pdf. Accessed: 2009-11
5. M. Toth-Taşcău, D. Bugariu, L. Bereteu, Design of a total hip prosthesis, Annals of the Oradea University, Fascicle of Management and Technological Engineering, Volume VIII (XVIII), 2009, pp.859-864, ISSN 1583 - 0691
6. I. Watt, S. Boldrik, E. van Langelaan, R. Smithuis: Hip - Total Hip Arthroplasty. Normal and abnormal imaging findings, The Radiology Assistant, the educational web site of the Radiological Society of the Netherlands, Available at: http://www.radiologyassistant.nl/en/. Accessed: 2009-11-15

PROIECTAREA UNOR PROTEZE DE ŞOLD PERSONALIZATE

Rezumat

Analizând modelele de implanturi folosite în România, pornind de la modelele obținute prin tehnici de imagistică medicală şi reconstrucție 3D, s-au proiectat trei modele de implanturi coxofemurale diferite. Obiectivul principal al conceperii acestor implanturi a fost reducerea gradului de eliminare a țesutului osos sănătos, necesar protezării totale clasice. Lucrarea prezintă tehnicile şi etapele de modelare CAD în vederea stabilirii formei optime a implantului de osteosinteză, pornind de la o structură de bază şi ajungându-se în final la modelul virtual al implantului medical folosit la osteosinteza articulației coxofemurale. Modele obținute vor servi realizării de ansambluri funcționale virtuale (diferite tipuri de protezări ale articulatei coxofemurale), care vor fi supuse analizelor numerice şi realizării practice a acestora, folosind tehnologii neconvenționale de fabricare rapidă a prototipurilor. Modelarea CAD a structurilor anatomice şi a elementelor de protezare s-a realizat utilizând tehnici convenționale disponibile în mediul CAD, SolidEdge V19. Prin modelarea convențională s-a urmărit o transpunere exactă a detaliilor de formă anatomică ale structurii osoase a articulației coxofemurale, în vederea obținerii unui model 3D al protezei de şold, care să copieze cu fidelitate toate neregularitățile osului. Această abordare permite suprafeței implantului să fie în contact permanent cu o structură osoasă, ducând aproape la eliminarea microdeplasărilor, ceea ce conferă stabilitate osteosintezei.

Scientific reviewers: **Liviu BERETEU, "Politehnica" University of Timişoara, România**
Ion DUMITRU, "Politehnica" University of Timişoara, România

SCIENTIFIC BULLETIN OF
THE „POLITEHNICA" UNIVERSITY OF TIMISOARA, ROMANIA
TRANSACTIONS ON MECHANICS
BULETINUL ŞTIINŢIFIC AL
UNIVERSITĂŢII „POLITEHNICA" DIN TIMIŞOARA, ROMÂNIA
SERIA MECANICĂ
Tom 54 (68) **ISSN 1224 - 6077** **Fasc 4, 2009**

A FINITE ELEMENT ANALYSIS OF THE IMPACT-CONTACT PROBLEM BETWEEN HYDRAULIC CYLINDRICAL ROD AND THE SUPPORT PRISM

Ştefan ŢĂLU[*], Mihai ŢĂLU[**]
[*] Technical University of Cluj-Napoca, Faculty of Mechanics, Department of Descriptive Geometry and Engineering Graphics, B-dul Muncii Street, no. 103-105, 400641, Cluj-Napoca, Romania, e-mail: stefan_ta@yahoo.com
[**] University of Craiova, Faculty of Mechanics, Department of Applied Mechanics, Calea Bucuresti Street, No. 165, Craiova, 200585, Romania, e-mail: mihai_talu@yahoo.com

Abstract. This paper investigates the low-velocity impact behaviour and impact-induced damages between hydraulic cylindric rod that falls and collides with the support prism of the part support system from horizontal Hydraulic Press – 2 MN. A three-dimensional finite element and transient dynamic analysis is performed to calculate the time-varying stresses, displacements, deformations and the factors of safety distribution throughout the support prism. A three-dimensional model of the support prism was generated based on the designed data. Finite elements analysis was performed using COSMOSWorks software. The predictive capability of the present numerical approach is successfully demonstrated through comparisons between theoretical and experimentally-measured values. The current computational model offers a relatively simple and efficient means of predicting the structural impact response between hydraulic cylindrical rod with the support prism. Results from the current analysis can be used for further studies in designing of the horizontal Hydraulic Press – 2 MN.

Keywords: horizontal Hydraulic Press, hydraulic cylindrical rod, support prism, finite elements analysis, impact

1. Introduction

Finite Element Analysis (FEA) is a method of numerical analysis, used for solving problems in many industrial applications, and many others.

In mathematical terms, FEA is a numerical technique used for solving field problems described by a set of partial differential equations.

As a powerful tool for engineering analysis, FEA is used during the product development process to solve problems ranging from very simple to very complex [1, 2].

FEA allows detailed visualization and provides a wide range of simulation options for controlling the complexity of both modelling and analysis of a system. Similarly, the desired level of accuracy required and associated computational time requirements can be managed simultaneously.

Benefits of FEA include increased accuracy, enhanced design and better insight into critical design parameters, virtual prototyping, fewer prototypes, a faster and less expensive design cycle and increased productivity [3, 4].

COSMOSWorks is a commercial implementation of FEA, capable of solving problems commonly found in design engineering.

A horizontal Hydraulic Press – 2 MN should be designed according an optimal cost-efficiency and long-term productive life for coping with the evolution of industrial technology, materials, energy sources and environmental regulations [5].

2. Materials and Methods

2.1. The prism support of part support system from horizontal Hydraulic Press – 2 MN

A standard prism support of part support system from horizontal Hydraulic Press – 2 MN was considered the baseline model for the FEA simulations (Figure 1).

A three-dimensional model of the support prism was generated based on the designed data and is shown in Figure1.

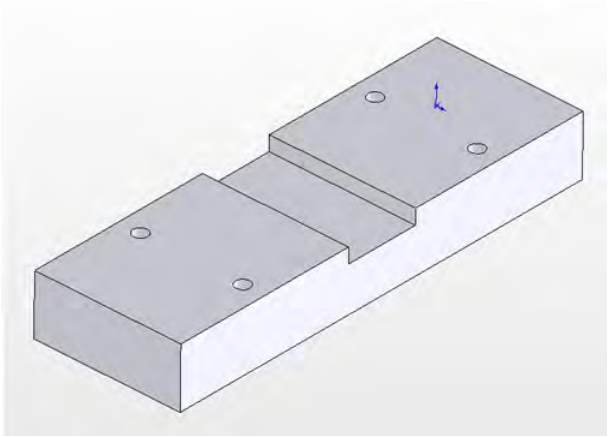

Figure 1 The prism support

2.2. Impact conditions

If during the work process there is a dysfunction as a result of accidental breakage or deformation of the material to be deformed or there is a failure of a safety element of the hydraulic system that controls displacement of the hydraulic linear motor rod, then there is an impact-contact between rod hydraulic cylinder and prism support.

Considering in this extreme case that the prism support takes over the entire stroke at the maximum displacement rod speed (in reality there are 2 prisms support that take this stroke), is important in transient dynamic analysis to calculate the time-varying stresses, displacements, deformations and the factors of safety distribution throughout the support prism. Study the impact-contact behavior is made on a time interval analysis by 6 μs from the moment of contact between rod hydraulic cylinder and prism support.

2.2. Meshing of the prism support

Finite elements analysis was performed using COSMOSWorks software.

Meshing of the analyzed structure in the finite elements is shown in figure 2.

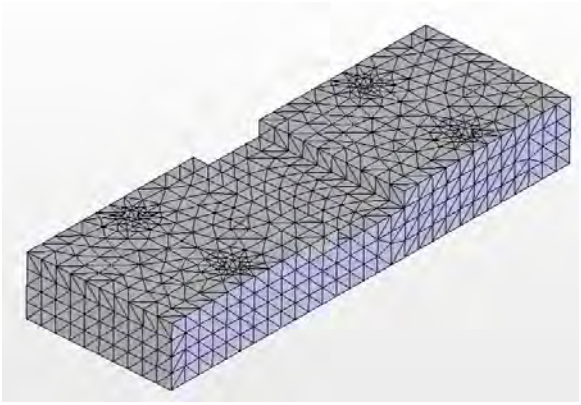

Figure 2 The meshing of the prism support

3. Results and Discussions

3.1. The stresses distribution

Graphical distribution of stresses by axes Ox, Oy, Oz and resultant are shown in figure 3, figure 4, figure 5 and figure6 (6 μs from the impact moment; deformation scale increased at 256.05).

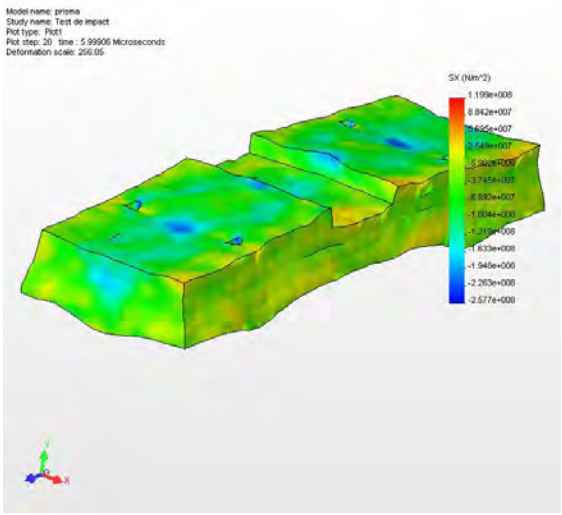

Figure 3 The stresses distribution by Ox axis

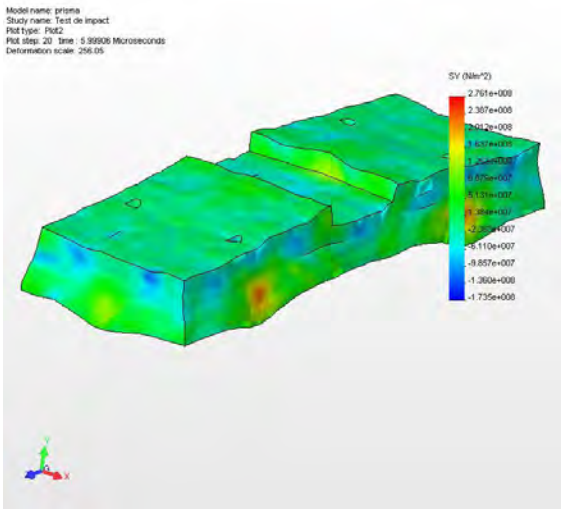

Figure 4 The stresses distribution by Oy axis

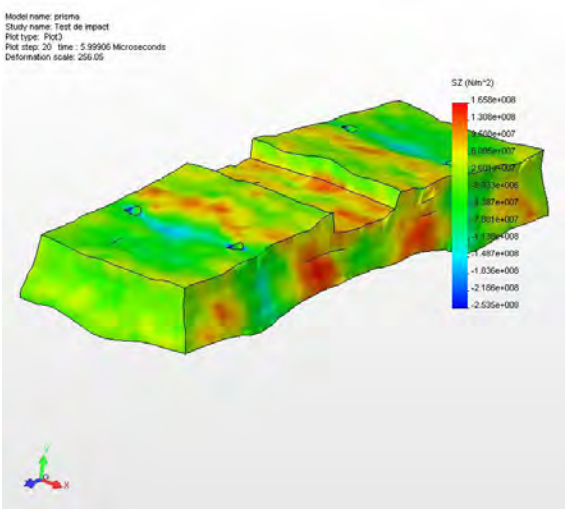

Figure 5 The stresses distribution by Oz axis

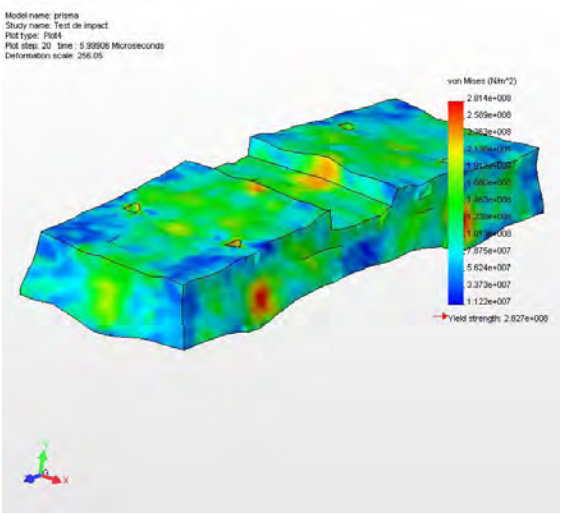

Figure 6 The resultant stresses distribution

3.2. The displacements distribution

Graphical distribution of resultant displacements are shown in:

- Fig. 7 (1 μs from the impact moment);
- Fig. 8 (2 μs from the impact moment);
- Fig. 9 (3 μs from the impact moment);
- Fig. 10 (4 μs from the impact moment);
- Fig. 11 (5 μs from the impact moment);
- Fig. 12 (6 μs from the impact moment);

all for deformation scale increased at 200.

3.3. The deformations distribution

Graphical distribution of deformations distribution ε_x, ε_y, ε_z by axes Ox, Oy, Oz are shown in Figure 13, Figure 14, Figure 15 (6 μs from the impact moment; deformation scale equal 200).

Graphical distribution of deformations distribution γ_{xy}, γ_{yz} and γ_{xz} are shown in Figure 16, Figure 17, Figure 18 (6 μs from the impact moment; deformation scale equal 200).

Graphical distribution of resultant deformations distribution ε and γ are shown in Figure 19 and Figure 20 (6 μs from the impact moment; deformation scale increased at 200).

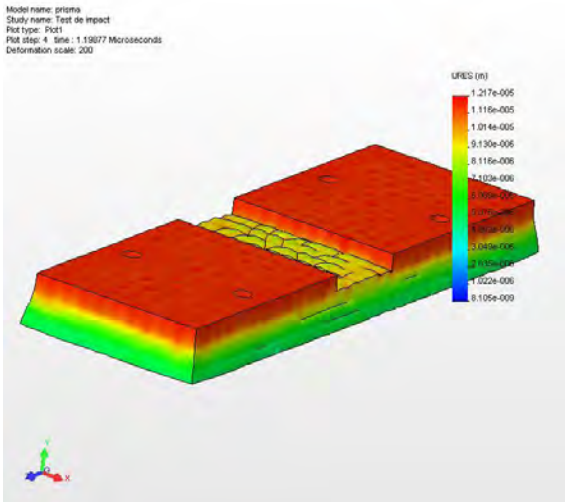

Figure 7 The resultant displacements distribution (1 μs from the impact moment)

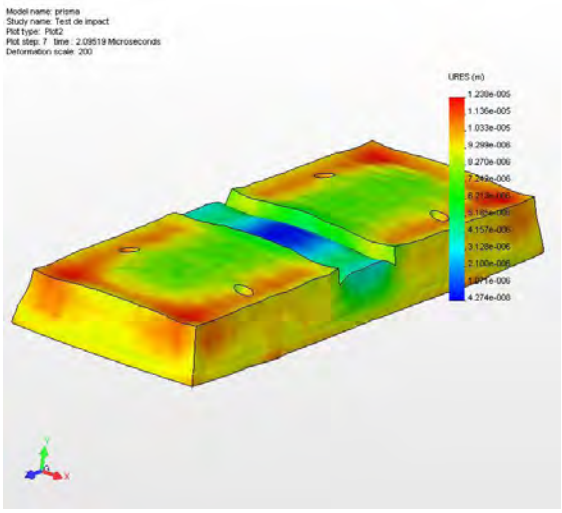

Figure 8 The resultant displacements distribution (2 μs from the impact moment)

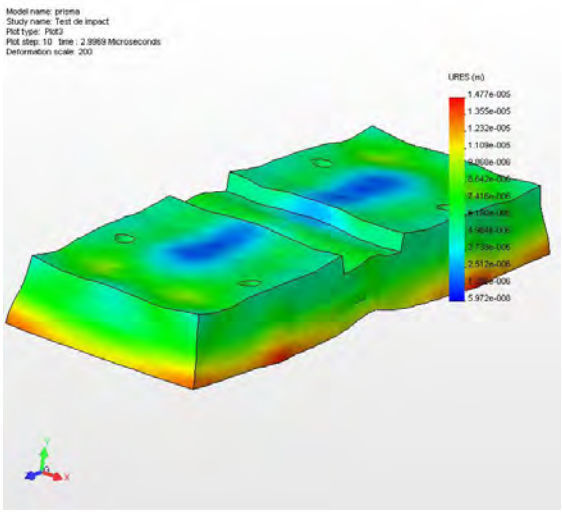

Figure 9 The resultant displacements distribution (3 μs from the impact moment)

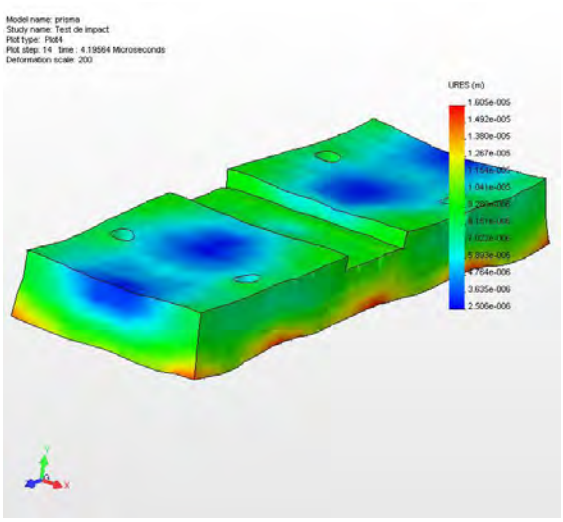

Figure 10 The resultant displacements distribution (4 μs from the impact moment)

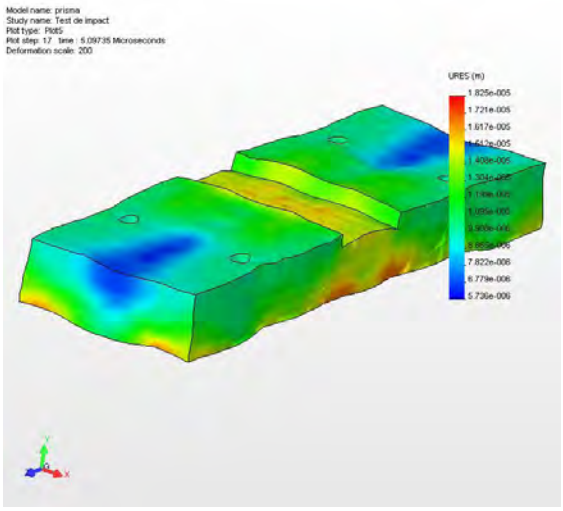

Figure 11 The resultant displacements distribution (5 μs from the impact moment)

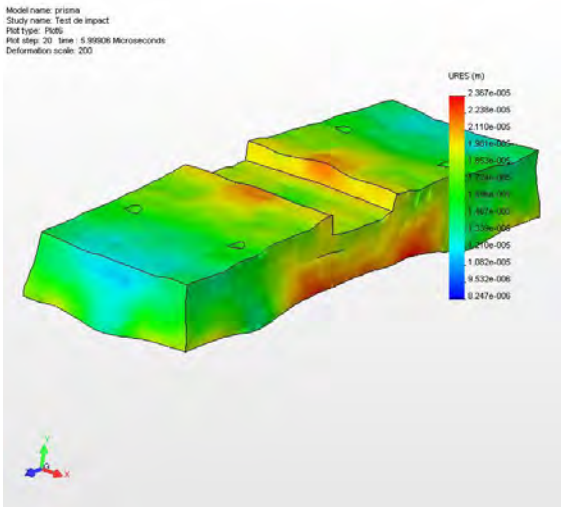

Figure 12 The resultant displacements distribution (6 μs from the impact moment)

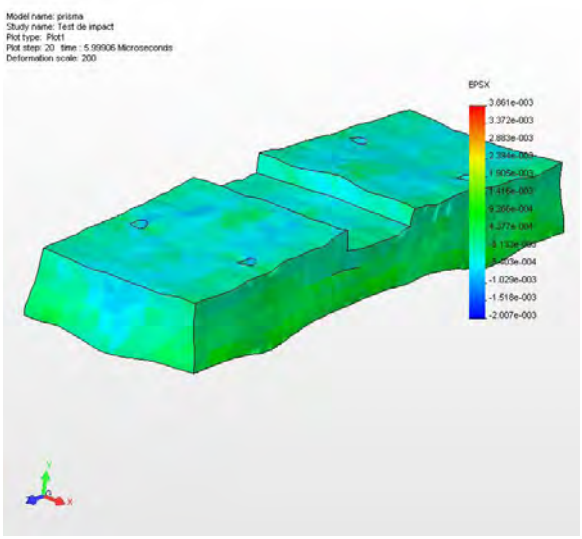

Figure 13 The ε_x deformations distribution by Ox axis

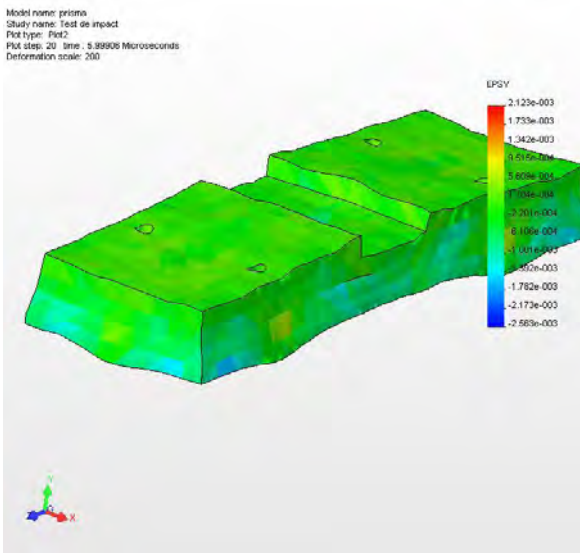

Figure 14 The ε_y deformations distribution by Oy axis

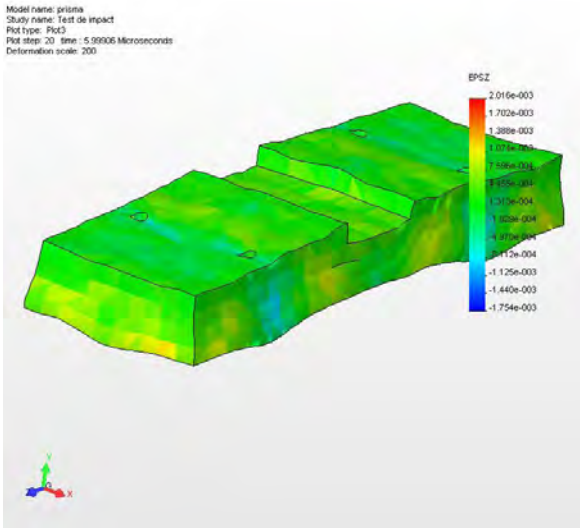

Figure 15 The ε_z deformations distribution by Oz axis

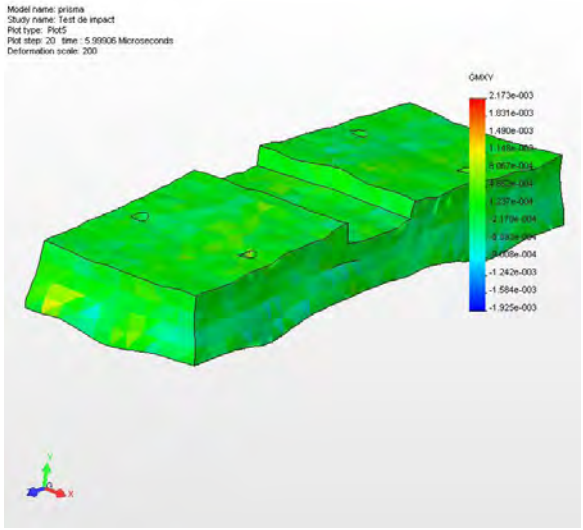

Figure 16 The γ_{xy} deformations distribution (6 μs from the impact moment)

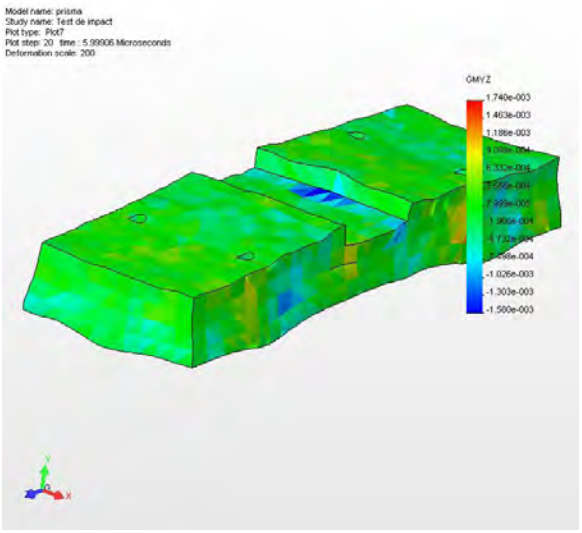

Figure 17 The γ_{yz} deformations distribution (6 μs from the impact moment)

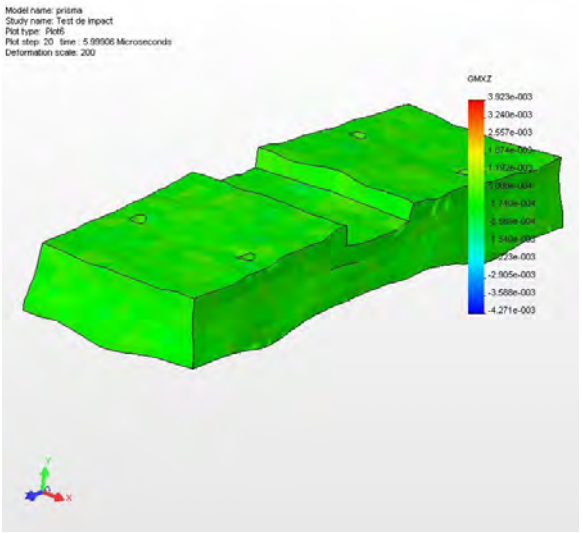

Figure 18 The γ_{xz} deformations distribution (6 μs from the impact moment)

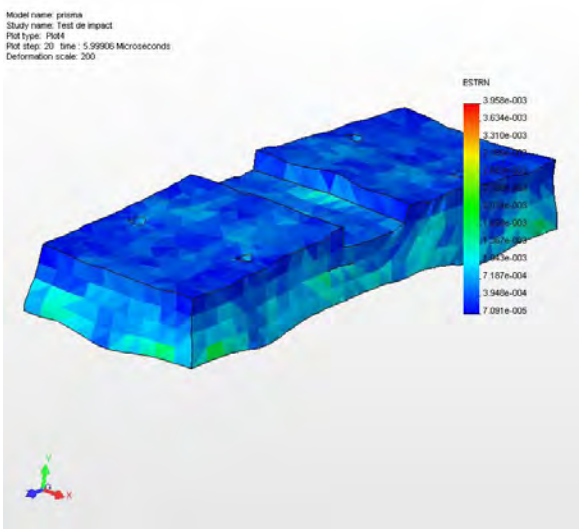

Figure 19 The resultant ε deformations distribution (6 μs from the impact moment)

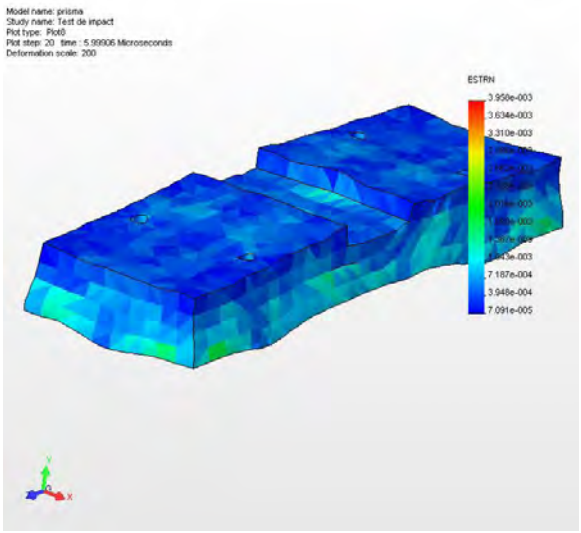

Figure 20 The resultant γ deformations distribution (6 μs from the impact moment)

3.4. The factors of safety distribution

Graphical distributions for factors of safety distribution are shown according:

- criterion: Max von Mises Stress; factor of safety distribution: Min FOS = 3.5 (Figure 21);
- criterion: Max Normal Stress; factor of safety distribution: Min FOS = 2.7 (Figure 22).

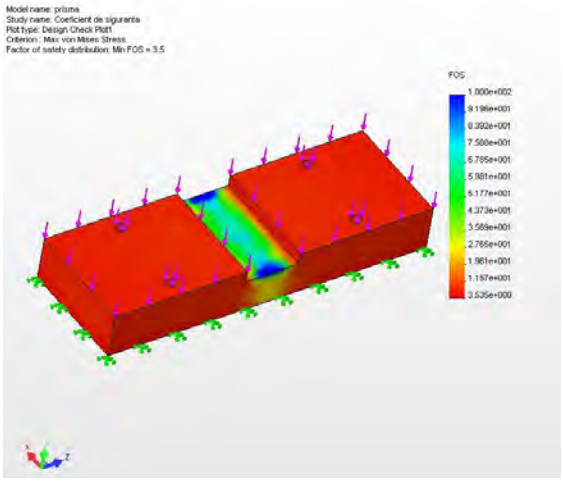

Figure 21 Factor of safety distribution: Min FOS = 3.5
Criterion: Max von Mises Stress

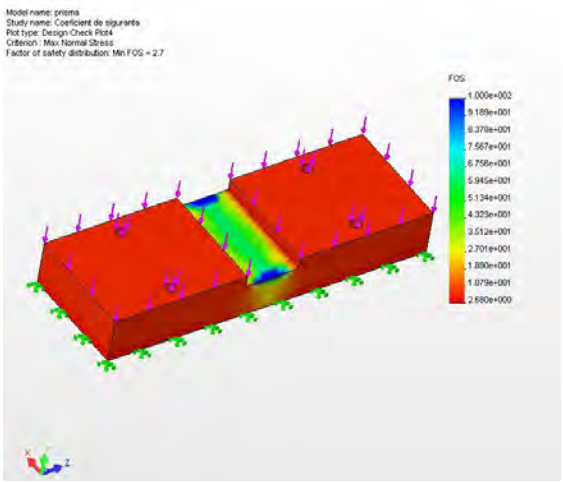

Figure 22 Factor of safety distribution: Min FOS = 2.7.
Criterion: Max Normal Stress

4. Conclusions

The low-velocity impact behaviour and impact-induced damages between hydraulic cylindrical rod that falls and collides with the support prism of the part support system from horizontal Hydraulic Press – 2 MN was made for determination of the time-varying stresses, displacements, deformations and the factors of safety distribution throughout the support prism.

A three-dimensional model of the support prism was generated based on the designed data.

Finite elements analysis was performed using COSMOSWorks software.

The predictive capability of the present numerical approach is successfully demonstrated through comparisons between theoretical and experimentally-measured values.

Acknowledgements

This work has partly been funded by the Romanian Ministry of Education, Research and Youth, through The National University Research Council, Grant PN–II–ID–PCE–2007–1, code ID_1107, 2007 – 2010.

References

1. J.E. Akin, Finite Element Analysis with error estimators, Publisher Butterworth-Heinemann, 2005, ISBN 13:9780750667227
2. D. Braess, Finite Elements: Theory, Fast Solvers, and Applications in Solid Mechanics – Third Edition, Cambridge University Press, UK, 2007, ISSN 1431-1550
3. D.L. Logan, First Course in the Finite Element Method – Fourth Edition, Thomson Learning, 2006.
4. D.W. Pepper, J.C. Heinrich, The Finite Element Method Basic Concepts and Applications – Second Edition, Publisher Taylor and Francis, 2005, ISBN 0-415-95062
5. O. Zienkiewicz, O.C. Zienkiewicz, R.L. Taylor, Finite Element Method for solid and structural mechanic, Publisher Butterworth-Heinemann, 2005, ISBN 10:0824759524

ANALIZA CU ELEMENT FINIT A PROBLEMEI DE IMPACT-CONTACT DINTRE TIJA CILINDRULUI HIDRAULIC ŞI PRISMA DE SPRIJIN

Rezumat Această lucrare investighează comportamentul la impact cu viteză redusă şi deteriorările produse de impact între tija cilindrului hidraulic care cade şi se ciocneşte cu prisma de sprijin a sistemului de sprijin a piesei pentru presa hidraulică orizontală de 2 MN. Analiza cu element finit tridimensional şi analiza dinamică tranzitorie s-a efectuat pentru a calcula variabilele în timp ale tensiunilor, deplasărilor, deformărilor şi factorilor de distribuţie de siguranţă în prisma de sprijin. Modelul tridimensional al prismei de sprijin a fost generat pe baza datelor proiectate. Analiza cu elemente finite a fost efectuată utilizând software-ul COSMOSWorks. Capacitatea de predicţie a abordării numeric prezente este demonstrată cu succes, prin comparaţii între valorile teoretice şi cele experimental-măsurate. Modelul actual computaţional oferă un mijloc relativ simplu şi eficient de a prevedea răspunsul structural de impact între tija cilindrului hidraulic cu prisma de sprijin. Rezultatele din analiza curentă pot fi folosite pentru studii suplimentare în proiectarea presei hidraulice orizontale de 2 MN.

Scientific reviewers: **Aurel RĂDUŢĂ, "Politehnica" University of Timişoara, România**
Mihaela POPESCU, "Politehnica" University of Timişoara, România

SCIENTIFIC BULLETIN OF
THE „POLITEHNICA" UNIVERSITY OF TIMISOARA, ROMANIA
TRANSACTIONS ON MECHANICS
BULETINUL ŞTIINŢIFIC AL
UNIVERSITĂŢII „POLITEHNICA" DIN TIMIŞOARA, ROMÂNIA
SERIA MECANICĂ
Tom 54 (68) **ISSN 1224 - 6077** **Fasc. 4, 2009**

RESEARCHES CONSIDERING „ENTRANCE EFFECT" IN CASE OF HEAT EXCHANGERS WITH WAVY FINS

Mihai NAGY* Ioan Daniel CĂRĂBAŞ[*], Ioan LAZA*, Paul ILIEŞ**
* Mechanical Engineering Faculty, Bv. Mihai Viteazu, No.1,
Timisoara 300222, România, email: mihai.nagi@mec.upt.ro, daniel.carabas@mec.upt.ro, laza_ionut@yahoo.com
**SC.RAAL SA. 420063, Bistrita, Str. Industriei nr. 4/A , România, email: paulilies@raal.ro

Abstract. The paper is based on experimental researches made on five compact heat exchangers, identical as appearance, construction and frontal dimensions, but with different thickness. In this paper there is proved the influence of "entrance effect" on thermal performances of these devices. There were analyzed the variation of thermal transfer global coefficient according to air flowing speed and the variation of Colborrn criterion according to Reynolds number

Keywords: entrance effect, heat exchangers, thermal transfer, limit layer

1. Introduction

Inside of experimental researches there was studied an aluminum fin, made in RAAL S.A. Bistrita, a wavy sinusoidal fin which is made by straps with a thickness, on casual, of 0,14; 0,16; 0,3; 0,5 mm.

If there is to be considered an x portion, a little one, (under 25% of wavy step) at the entrance of the fluid on a wavy wall, this portion may be compared with a plane wall, with the speed of the fluid w_w parallel with the wall. There can be observed that (figure 1) that a layer of fluid is getting a shape, where there is a boundary layer motion, named as a hydraulic limit layer.

This layer has got at the entrance on the wall a very, very small thickness δx and it grows with an x coordinate. No mater that the average stream is laminar or turbulent, the limit layer will have always a laminar effect, it is only that the thickness of that limit layers the one who varies upon the degree of turbulence of the core of the stream.

On the surface of the wall there is formed as well a hydraulic limit layer, where w_x speed varies from zero to a w_∞ value, and thermal limit layer too, where the temperature of the T fluid varies T_p (temperature of the wall) to T_∞ (temperature of the fluid uninfluenced by the presence of the wall) [4].

The thickness of both limit layers may be admitted as having a parabolic variation [2], but it will be commonly different for the two layers:

δ_x – the thickness of hydraulic limit layer,

δ_t – the thickness of thermal limit layer.

2. Theoretical consideration

According to Plhausen relation [1], the link between the two layers is:

$$\partial_t = \frac{\partial x}{\sqrt[3]{\mathrm{Pr}}} \quad (1)$$

For air with Pr=0,7 there is obtained:

$$\partial_t = 1.124 * \partial_x \quad (2)$$

The dimensions of δ_x and δ_t depend on the "x" coordinate and they grow with this coordinate untill a limit value determined by Re_{cr}. In the boundary limit layer the heat exchange by

conduction is equal to the heat transmissive to the fluid by convection:

$$\dot{q} = -\lambda_f \left(\frac{\partial T}{\partial y}\right)_{y\to 0} = \alpha (T_p - T_\infty) \qquad (3)$$

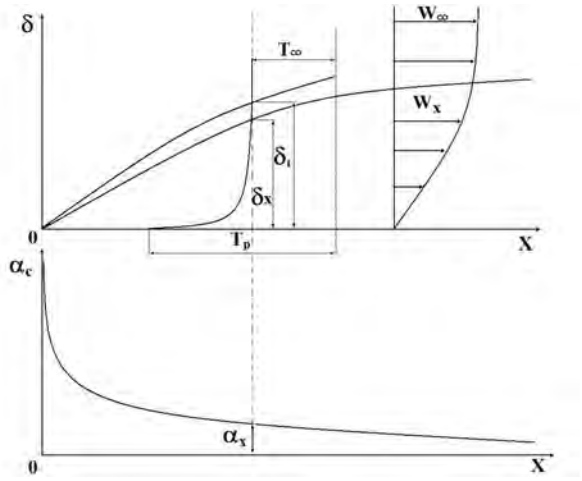

Figure 1. Variation of limit layer at the entrance on a plane surface

The y axis is perpendicular on the wall and λ_f – is the thermal conductivity of limit layer.

It may be adopted on first approximation as:

$$\left(\frac{\partial T}{\partial y}\right)_{y\to 0} \cong \frac{T_p - T_\infty}{\partial_t} \qquad (4)$$

and there is obtained like this the value of convection coefficient α_x in the area where the thickness of limit layer is δ_t

$$\alpha_x \cong \frac{\lambda_f}{\delta_t} \qquad (5)$$

The heat exchange between the fluid and the wall is the most effective at the entrance limit of the wall where the thickness of limit layer is a very small one. There is found that, at the beginning, when the limit layer gets to zero, the ''α_x'' convection thermal transfer coefficient has the maximum value. This phenomenon is well known under the denomination of "entrance effect" [4-6]. This effect may be made at the entrance of any surface, for a short length.

By solving the integral equation of limit layer [2] there is obtained the expression of limit layer thickness:

$$\frac{d}{dx}\int_0^\delta \rho\, w_x^2\, dy - w_0 \frac{d}{d_x}\int_0^\delta \rho\, w_x\, dy = -\tau_0 \qquad (6)$$

where there were scored, beyond the amounts from 2nd figure 2. the following τ_0 [N/m$_.$] – friction force, reported to the unit of surface.
Solving of equation (6) leads to:

$$\delta = c\sqrt{\frac{x\,\nu}{w_0}} = c\, x\, Re_x^{-1/2} \qquad (7)$$

The value of c is [4]:

c = 3,40 - according to Blasius
c = 4,64 - according to Pohlhausen
c = 5,83 - according to Miheev

The relations (5) and (7) prove that ''α_x'' is as bigger as "x" is smaller and it is like this as much as w_x speed of entrance on the fin is bigger.

Because of the complex phenomena which occure in this case, it is the researching on the stall the only one who can respond at the questions involving thermic and fluido-dynamic performances of this kind of surfaces with wavy fins.

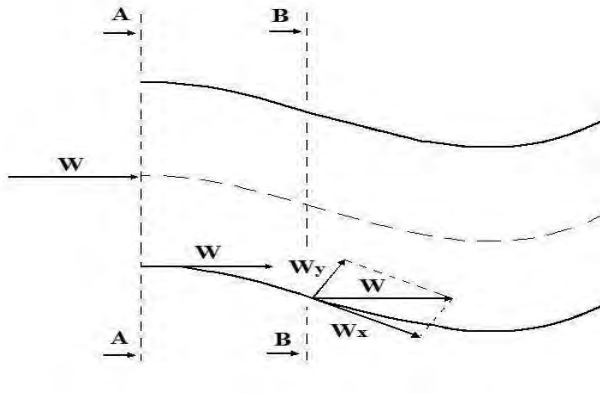

Figure 2. Variation of limit layer at the entrance on a plane surface

The wavy fins are made on a certain dimension and they are discharged on the thickness compulsory by device.

The correct discharge is made on the A-A section (Figure 2) and not on the B-B. If the fluid gets entered after the B-B section, the ''w'' speed of the fluid is to be decomposed on the two perpendicular directions, x and y, (in the A-A section the''w'' speed of the fluid is not to be decomposed) so the effect of thermal transfer is reduced (theory also verified on experimental researches).

If there is taken into consideration a random section in the wavy wall of the fin, according to the direction of fluid flow and the system is there framed in the coordinate axis y-x (Figure 3) it may be written the equation of the ambit:

$$y = h \sin \frac{2\pi}{L} x \qquad (8)$$

where h - is the maximum amplitude and L - waving step.

Because h is very short according to the L length, which represents in this case the waving step, or the wave length, the perturbation speeds in a point P of the ambit (w_x, w_y) are very small. Admitting that the speed from the infinite w_∞ is

directed on the x axis, it may be written for the P point (which might be confound with abscissa axis).

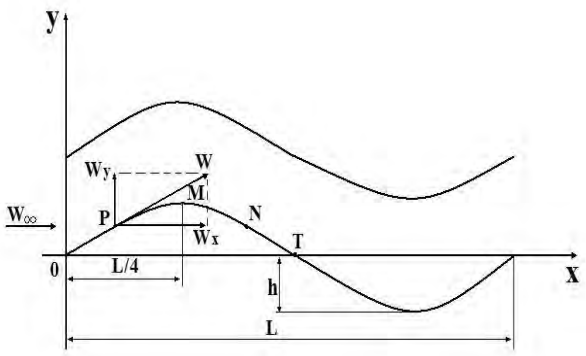

Figure 3. Channel with wavy walls

$$\left(\frac{dy}{dx}\right)_p = \frac{2\pi h}{L}\cos\frac{2\pi}{L}\chi \cong \left(\frac{w_y}{w_\infty}\right)_{y=0} \quad (9)$$

From the above equation there is obtained the variation of speeds:

$$w_y = w_\infty \frac{2\pi h}{L}\cos\frac{2\pi}{L}x \quad (10)$$

$$w_x = w_\infty \frac{2\pi h}{L}\sin\frac{2\pi}{L}x \quad (11)$$

It is certain that the variation of speeds inside the channel is sinusoidal.

3. Experimental Researches

3.1. The Test Stall

There was used a special stall for testing heat exchangers (Figure 4.), a stall which simulates on high fidelity the real working mode of the tested devices.

The stall is gifted with European-level apparatus and it is one of the most modern and complex stalls in the country.

Figure 4. Overall view of a test stall

The stall was conceived and realized in order to allow tests for all kind of heat exchangers, coolants which use air as a cold fluid the air and, as a hot fluid, the water, the oil or the hot air.

3.2. Tested Exchangers

The heat exchangers are on water-air, oil-air or air-air type and they may be used without operating modifying on the installation scheme.

In order to study thermal and fluid-dynamic performances, there were used aluminum heat exchangers, on air-air type; these devices are on boards and bars type (figure 5.).

Figure 5. 400x400xGxp radiator, with wavy fins

These devices have identical frontal dimensions, with identical water channels on rectangular section and air channels provided with wavy fins with a constant high of 8,8 mm. and the step p = 4 mm. (figure 6).

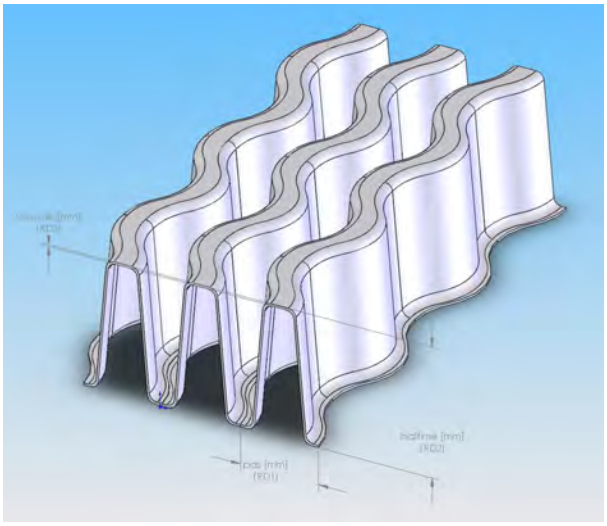

Figure 6. Wavy fin used for tested radiators

At the tested radiators it was varied the thickness of the G matrix (30; 45; 65; 95 şi 115 mm.), mentioning that the performances of these

devices depend on the geometry and on the length of the channel.

3.3. Processing Experimental Data

Data processing is made in LabView 7.0. This program (Figure 7) observes the parameters on the stall, it designees their graphic representation, is actions from distance the cool air obdurate, it communicates with an Excel file where the data are computed after which they are taken and shown in the graphic interface, and also is the record of the value of valid experiments (<2%).

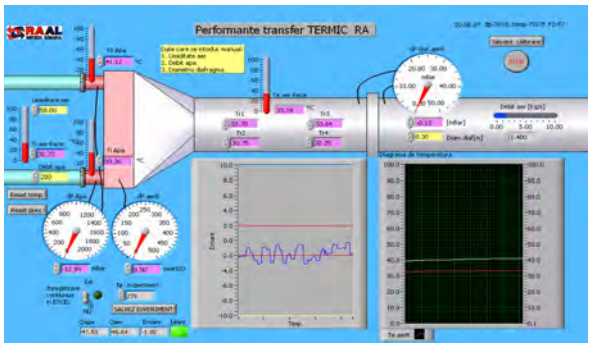

Figure 7. Data acquisition program interface

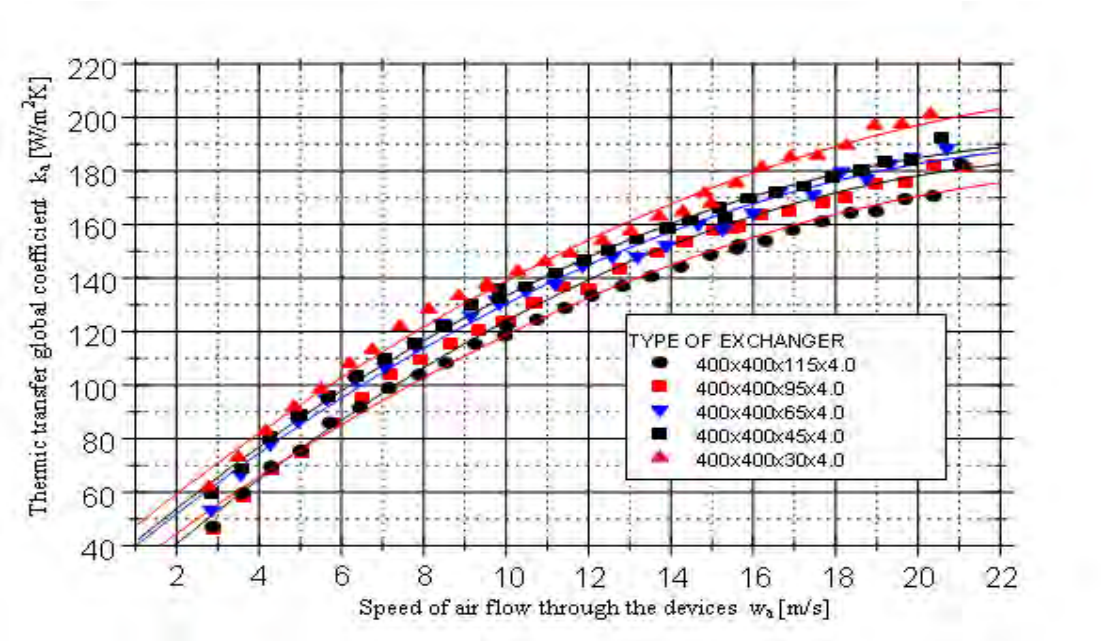

Figure 8. Thermic transfer global coefficients for the heat exchangers family with cu p=4.0 mm.

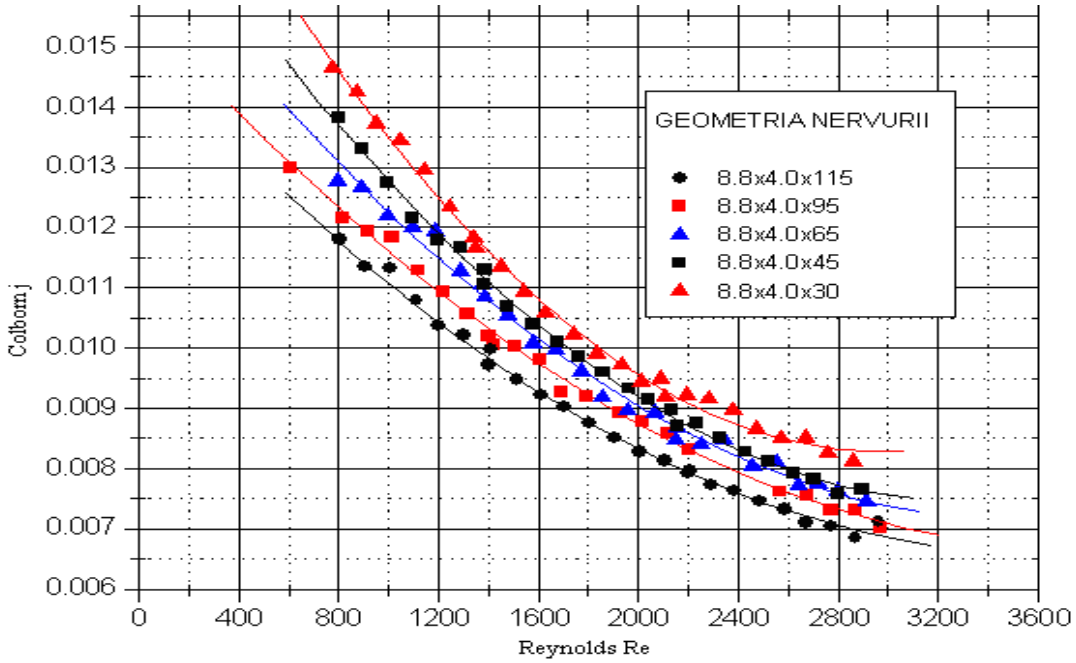

Figure 9. Colborn variation for the wavy fins surfaces with 4,0 mm step

Thermal transfer global coefficients for the same heat exchangers family tested in almost identical condition, on the first analysis, should have been identical, so the variation curves should have been overlapped [3].

This theory is available if there isn't considered the thickness of air channel which is short for these radiators (from 30 mm. to 115 mm.) and also it isn't considered the entrance effect, which is as bigger as the thickness of heat exchangers is smaller.

Colborn criteria variation sketching according to Reynolds number means the generalization of experimental results about thermal performances of these finally surfaces, where:

$$J = \frac{Nu}{\mathrm{Re}\,\mathrm{Pr}^{1/3}} = St\,\mathrm{Pr}^{2/3} \qquad (12)$$

$$\mathrm{Re} = \frac{wl}{\nu} \qquad (13)$$

The above results may be appreciated both qualitative and quantitative and the diagrams may be rigorously used for designation of similar finely surfaces (geometry of nearby fin) with no consideration for the attempt conditions.

4. Conclusions

It is observed that heat exchange between thee fluid and the wall is the most effective at the entrance limit of the wall where the thickness of limit layer is a very small one. It is determined that, at the beginning, when the limit layer tends to zero, the ''α_x'' thermal transfer convection coefficient has the maximum value. It is also determined that the phenomenon called "end effect" is obtained at the entrance of the fluid on the contact surface.

By solving the integral equation (6) it is obtained the thickness of limit layer (8), this is why there is proved that ''α_x'' is as bigger as ''x'' is smaller and as well as also the w_x entrance speed on the fin is bigger.

In case of skatching k thermal transfer global coefficient variation according to speed, the above diagrams offer information about the dimension order of thermal transfer global coefficients, the variation mode of this amount, but they cannot be used in order to design another devices except if the devices meant to be designed would of work in exactly the same conditions. (speeds, temperature and air humidity and devices thickness).

After sketching Colborn j variation according to Reynolds Re number it is observed that obtained results may be appreciated both quantitative and qualitative and the diagrams may be rigorously used for designation of similar finly surfaces with no consideration for the attempt conditions.

The values of Colborn number are as bigger as the length of the channel is shorter and also the fin step is shorter, too.

The differences between Colborn values for the same family and for the same Reynolds are explained due to entrance effect. It is proved this way that the theory about entrance effect is correct.

References

1. I. Leca, Transfer of heat and mass. Theory and applications. Didactic and Pedagogic Publishing House, Bucharest, 1983.
2. M. Nagi, Determin ation of the prediction equation for the fluid laminar flowing through sinusoidal fins. Scientific Bulletin , U.T.T. Tom 41(55) Mechanics, 1996, pp. 110-115.
3. M. Nagi, P. Ilieş, A. Negoiţescu, The detrmination of the optimal circulation fluids speeds through the heat Exchangers. DAAAM International, VIENA, AUSTRIA.2008, pp.943-944, ISSN 1726-9679, ISBN 978-3-901509-68-1**,** ISI PROCEEDINGS.
4. M. Nagi, D. Iorga,, I. Laza, L. Mihon, D. Ostoia, Heat exchangers, vol.1, Mirton Publishing House, Timişoara, 2006.
5. M. Nagi, A. Negoiţescu, Studies concerning "the entrance efect" on the discontinue fins of the heat exchangers, Termiche prozesse., Rumanisch-Deutches Symposion, pp.171-176, 2008
6. M. Nagi, L.D. Negru, I. Laza, D. Lelea, Theoreticaland experimental studies about the alternatives of comparing oil coolers used for engines with internal combustion (in serbian language) OSMI Strucni skup o opremi u procesnoj industriji Beograd, 26-27 oct. 1994. Procesna tehnika Nr.3 – 4, 1994 pp.30 - 32.

CERCETĂRI PRIVIND "EFECTUL DE INTRARE" ÎN CAZUL SCHIMBĂTOARELOR DE CĂLDURA CU NERVURI ONDULATE

Rezumat:

Lucrarea are la bază cercetări experimentale efectuate pe cinci schimbătoare de căldură compacte identice ca formă, construcţie şi dimensiuni frontale dar cu grosimi diferite.

Se demonstrează influența “efectul de intrare” asupra performanțelor termice ale acestor aparate. S-au analizat variația coeficientului global de transfer termic în functie de viteza de curgere a aerului şi variația criteriului Colborrn în funcție de numarul Reynolds.

Scientific reviewers: **Dănilă IORGA, “Politehnica” University of Timişoara, Romania**
Eugen GHITA,”Politehnica” University of Timişoara, Romania

SCIENTIFIC BULLETIN OF
THE „POLITEHNICA" UNIVERSITY OF TIMISOARA, ROMANIA
TRANSACTIONS ON MECHANICS
BULETINUL ŞTIINŢIFIC AL
UNIVERSITĂŢII „POLITEHNICA" DIN TIMIŞOARA, ROMÂNIA
SERIA MECANICĂ
Tom 54 (68) **ISSN 1224 - 6077** **Fasc. 4, 2009**

NUMERICAL INVESTIGATION OF HEAT TRANSFER AND PRESSURE DROP IN THE SHELL-SIDE OF A SHELL-AND-TUBE HEAT EXCHANGER

Viorica CEBRUCEAN (HAREA)*, Ioana IONEL*, Dumitru CEBRUCEAN*
* Faculty of Mechanical Engineering, Bv. Mihai Viteazu, No.1,
Timisoara 300222, Romania,
e-mail: harea_viorica@yahoo.com, ioana.ionel@mec.upt.ro, dumitru_cebrucean@yahoo.com.

Abstract. Shell-side heat transfer and pressure drop of a shell-and-tube heat exchanger with single segmental baffles has been numerically investigated. The main objective is to compare the results of this work with our previous numerical results in which the properties of the shell-side fluid were kept constant. The numerical simulations have been performed using the commercial CFD software package FLUENT 6.2. The model has been designed with 8 segmental baffles and baffle cut of 25%. Numerical results have shown that the pressure drop has slightly decreased and the fluid properties have almost no effect on heat transfer as compared to our previous study.

Keywords: shell-and-tube heat exchangers, segmental baffles, heat transfer, pressure drop, CFD

1. Introduction

Shell-and tube heat exchangers are widely used apparatuses in chemical, petroleum referring and energy industries. They are characterized by high heat transfer coefficient, compactness, relatively low cost, ease of construction and maintenance. Shell-and-tube heat exchangers provide relatively large ratios of heat transfer area to volume and weight and they can be easily cleaned. They offer great flexibility to meet almost any service requirement [3, 7, 14].

A shell-and-tube heat exchanger is a cylindrical vessel housing a set of tubes (usually called the tube bundle). The heat transfer occurs between the fluid flowing over the tubes and the fluid flowing inside the tubes. The fluid flow inside the tubes is said to be "tube-side" and the fluid flow within the space between the tubes and the shell is said to be "shell-side". Figure 1 shows a scheme of a segmental baffled one-shell pass one-tube pass shell-and-tube heat exchanger [2].

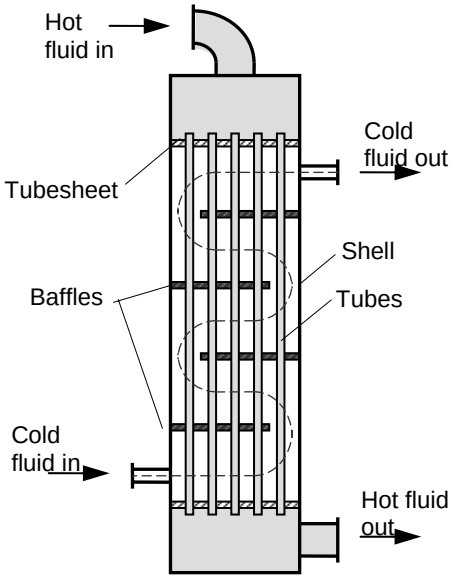

Figure 1 1-1 Shell-and-tube heat exchanger with single segmental baffles and fixed tubesheets

The heat transfer of shell-and-tube heat exchangers can be improved by means of baffles. Among which, segmental baffles are the most commonly used in conventional shell-and-tube type heat exchangers in order to increase the heat transfer rates, as well as to provide support to tube bundle and prevent vibration of the tubes caused by flow-induced eddies. There are several types of segmental baffles: single, double, triple and no-tubes-in-window segmental baffles [2, 7, 11]. The single and double segmental baffles are the most frequently used in industries. They divert flow most effectively across the tubes. The triple and no-tubes-in-window segmental baffles are used for low pressure drop applications.

This study aims to numerically investigate the shell-side heat transfer and pressure drop for liquid flow in a shell-and-tube heat exchanger with single segmental baffles. The results of this work have been compared with our previous numerical results [1] in which the properties of the shell-side fluid were kept constant. The work has been carried out by means of Computational Fluid Dynamics (CFD). The commercial CFD software package FLUENT 6.2 is used to perform numerical simulations and the pre-processor GAMBIT 2.2 is used to create and generate the mesh.

2. Previous work

Theoretical and experimental studies on shell-and-tube heat exchangers with and without segmental baffles, and variable geometries were carried out by a number of researchers [3, 14, 15]. Tinker [15] examined several heat exchangers with different shell diameters varying from 90 to 260 mm using principally oil as shell-side fluid and in one test water. Tube outside diameters and tube pitch varied from 10 to 16 mm and from 11.5 to 19 mm, respectively. Donohue [3] collected available experimental data from different investigators and identified factors which influence heat transfer coefficient and pressure drop in unbaffled and baffled shell-and-tube heat exchangers. Shell-side heat transfer and pressure drop in baffled shell-and-tube heat exchangers can be estimated using a method given in [14]. Gaddis and Gnielinski [6] presented a procedure for calculating the pressure drop in the shell side of shell-and-tube heat exchangers with segmental baffles and compared the results with available experimental data.

One of the most important parameters used in the design of shell-and-tube heat exchangers is the space between two adjacent baffles [7, 14]. Closer spacing causes higher heat transfer, but this leads to poor stream distribution and higher pressure drop. On the other hand, higher baffle spacing reduces the pressure drop, but this will lead to predominantly longitudinal flow, which decreases the heat transfer. As suggested by Taborek [14], the space between the baffles could vary between the minimum of 20% of shell diameter and a maximum equal to the shell diameter. Mukherjee [11] noted that the optimum baffle spacing normally ranges from 0.3 to 0.6 times the shell diameter.

The effect of baffle spacing on heat transfer area and pressure drop was well studied by Saffar-Avval and Damangir [13] and Khalifeh Soltan et al. [8]. They concluded that the baffle spacing has a decisive effect on pumping power and noticeable effect on required heat transfer area. Also, a guideline was developed to calculate the optimum baffle spacing for single phase shell-and-tube heat exchanger. The optimum ratio of baffle spacing to shell diameter was studied by Eryener [4]. He applied a method based on the thermoeconomic analysis and performed calculations for the ratios of baffle spacing to shell diameter in the range from 0.01 to 1.

Another important parameter for the design of shell-and-tube heat exchangers is the baffle cut, which can vary between 15% and 45% of the shell inside diameter. Several investigators have recommended and suggested to use baffle cuts of 20-35% [7, 11].

The heat transfer in shell-and-tube heat exchangers can be negatively affected by the baffle-shell leakage. Li and Kottke [9] experimentally investigated the effect of the leakage between baffles and shell on pressure drop and local heat transfer in a segmental baffled shell-and-tube heat exchanger. They found that in the Reynolds range from 500 to 16000, the baffle-shell leakage can greatly reduce the pressure drop (by 69-74%) and the per-compartment average heat transfer (by 17-21%).

Although, segmental baffles can improve and enhance the heat transfer in the shell-side of heat exchanger, they have many disadvantages as compared to helical baffles, rod baffles, disk-and-doughnut baffles [3, 10, 12, 14,16]. Li and Kottke [10] showed that the disc-and-doughnut baffles have a higher effectiveness of heat transfer to pressure drop than single-segmental baffles because of partly a lower percentage of baffle-shell leakage and a higher percentage of the main stream. However, disc-and-doughnut baffles have not achieved the same popularity in industry as segmental baffles, mainly because of manufacturing problems and the lack in the

literature of comparable data on heat transfer and pressure loss. Peng et al. [12] designed and tested two different shell-and-tube heat exchangers with continuous helical baffles. The results of their study indicate that the use of continuous helical baffles will result in nearly 10% increase in heat transfer coefficient compared with that of conventional segmental baffles for the same shell-side pressure drop. Recently, Wang et al. [16] have numerically investigated the performance of a combined multiple shell-pass shell-and-tube heat exchanger with continuous helical baffles and compared with a shell-and-tube heat exchanger with segmental baffles. The numerical results have shown that, under the same shell-side pressure drop, the overall heat transfer rate of the heat exchanger with continuous helical baffles is ~5.6% higher than that of conventional segmental baffles. Also, they found that, under the same mass flow rate and overall heat transfer rate, the average overall pressure drop is 13% lower for continuous helical baffles.

Although, heat exchangers with continuous helical baffles are superior to the heat exchangers with segmental baffles, disc-and-doughnut baffles or discontinuous helical baffles and a manufacture method of them has been proposed, they will remain under the shadow of the conventional shell-and-tube heat exchangers as long as the cost of construction will be higher and the manufacture will be more complicated in comparison to the conventional heat exchangers.

3. Numerical analysis

Numerical analysis has been carried out in order to study the effect of fluid properties on shell-side heat transfer and pressure drop and to compare the results with our previous work [1] in which the properties of the shell-side fluid were kept constant.

The real shell-and-tube heat exchanger investigated in [1] is a vertical stainless steel column (17.5 W/m K) with a shell inside diameter of 207 mm. The tube bundle contains 19 straight tubes with an effective heat exchange length of 690 mm. The tubes have an inner diameter of 21 mm and an outer diameter of 25 mm, and the tube pitch is 38 mm. This heat exchanger is an important device in our lab scale facility for biomass co-firing and flue gas cleaning [1, 2].

As mentioned earlier, baffles in the shell side of heat exchangers can significantly improve the heat transfer, but at the cost of high pressure drop. To maintain the pressure drop of the shell-side fluid within reasonable limits and higher ratio of heat transfer coefficient, a number of 8 segmental baffles would be necessary to use. Based on theoretical estimations, a baffle cut of 25% and space between two adjacent baffles of 75 mm will be considered in this study. The shell-side inlet and outlet nozzles have an inner diameter of 21 mm. It was shown that the pressure drop in the shell inlet and outlet cannot be neglected when the shell inlet and outlet diameters are small [1, 6].

The shell-side of heat exchanger is shown in figure 2.

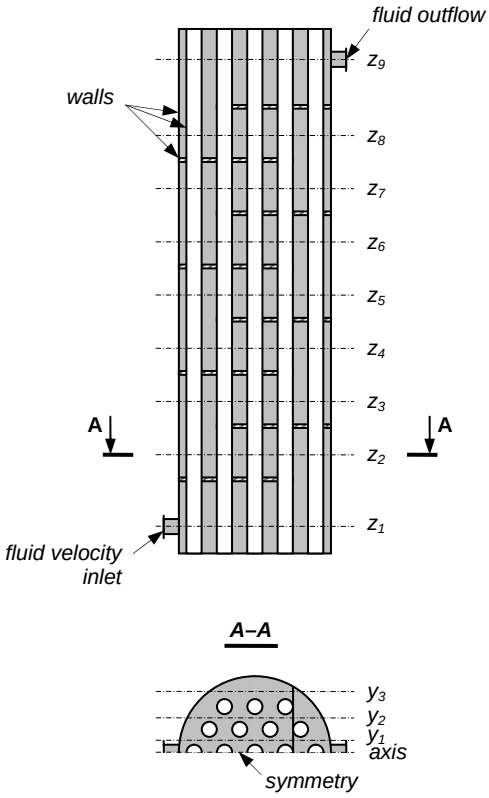

Figure 2 Section along the tube axis and half cross-section of the shell-side of heat exchanger

Due to the symmetry plane, only the half cross-section of the shell-side has been created. There are also indicated different planes along the *z*-axis and *y*-axis.

The computational domain has been meshed with the unstructured Tet/Hybrid grids, which are generated by GAMBIT 2.2. The numerical simulations have been performed using the commercial CFD software package FLUENT 6.2. Segregated solver and standard laminar model were employed and energy equation has been included. The pressure-velocity coupling is solved using the SIMPLE algorithm, and second order upwind scheme has been chosen to discretize momentum and energy equations.

The governing equations of continuity, momentum and energy are solved by a finite volume method.

Created model in GAMBIT was exported to FLUENT in which the following boundary conditions for the shell-side of heat exchanger were set up: the working fluid was selected from the software database as water liquid; the water inlet conditions were defined as velocity inlets, which correspond to the mass flow rates ranged from 5 to 25 kg/h, and temperature of 293 K; the temperature of 363 K was set for the tube wall, and the exterior wall was modeled as adiabatic.

The water properties are constant except for water density and viscosity, which are calculated as a function of temperature according to the following polynomial equations:

– for density,

$$\rho = 0.000019t^3 - 0.006512t^2 + \\ + 0.039t + 999.96 \quad (1)$$

– for dynamic viscosity,

$$\mu = 0.000027t^4 - 0.007751t^3 + \\ + 0.878t^2 - 51.95t + 1746.45 \quad (2)$$

4. Results and discussions

Figure 3 reflects the change of temperature field and temperature distribution in the shell side of heat exchanger at the maximum mass flow rate simulated of 24.61 kg/h.

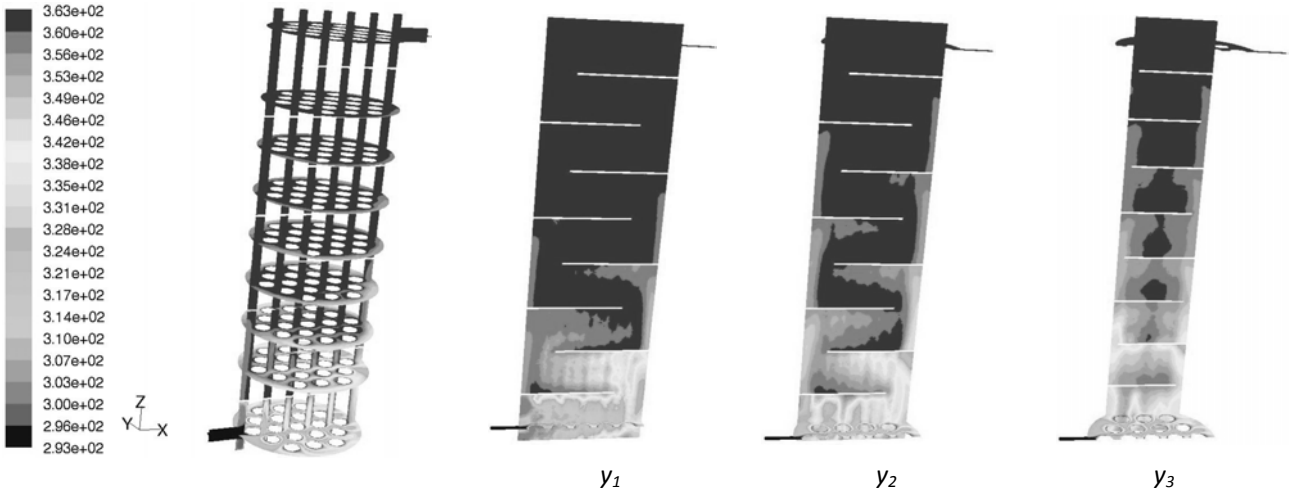

Figure 3 Shell-side temperature contour along *z*-axis at different *y*-planes (L_m = 24.61 kg/h, T_{in} = 293 K => T_{out} = 362.5 K)

The water inlet temperature of 293 K (i.e., 20°C) and the tube wall temperature of 363 K (i.e., 90°C) were set during simulations. Under these conditions, the outlet temperature of 362.5 K is achieved. Also, it can be observed from figure 3 that the temperature of fluid increases faster at $y = 0$, which corresponds to the symmetry boundary, and more slowly near the shell wall, at $y = 0.0825$ m.

Compared to the results from [1] the temperature increased too little, only by 0.4 K. However, the results have shown that the heat transfer can be easily improved by baffling the shell-side of heat exchanger. When the model of the heat exchanger without baffles was numerically investigated only the temperature of fluid in the core increased [1].

The average temperature distribution along the heat exchanger at different mass flow rates is shown in figure 4. As can be seen, the increase in the mass flow rate results in slow decrease of the temperature. The temperature profiles were almost similar to those from [1]. Moreover, the temperature profile in the heat exchanger with single segmental baffles are more uniform than that without the baffles.

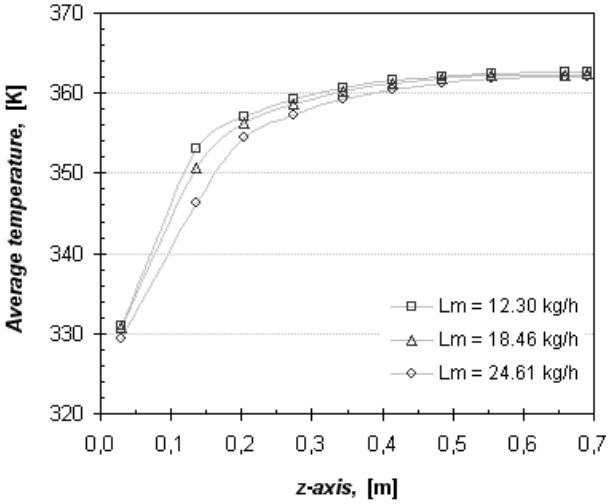

Figure 4 Average temperature distribution along *z*-axis

The pressure drop versus mass flow rate is shown in Figure 5. Pressure drop has slowly decreased as compared to [1]. This is mainly because of the viscosity change, which decreases from 1002×10^{-6} (at 20°C) to approximately 320×10^{-6} kg/m s (at 90°C). Thus, the viscosity has a significant impact on pressure drop.

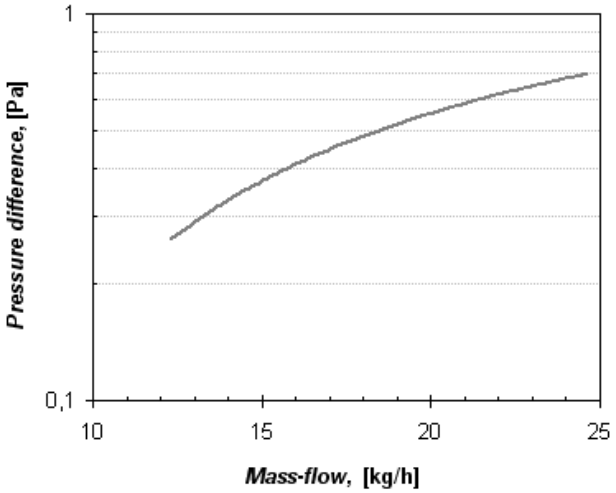

Figure 5 Shell-side pressure drop as a function of mass-flow rate

Previous results [1] have shown that the shell-side pressure drop increases rapidly with a decrease in diameter of the shell inlet and outlet nozzles. This is an important fact that cannot be neglected and should be taken into account when the shell-side pressure drop is calculated.

5. Conclusions

Heat transfer and pressure drop in the shell-side of a shell-and-tube heat exchanger with single segmental baffles has been numerically analyzed in this work. The shell-side of heat exchanger is baffled with 8 segmental baffles, baffle cut of 25%, baffle space of 75 mm and the shell-side inlet and outlet nozzles with inner diameters of 21 mm.

Numerical results have shown that the temperature increased, surprisingly, too little, only by 0.4 K as compared to our previous results. From this point, it could be concluded that the fluid properties has no major effect on the fluid outlet temperature. However, the heat transfer can be easily improved by baffling the shell-side of heat exchanger. When the shell-side of heat exchanger without baffles was numerically investigated only the temperature of fluid in the core increased and the fluid outlet temperature was lower than that in the baffled shell.

Pressure drop has slowly decreased as compared to our previous results. This is due to the viscosity decrease with temperature increase. The major finding of our numerical results is that the shell-side pressure drop increases rapidly with a decrease in diameter of the shell inlet and outlet nozzles. This is an important fact that cannot be neglected and should be taken into account when the shell-side pressure drop is calculated.

References

1. D. Cebrucean, V. Cebrucean, Numerical study of a shell-and-tube heat exchanger for heating rich monoethanolamine using hot flue gases. Part I: Shell side. Proceedings of the 3rd International Conference on Thermal Engines and Environmental Engineering, 2009, pp. 143-147, ISSN 978-960-6766-02-42
2. V. Cebrucean, Theoretical and numerical study of heat transfer and fluid flow in a shell-and-tube heat exchanger. MSc Thesis. Timisoara, Romania, 2009
3. D. A.. Donohue, Heat transfer and pressure drop in heat exchangers. Industrial and Engineering Chemistry, Vol. 41, No. 11, 1949, pp. 2499-2511, ISSN 1520-5045.
4. D. Eryener, Thermoeconomic optimization of baffle spacing for shell-and-tube heat exchangers. Energy Conversion and Management, Vol. 47, No. 11-12, 2006, pp. 1478-1489, ISSN 0196-8904.
5. Fluent User's Guide. Fluent Inc., 2003
6. E. S. Gaddis, V. Gnielinski, Pressure drop on the shell side of shell-and-tube heat exchangers with segmental baffles, Chemical Engineering and Processing, Vol. 36, No. 2, 1997, pp. 149-159, ISSN 0255-2701.
7. S. Kakac, H. Liu, Heat exchangers. Selection, rating and thermal design, 2nd Edition. CRC Press, 2002, ISBN 08493-09026.
8. B. Khalifeh Soltan, M. Saffar-Avval, E. Damangir, Minimizing capital and operating costs of shell-and-tube condensers using optimum baffle spacing, Applied Thermal Engineering, Vol. 24, No. 17-18, 2004, pp. 2801-2810, ISSN 1359-4311.
9. H. D. Li, V. Kottke, Effect of the leakage on pressure drop and local heat transfer in shell-and-tube heat exchangers for staggered tube arrangement, International Journal of Heat and Mass Transfer, Vol. 41, No. 2, 1998, pp. 425-433, ISSN 0017-9310.
10. H. D. Li, V. Kottke, Analysis of local shell-side heat and mass transfer in the shell-and-tube heat exchanger with disc-and-doughnut baffles, International Journal Heat and Mass

Transfer, Vol. 42, No. 18, 1999, pp. 3509–3521, ISSN 0017-9310.
11. R. Mukherjee, Effectively design shell-and-tube heat exchangers" Chemical Engineering Progress, Vol. 94, No. 2, 1998, pp. 21-27, ISSN 0360-7275.
12. B. Peng, Q.W. Wang, C. Zhang, G. N. Xie, L. Q. Luo, Q.Y. Chen, M. Zeng, An experimental study of shell-and-tube heat exchangers with continuous helical baffles, Journal of Heat Transfer, Vol. 129, No. 10, 2007, pp. 1425-1431, ISSN 0022-1481.
13. M. Saffar-Avval, E. Damangir, A general correlation for determining optimum baffle spacing for all types of shell and tube exchangers. International Journal of Heat and Mass Transfer, Vol. 38, No. 13, 1995, pp. 2501-2506, ISSN 0017-9310.
14. J. Taborek, Shell-and-tube heat exchangers: Single-phase flow. In: Heat exchanger design handbook, Section 3.3, Schlunder, E.U. et al., (eds.) Hemisphere, 1983, ISBN: 08911-61252.
15. T. Tinker, Shell side heat transfer characteristics of segmentally baffled shell-and-tube heat exchanger. In: Annual Meeting of the American Society of Mechanical Engineers, 1947.
16. Q. Wang, Q. Chen, G. Chen, M. Zeng, Numerical investigation on combined multiple shell-pass shell-and-tube heat exchanger with continuous helical baffles, International Journal of Heat and Mass Transfer, Vol. 52, No. 5-6, 2009, pp. 1214-1222, ISSN 0017-9310.

MODELAREA NUMERICĂ A PROCESULUI DE TRANSFER DE CĂLDURĂ ŞI DE CURGERE ÎN SPAȚIUL EXTRATUBULAR A UNUI SCHIMBĂTOR DE CĂLDURĂ CU FASCICUL DE ȚEVI ŞI MANTA

Rezumat

În lucrarea dată a fost studiată modelarea numerică a transferului de căldură şi pierderilor de presiune în spațiul extratubular al unui schimbător de căldură cu fascicul de țevi şi manta, cu şicane de tip segment. Obiectivul principal a fost compararea rezultatelor cu cele obținute anterior, în care proprietățile fluidului au fost definite drept constante.

Simularea numerică a fost efectuată cu ajutorul softului comercial CFD FLUENT-6.2.

Modelul studiat a conținut 8 şicane de tip segment cu partea decupată de 25% din diametrul interior al mantalei. Rezultatele numerice au arătat că pierderile de presiune au scăzut uşor şi proprietățile fluidului nu au nici un efect asupra transferului de căldură în comparație cu studiul efectuat anterior.

Scientific reviewers: **Ioan LAZA, "Politehnica" University of Timişoara, România**
Liviu MIHON, "Politehnica" University of Timişoara, România

SCIENTIFIC BULLETIN OF
THE „POLITEHNICA" UNIVERSITY OF TIMISOARA, ROMANIA
TRANSACTIONS ON MECHANICS
BULETINUL ŞTIINŢIFIC AL
UNIVERSITĂŢII „POLITEHNICA" DIN TIMIŞOARA, ROMÂNIA
SERIA MECANICĂ
Tom 54 (68) **ISSN 1224 - 6077** **Fasc. 4, 2009**

FINITE ELEMENT MODELLING FOR CMT JOINING DISSIMILAR MATERIALS GALVANIZED STEEL-ALUMINIUM

Mihai HLUŞCU
Mechanical Engineering Faculty, Bv. Mihai Viteazu No. 1, 300222 Timişoara, Romania
e-mail: mihai.hluscu@mec.upt.ro

Abstract. Cold Metal Transfer (CMT) is an important procedure it is recommended to join plates for join plates for galvanized steel-aluminium alloy. Distributions of different components of stresses, movements, as the distorted of the model are presented. The scope is to develop the joining technology obtained and to use it in automotive industry with real economic and qualitative effects.

Keywords: CMT, finite element modelling, mechanical testing

1. Introduction

The combination of different materials is a permanence problem because its implications. In order to create appropriate technologies of conjunction, there have been developed complex and experimental programmes with interdisciplinary participation.

2. Mechanical testing on joined probes

In order to check the joining technology of the galvanized steel with aluminum, using the CMT process mechanical testing were made on 4 probes; probes 1-3 were made manually, and probe 6 was mechanized made using the parameters in table 1.

For aluminum-galvanized steel joints (probes 1, 2, 3 and 6) the following conclusions can be mentioned:

For probes 1, 2, 6 resistance mechanical characteristics (F_{max} and R_m fracture resistance) have high values F_{max}=3,26KN and $R_{m,med}$=82,24Mpa, respectively.

This indicates a corresponding joining; but for probe 3 - samples were joined using the same resistance mechanical characteristics – the joining was not a corresponding one. The resistance mechanical characteristics used were F_{max}=2,35KN and R_m=58,95Mpa, respectively values which were 28% smaller than for probes 1, 2 and 6.

3. Finite element modelling of welded joints

In order to generate the geometric model the following have been defined:

- 4 points with the PIT command
- 2 points with the PTGEN command
- 1 surface with the SF2CR command
- 1 volume with the VLEXTR command
- 1 volume with VLGEN command (translation copying)
- 1 volume with VLCRSF command (that defines the weld)

Totally the model is described by 18 points, 32 curves, 17 surfaces and 3 volumes.
The types of used elements are:

SOLID with 8 nodes for the base material

TETRA 4 with 4 nodes for welding

Table 1 Mechanical testing aluminium – galvanized steel joining

Probe no.	Test no.	Welding size		F_{max} [KN]	$F_{max,med}$ [KN]	R_m [MPa]	$R_{m,med}$ [MPa]
		l [mm]	H [mm]				
1	1	20	2	3,08	3.16	77	79.10
	2	20	2	4,24		106	
	3	20	2	1,92		48	
	4	20	2	2,79		69,75	
	5	20	2	1,85		46,25	
	6	20	2	3,28		82	
	7	20	2	4,99		124,75	
2	1	20	2	1,86	3.05	46,5	76.25
	2	20	2	0,63		15,75	
	3	20	2	0,59		14,75	
	4	20	2	0,5		12,5	
	5	20	2	3,47		86,75	
	6	20	2	3,5		87,5	
	7	20	2	3,37		84,25	
3	1	20	2	2,23	2.35	55,75	58.95
	2	20	2	1,92		48	
	3	20	2	1,5		12,5	
	4	20	2	2,19		54,75	
	5	20	2	2,94		73,5	
	6	20	2	2,51		62,75	
6*	1	18,6	2	3,37	3.58	90,59	91.36
	2	20	2	3,91		97,95	
	3	19,5	2	3,7		94,87	
	4	21,2	2	3,5		82,93	
	5	19	2	3,44		90,52	

*mechanised

Material properties:

- Zinc plates sheet: EX-2,1x10^5MPa, μ=0,3 Poisson's coefficient
- AlMg plate : EX= 7x10^4MPa; μ=0,24 Poisson's coefficient
- AlMg3 filler material: EX= 7x10^4MPa; μ=0,24 Poisson's coefficient

The division of the 3 volumes was successively realized starting with the zinc plated sheet, after defining the specific material properties for each component part of the joint.

The zinc plated sheet is described by 9600 volume elements „solid" with 8 nodes.

For the AlMg plate other 9600 elements have been used (from 9600 up to 19200), SOLID elements having EX= $7 \cdot 10^4$ MPa and μ=0.24.

The welding, geometrically described by the volume „3" was divided in 1800 solid elements of the type TETRA 4.

In order to achieve a closer division to the real model the number of elements and sizes of each element have been selected so that the linking of nodes is done only in the weld area. This has been accomplished by selecting the above mentioned nodes with the following commands:

-INITSEL, ND, 1, 1

SELINP, ND, 19353, 20008,1,1

SELINP, ND, 26569, 27224,1,1

NMERGE,1, 500000, 1, 0.00001,0,0,0

Totally 574 nodes have been linked; the total number of nodes has been reduced with 287 after the NCOMPRES command.

The total number of nodes is: 26773

In order to perform the tensile testing imposed to the null movement on all directions on the curve 17 that limits the inferior part of the AlMg plate, edge on the same face with the weld, the command DCR,17,Al,0,17,1 has been used. Forces have been applied on the nodes situated on the superior edge of the zinc plated sheet; this edge is situated in the same vertical plan with that having the imposed null movements command: FCR, 8, FY, 20, 8, 1.

The value of the force applied on all the 41 nodes is 20 N, there results a total of 820 N.

The imposed loading and movements are represented in figure 1.

Once the model is realized the necessary options are specified in order to achieve the static analyses using the commands:

- A_STRESS, 1,-1, 1, 1, 1, 0, 0, 0, 1, 1

STRESS,1, and the static analyses has been made with the command R_STATIC

After performing the analyses the program furnished the results required by the command A_STRESS in a file with the extension *.out.

Distribution of different components of stresses, movements, as well as the distorted of the model are presented with the value indicated in figures 1, 2, 3, 4, 5, 6, 7:

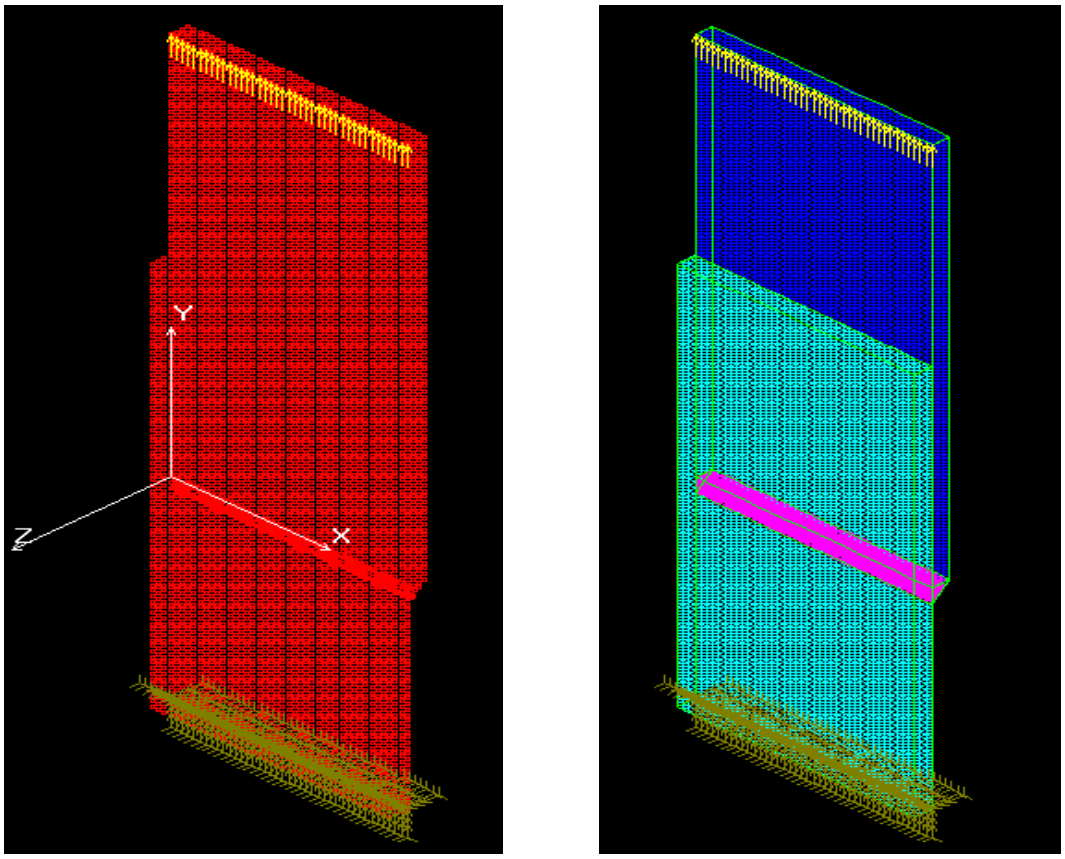

a) b)

Figure.1 Discredited model scheme:
a) nodes of the model b) elements of the model

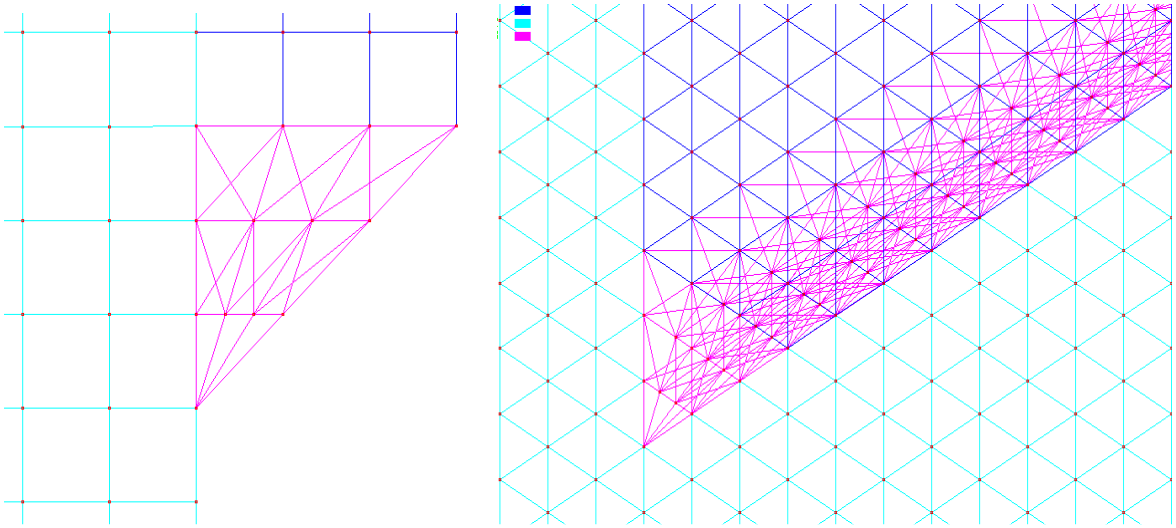

Figure.2 Details regarding the discreditation of the joint
a) front plan view b) space view

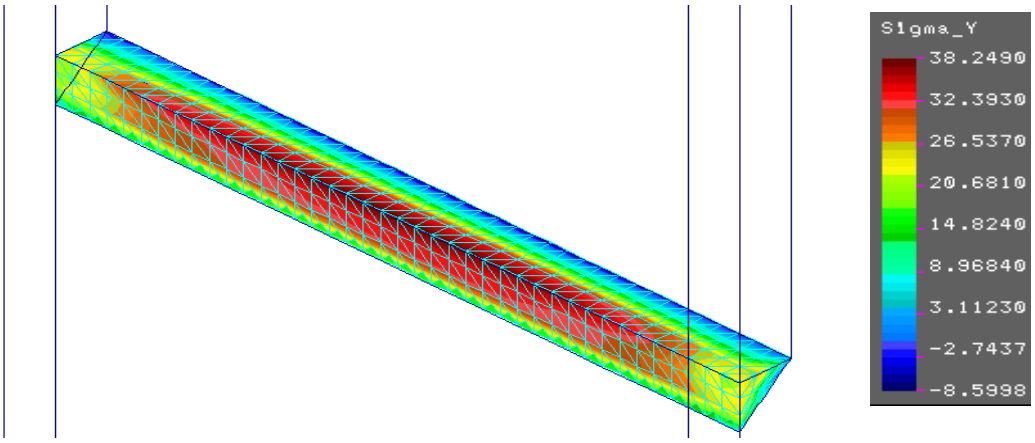

Figure3 Normal stresses distribution on the force direction in the joint

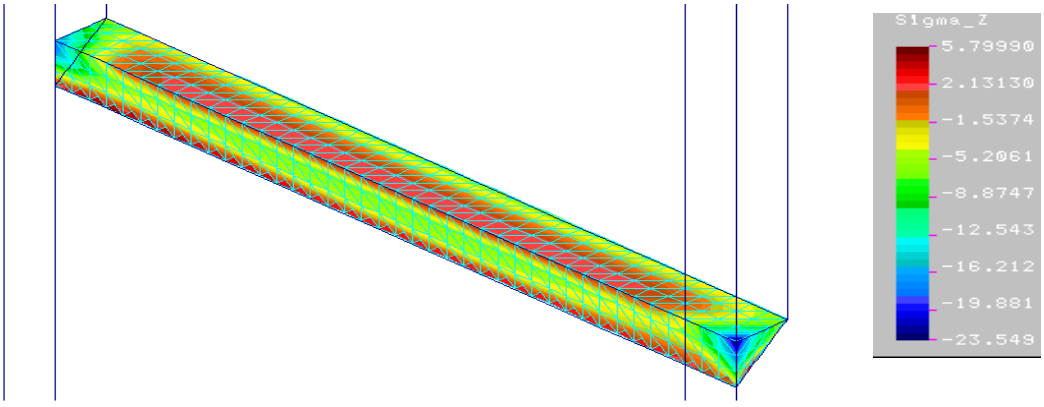

Figure 4 Normal stresses distribution on the perpendicular direction on the force direction in the joint

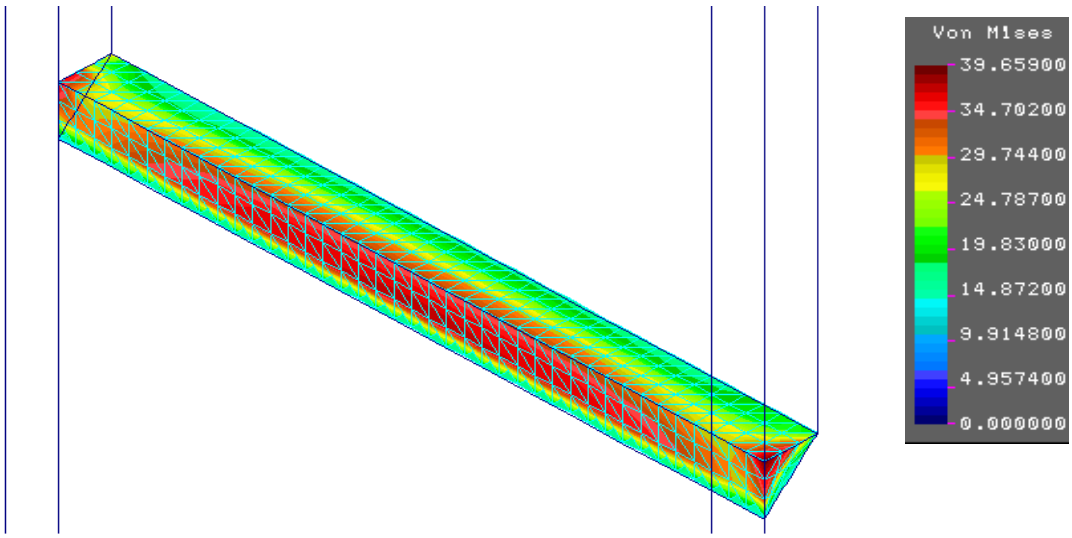

Figure5 Equivalent stresses distribution according to the fifth theory in the joint

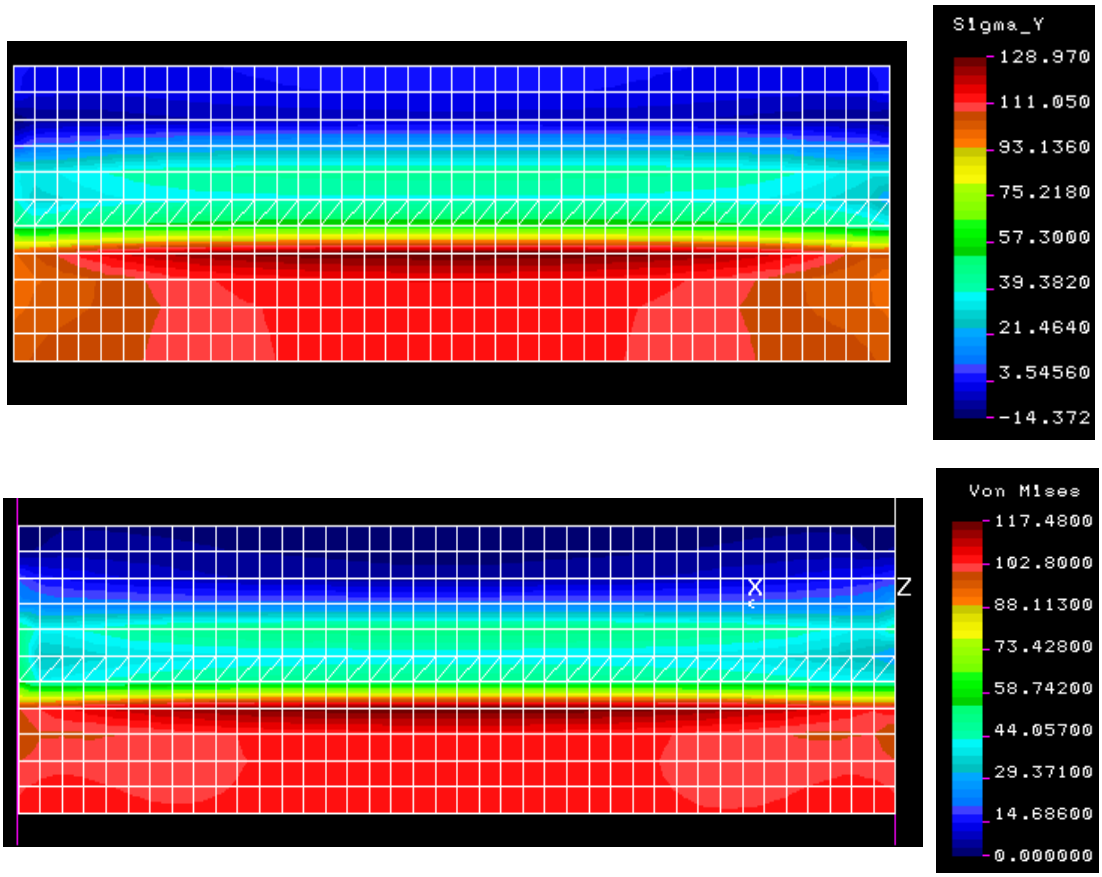

Figure 6 Normal stresses distribution, σ_y, and of the equivalent ones, $\sigma_{ech(5)}$, in the joint

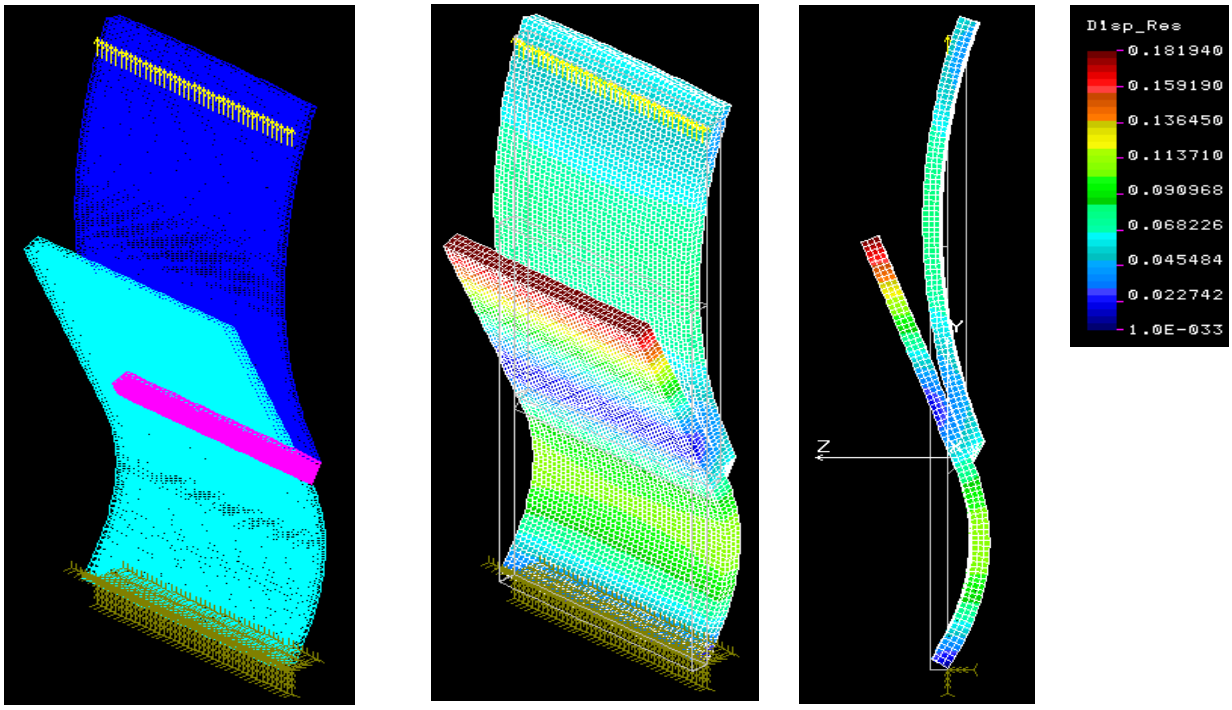

Figure 7 Model deformation and distribution of movements on the force direction

4 Conclusions

4.1 CMT is an important procedure at present, patented by the firm Fronius, it is recommended to join plates for galvanized steel – galvanized steel and dissimilar joints galvanized steel – aluminium alloy [12].

4.2 It insists on realizing dissimilar aluminium alloy – galvanized steel indicating the parameters

4.3 The experimental developed modelling confirms the results of the program.

References

1. B. Bouai , Low heat process enchance jointing of coated sheet metals, Welding Journal, 2003, 82(1), pp. 26-31 , ISSN 0043-2296
2. J. Bruckner, Cold metal transfer has a future joining steel to aluminium, WELDING JOURNAL, 2005, vol. 84, nr. 6, pp. 38-40, ISSN 0043-2296
3. Y. C. Chen, Role of zinc coat in friction stir lap welding Al and zinc coated steel, MATERIALS SCIENCE AND TECHNOLOGY, 2008, vol. 24, nr.1, pp. 33-39, ISSN 0267-0836
4. S. B. Lin, C.L. Fan, J.L. Song, C.L Yang, Research on CMT welding of nickel-based alloy with stainless steel, CHINA WELDING, 2007, vol. 16, nr.3, pp. 23-26, ISSN 1004-5341
5. W. Lutz, Hot exhaust component perfectly „cold'' welded with a robot, PRAKTIKER, 2007, vol. 59, nr. 5, pp. 162-164, ISSN 0554-9965
6. J. Matusiak, J., Low heat input MIG/MAG welding and braze welding methods designed for joining of heat sensitive materials and elements, BIULETYN INSTYTUTU SPAWALNICTWA, 2007, vol. 51, nr. 6, pp. 41-46, ISSN 0867-583X
7. M. Popescu, A. Magda, C. Codrean, C. Locovei, E. Moga-Modrea, Problems when performing dissimilar joints galvanized steel-aluminium alloy using the CMT process, Scientific Bulletin of the POLITEHNICA University of Timişoara, Transactions on Mechanics, tom 54(68), fasc 1, 2009, ISSN 1224-6077
8. L. Quintino, G. Pimenta, D. Iordachescu, R. M. Miranda, N. V Pepe, MIG Brazing of galvanized thin sheet joints for automotive industry, Material and Manufacturing Processes, 2006,vol. 21, issue 1, pp. 63-73, ISSN 0361-8773
9. H. M. Staubach , Joining of steel-aluminium mixed joints with energy reduced GMA processes and filler materials on an aluminium and zinc basis, WELDING AND CUTTING, 2008, vol. 7, nr. 1, pp. 30-34, ISSN 0036-7184
10. R. G Trommer, From the experience of a waged welder – spatter – free welding and brazing with the CMT process, PRAKTIKER, 2005, vol. 57, nr. 9, pp. 250, 252-254, ISSN 0554-9965
11. J. Wilden, J.P Bergmann, Low temperature brazing of zinc coated steel and steel/aluminium joints by setting ZnAl – alloys as brazing material, BRAZING AND SOLDERING, PROCEEDINGS, 2006, apr, pp. 32-39, ISBN 0-87170-838-8
12. X. R. Yang, Welding of thin sheet metals by MIG/MAG process with CMT, Welding Technology in Energy Engineering, IFWT 2005, Proceedings, 2005, 21-23 sep, pp. 2008-2012, ISBN 7-1111-7383-X

MODELAREA CU ELEMENT FINIT PENTRU IMBINARILE CU DISIMILARE DIN MATERIALE DISIMILARE OTEL GALVANIZAT-ALUMINIU REALIZATE CU PROCEDEUL CMT

Rezumat

CMT este un procedeu de mare actualitate, cu aplicabilitate la realizarea de îmbinări cu disimilare ale tablelor din oțel galvanizat şi aliaje de aluminiu.

Sunt prezentate distribuțiile diferitelor componente ale tensiunilor, deplasărilor, precum şi deformațiilor modelului.

Scopul dezvoltării acestei tehnici de îmbinare este utilizarea ei în industria constructoare de autovehicule, cu reale efecte economice şi calitative.

Scientific reviewers: **Liviu BERETEU, "Politehnica" University of Timişoara, România**
Ion DUMITRU, "Politehnica" University of Timişoara, România

SCIENTIFIC BULLETIN OF
THE „POLITEHNICA" UNIVERSITY OF TIMISOARA, ROMANIA
TRANSACTIONS ON MECHANICS
BULETINUL ŞTIINŢIFIC AL
UNIVERSITĂŢII „POLITEHNICA" DIN TIMIŞOARA, ROMÂNIA
SERIA MECANICĂ
Tom 54 (68) **ISSN 1224 - 6077** **Fasc. 4, 2009**

RELEVANT ASPECTS OF THE REAL TIME MONITORING FOR AIR POLLUTION USING A LIDAR SYSTEM IN TIMISOARA EPISODE

Nisulescu Gheorghe Catalin*, Popescu Francisc*
* Faculty of Mechanical Engineering, Bv. Mihai Viteazu No 1, 300222 Timişoara, Romania, cnisulescu@mec.upt.ro, ingfrancisc@imx.net

Abstract. The paperwork presents the advantage of using Lidar systems for studying of air pollution. Taking in consideration that the LIDAR system offers possibility to get results in real time, developing of a air monitoring program for different episodes in real time which will offer processing data results is a good way for process improvement.

Keywords: air pollution, Lidar, real time

1. Introduction

In Timişoara area, high concentrations of gases and particles from coal combustion and motor vehicles have produced severe loss of air quality and significant health effects. On a regional scale, troposphere ozone formation and acid deposition have been the major threats. Emissions of carbon dioxide and other radioactively active gases together with stratospheric ozone depletion represent planet-scale assaults on the quality of our atmospheric environment.

Remote sensing systems are now often used for detection of airborne pollutants. These systems deliver information about the concentrations in a certain region which is covered from a light beam between emitter and receiver. This results in an average value which represents mostly better the pollution level in a particular area then a point measurement.

2. LIDAR technique

Optical remote sensing techniques are used today for monitoring atmospheric characteristics due to the fact that, conform to the diffraction theory, an obstacle could be "seen" by an electromagnetic wave having a wavelength on the same magnitude as the geometric dimension of the obstacle. So, using a light beam (wavelength nm, μm) one can detect atmospheric components, which are "invisible" for other sounding waves.

The speed of light is also a good argument, because it provides real time response. Another aspect is that a lot of phenomena are produced at the interaction between a light beam and atmospheric constituents, most of these phenomena are specific to the constituent's type.

Very important among optical remote sensing techniques are the Lidars based on the use of pulse or continuous lasers as they are characterized by high sensitivity and a long range of penetration. **LIDAR** (**LI**ght **D**etection **A**nd **R**anging) are laser based systems for atmosphere sounding, which allow suspended particulate

detection along the sounding direction, with a very good precision and in a very short time (seconds). After the development of new lasers and photo detectors in the following years, various types of ground-based Lidar systems (including ceilometers) have been continuously used to probe the earth's atmosphere and to detect a variety of air pollutants, such as O_3, NOx, SO_2, Hg, toluene, benzene and measure aerosol optical properties (optical depth, spatial distribution and layering, diurnal variation, etc.)

2.1 Principle and operation

LIght Detection And Ranging (LIDAR) makes use of a laser to excite backscattering in the atmosphere. This backscattered signal is observed using a telescope receiver, which collects the light and send it to the receiver optics (figure 1).

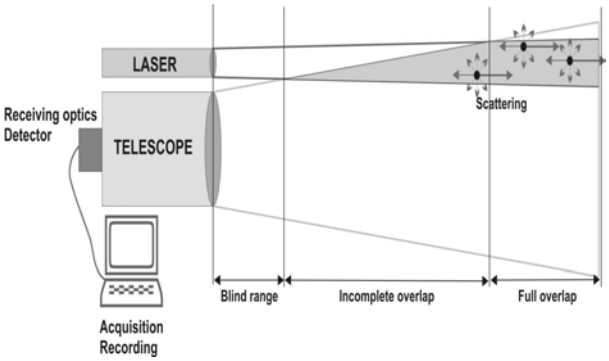

Figure 1 Basic principle of LIDAR system

The role of the optical chain is to select specific wavelengths, split between them and direct them to photo detectors, which convert the optical signal into electrical signals. These electrical signals are recorded as a function of time by analog-to-digital converters and/or photon counting devices and the results are stored onto a computer.

2.2 LIDAR specifications

LIDAR components (figure 2) characteristics are presented below:

Laser:
Laser type: Nd: YAG solid state,
Wavelengths: 1064, 532, 355 nm;
Energy per Pulse: 200 mJ at 1064 nm, 100 mJ at 532 nm, 35 mJ at 355 nm;
Pulse duration: 6-9 ns;
Spectral line bandwidth of laser: 1 cm^{-1};
Laser characteristics: Laser system with power supply and air – water cooling system in closed circuit;
Repetition rate: 1 – 30 Hz;
Laser beam diameter: 6 mm;
Laser beam divergence: < 0.75 mrad;

Telescope characteristics:
Optical design: Cassegrain reflector;
Mirrors with magnesium fluoride over coat and with maximum reflectivity's in spectral range 266 -1064 nm;
Diameter of principal mirror: 30 - 40 cm;
Focal length: 1500-3000 mm;
Focal Ratio (F/D): f/3-f/10;
Focal Length: 26- 40 mm**)**

Photo detectors:
Wavelength range: 270– 650 nm;
Peak Sensitivity at 630 nm;
Photomultiplier tube extended read multialkali, (for Lidar application) ;
Radiant cathode Sensitivity: > 65 mA/W;
Gain: ~ 4E+6) **;**
Width single photon pulse < 2 ns;
Operational conditions: -30°C … + 50°C;

Figure 2 LIDAR equipment

2.3 Goal of LIDAR system

The goal is to gain better understanding of atmospheric and climatologically processes.

Planetary boundary layer height, base and height of clouds, global wind profiles and altitude where aerosol intrusion appears in free troposphere can be observed using LIDAR system.

In figure 3 is presented a sample for a range corrected signal (RCS).

Air monitoring web application offers multiple possibilities like connection through specific IP, discovering file with LIDAR data, copying data into specific location (back-up), searching using different filters, showing specific

RCS, monitoring different location in the same time.

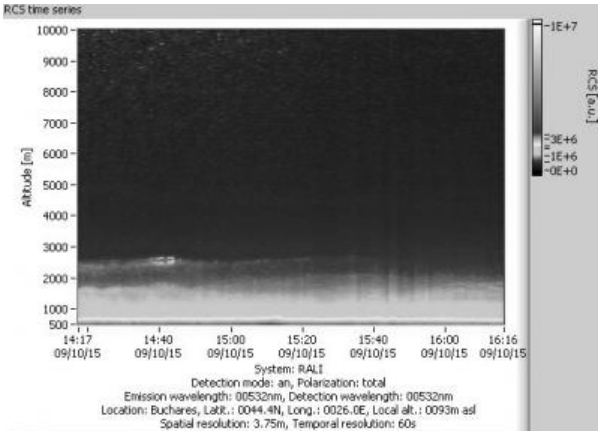

Figure 3 RCS sample

3. Air monitoring application

Air monitoring system works automatically, based on set policies, without user intervention (figure 4). Using a web browser you can access the system through air monitoring web application interface. Statistical information will be presented in home page and also information useful for user like system messages, status of transfer, storage size. Administrator can set policies accordingly with him consideration.

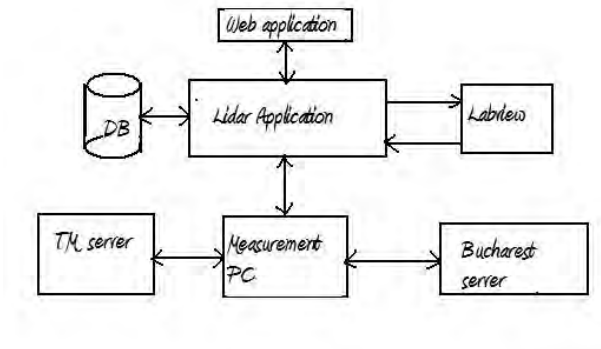

Figure 4 Application schema

User can perform using different filter options searching for specific files or monitoring locations. Application performs automatically content processing. LIDAR data are processed and a RCS is displayed. User can see the resulted RCS from different period or location. User can transfer raw data as well as processed data from the measurement station until the central server. This transfer can be made manual or automated.

4. Conclusion

Air monitoring application allows managing the transfer of content from measurement station to a temporary server, processing of data and the sending of the information to a central server. All the data obtained will be used to get advanced control systems for continuous, real-time monitoring of the atmosphere in polluted urban regions.

We have to find the way to reduce all pollutants in Timisoara area and that the measurement has to be permanent and extend in other areas of the city.

The air monitoring with the LIDAR system allows identification of the aerosol vertical distribution and will add a major contribution to the EARLINET network

As cities continue to grow in size and in their share of the growing global population and economic wealth, their environmental impacts will of necessity continue to be a central theme in the move towards global sustainability. Urbanization brings with it many transformations of nature including pollution. Every city will have a crucial role to play in the minimization of activities contributing to ozone depletion and global warming. The environmental sustainability of cities requires looking both outward and inward in managing the processes of change. The CO, O_3, SO_2, NO, NO_2, CH_4, total and non methane hydrocarbons concentration data sets were investigated from two types of air quality monitoring stations (urban traffic and rural background) in Timisoara.

5. Acknowledgement

I want to acknowledge for contract POSDRU/6/1.5/S/13 of “Politehnica” University of Timisoara and Norway Grants for RADO contract STVES 115266 for opportunity of participating in these programs.

References

1. S. Kshudiram, The Earth’s Atmosphere Its Physics and Dynamics, USA, 2008, ISBN 978-3-540-78426-5
2. M. V. Micea, Design and Implementation of Real-Time Systems for Critical Applications of Digital Signal Acquisition and Processing", PhD Thesis, Department of Computer Science & Engineering, "Politehnica" University of Timisoara, Romania, 2004.
3. J. H. Seinfeld, S. N. Pandis, Atmospheric chemistry and physics from air pollution to climate change, 2nd edition, Published by John Wiley & Sons, Inc., Hoboken, New Jersey, USA, 2006, ISBN 978-0-471-72018-8

4. P. Sturm, Emission Measurements & Air Quality Monitoring, Graz, 1999, ISSN 1453-7394
5. S. Ştefan, Doina Nicolae, Mihaela Caian, Secretele aerosolului atmosferic in lumina laserilor , Ed. Ars Docendi, Bucureşti, 2008, ISBN 978-973-558-357-6
6. C. Weitkamp, Lidar Range – Resolved Optical Remote Sensing of the Atmosphere, 2005, ISBN 0-387-40075-3

ASPECTE RELEVANTE ALE MONITORIZARII IN TIMP REAL A POLUARII AERULUI FOLOSIND SISTEME LIDAR IN EPISODUL TIMIŞOARA

Rezumat

Lucrarea prezintă avantajul utilizării sitemelor Lidar pentru studiul poluării aerului. Luând în considerare că sistemul Lidar oferă posibilitatea să obținem rezultate în timp real, dezvoltarea unui program informatic de monitorizare a aerului pentru diferite episoade de lucru va oferi rezultatele datelor procesate, este o bună cale pentru îmbunătățirea sistemului.

Scientific reviewers: **Ioana IONEL, "Politehnica" University of Timişoara, Romania**
Winfred Maria RUSS, Technical University of Munchen, Germany

SCIENTIFIC BULLETIN OF
THE „POLITEHNICA" UNIVERSITY OF TIMISOARA, ROMANIA
TRANSACTIONS ON MECHANICS
BULETINUL ŞTIINŢIFIC AL
UNIVERSITĂŢII „POLITEHNICA" DIN TIMIŞOARA, ROMÂNIA
SERIA MECANICĂ
Tom 54 (68) **ISSN 1224 - 6077** **Fasc. 4, 2009**

EFFICIENCY OF FIRST GENERATION PHOTOVOLTAIC PANELS

Delia CĂLINOIU*, Ioana IONEL*
Mechanical Engineering Faculty, Bv.Mihai Viteazu, No. 1, Ro-30022, Timişoara, România
e-mail: delia.calinoiu@mec.upt.ro , ioana.ionel@mec.upt.ro

Abstract. Photovoltaic is one of the fastest growing industries at present. Over the last five years, the production of photovoltaic solar cells has steadily increased at an annual average from 40 %, driven not only by the progress in materials and processing technology, but by market introduction programs in countries around the world. This growth is mainly being attained by an increase in manufacturing capacities based on the technology of crystalline, single junction devices. Consistent with the time needed for any major change in energy infrastructure, another 20 - 30 years of sustained and aggressive growth will be required for photovoltaic to substitute a significant share of conventional energy sources. This paper presents experimental results regarding photovoltaic panel's effectiveness and assessments about the capability of a 180 W independent photovoltaic system to supply consumers.

Keywords: Solar cell, Photovoltaic panel, Independent photovoltaic system.

1. Introduction

The current levels of dependence on fossil fuels, the need of reducing the carbon emissions associated with energy use and the prospects of developing a new and extremely innovative technology sector, make photovoltaic increasingly attractive. However, the high production cost of electricity, due to the significant capital investment cost, is the main barrier to large - scale deployment of photovoltaic systems [1-4].

Competition is increasing. New technologies are being developed. Solar photovoltaic systems today are more than 60 % cheaper than they were in the 1990's.

However, different solar cell technologies have grown at different rates and over 85 % of the current production is based on silicon wafer or silicon ribbon technology. This is a well - established technology, which achieves sufficient efficiency for at least 20 years of lifetime and constitutes a low - risk investment with high demands for return on investments [5-8].

2. Photovoltaic market development

Photovoltaic has enjoyed extraordinary growth during the last few years with overall growth rates between 50 % and 60 % making further increase of production facilities an attractive investment. Figure 1 demonstrates the current growth. The White Paper target, already exceeded in 2006, has been more than tripled in 2008, marking the success of the European sector. In 2010 the total cumulative capacity installed in the European Union could be as much as 16000 MW. The European photovoltaic industry currently has an important role in photovoltaic technology development, capturing about 30 % of the world market of photovoltaic modules.

Photovoltaic is the field of technology and research related to the devices which directly

convert sunlight into electricity. The solar cell is the elementary building block of the photovoltaic technology. Solar cells are made of semiconductor materials, such as silicon. One of the properties of semiconductors that makes them most useful is that their conductivity may easily be modified by introducing impurities into their crystal lattice.

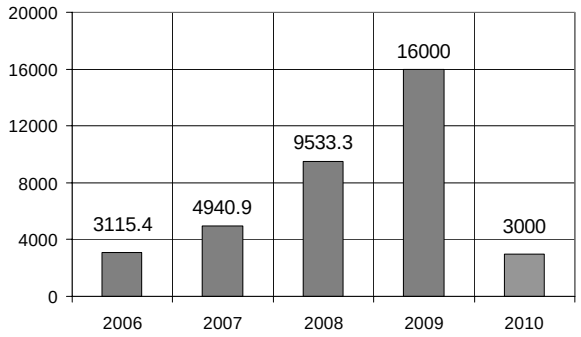

Figure 1. Comparison of the recent photovoltaic growth (in MW) in the EU with the White Paper objectives [EurObserv' ER, 2009]

There are several types of solar cells. However, more than 90 % of the solar cells currently made worldwide consist of wafer- based silicon cells. They are either cut from a single crystal rod or from a block composed of many crystals and are correspondingly called mono-crystalline or multi-crystalline silicon solar cells. Wafer-based silicon solar cells are approximately 200 μm thick. Another important family of solar cells is based on thin-films, which are approximately 1-2 μm thick and therefore require significantly less active, semi-conducting material. Thin-film solar cells can be manufactured at lower cost in large production quantities; hence their market share will likely increase in the future. However, they indicate lower efficiencies than wafer-based silicon solar cells, which means than more exposure surface and material for the installation is required for a similar performance.

3. Photovoltaic technology

Photovoltaic cell is an electronic device similar with a diode. As primary material for manufacturing a semiconductor is used, often crystalline or polycrystalline silicon on the surface which is formed by various technological methods layer containing impurities to obtain the p - n junction. Figure 2 presents a simplified design scheme for a PV cell.

For instance, in the fabrication of a photovoltaic solar cell, silicon, which has four valence electrons, is treated to increase its conductivity. Because the p - type silicon is in intimate contact with the n - type silicon a p - n junction is established and a diffusion of electrons occurs from the region of high electron concentration (the n - type side) into the region of low electron concentration (p - type side). When the electrons diffuse across the p - n junction, they recombine with holes on the p - type side. However, the diffusion of carriers does not occur indefinitely, because the imbalance of charge immediately on either sides of the junction originates an electric field. This electric field forms a diode that promotes current to flow in only one direction. Ohmic metal - semiconductor contacts are made to both the n - type and p - type sides of the solar cell, and the electrodes are ready to be connected to an external load.

When photons of light fall on the cell, they transfer their energy to the charge carriers. The electric field across the junction separates photo-generated positive charge carriers (holes) from their negative counterpart (electrons). In this way an electrical current is extracted once the circuit is closed on an external load.

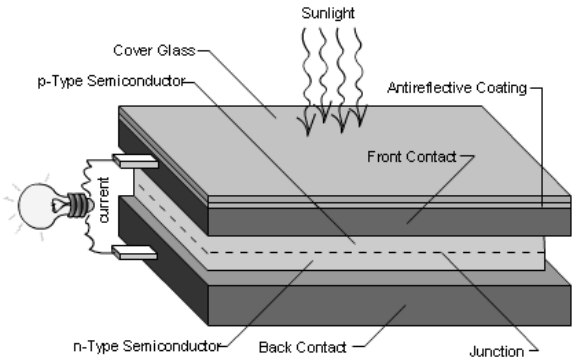

Figure 2. Solar cell [***www.energy.ca.gov]

A number of solar cells electrically connected to each other and mounted in a single support structure or frame is called a "photovoltaic module".

Modules are designed to supply electricity at a certain voltage, such as a common 12 volt system. The current produced is directly dependent on the intensity of light reaching the module.

Several modules can be wired together to form an array. Photovoltaic modules and arrays produce direct - current electricity. They can be connected in both series and parallel electrical arrangements to produce any required voltage and current combination. There are two main types of photovoltaic system figure 3.

Grind - connected systems (on - grid systems) are connected to the grid and inject the electricity into the grid. For this reason, the direct

current produced by the solar modules is converted into a grid - compatible alternating current. However, solar power plants can also be operated without the grid and are then called autonomous systems (off - grid systems).

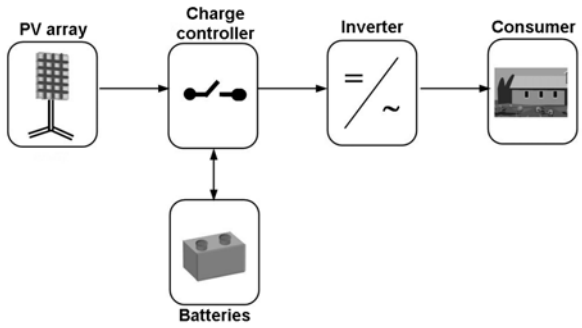

Figure 3. The principle design of a photovoltaic system with alternating current output [Fraunhofer ISE, Freiburg, Germany]

More than 90 % of photovoltaic systems worldwide are currently implemented as grid-connected systems. The power conditioning unit also monitors the functioning of the system and the grid and switches off the system in case of faults.

4. Experimental results

In photovoltaic generator design must take into account the maximum temperature of the solar cells such as to provide the necessary power. Obviously this situation it's meet in the summer days when the temperature of solar cells often exceed 60 °C.

This behavior of solar cells in relation to temperature is a drawback, since the mid-day when solar radiation is maximum conversion efficiency is minimal.

To prevent battery overcharging or complete discharging a loading controller it's used, mounted between the photovoltaic generator and battery. A load regulator usually contains a protection diode for discharge, which prevents battery discharge at night by the photovoltaic generator.

Photovoltaic modules consist in 36 crystalline solar cells; model IS75P with anti - reflection layer. The size of one panel is 125 x 125 mm and provide a power of 75 W at 16.6 V respectively 90 W at 17.6 V.

Thanks to New Ultratron technology developed by Istar Solar the modules have a higher output power. This allows the operation of the cell even at low intensity of the sun. The irradiance was measured with the pyranometer located on the co - planar plane with modules.

The characteristics of photovoltaic modules that were used in the experiment are given in the table 1.

Table 1 The characteristics of **IS75P** photovoltaic module

Characteristics	Value
Peak power	75 W
Voltage rating	12 V
Amperage at peak power	4.5 A
Flask current	4.8 A
Open circuit voltage	21V
Voltage at peak power	16.6V
Temperature rating	46 (±2) °C
Maximum voltage	715
Operation temperature	–40… + 90 °C
Dimensions (L x W x H) mm	1190 x 550 x 35 mm
Weight	9.3 kg

The table 2 shows a sample of measured data. The significance of measures are the following: solar radiation measured on the surface of both photovoltaic modules, the current that is given by the photovoltaic modules, the voltage of modules terminals, the power provided by modules, temperature, humidity and environment pressure in which measurements was made.

Table 2. Sample of measured data for **IS75P** PV

Nr.	G [W/m^2]	I [A]	U [V]	P_{out} [W]	t [°C]
1	35	0.24	25.8	6.19	23
2	51	0.34	25.6	8.7	24.5
3	106	0.37	25.7	9.5	25.3
4	130	0.40	25.7	10.28	27.1
5	315	0.65	25.8	16.7	28.4
6	580	2.11	26.2	55.28	27.4
7	762	3.51	26.6	93.36	27.2
8	757	3.60	26.9	96.84	26.6
9	715	3.32	26.9	89.3	26.6
10	448	2.51	26.8	67.26	26.4
11	119	2.50	26.5	66.25	26.5
12	114	2.48	26.3	65.22	26.9
13	115	1.73	26.1	45.15	26.9
14	515	1.94	26.1	50.63	27.4
15	331	1.30	25.9	33.67	27.4
16	210	1.46	25.9	37.81	27
17	292	1.59	25.9	41.18	27.3
18	155	1.97	25.9	51.02	27.6
19	180	1.6	26.1	41.76	28.3
20	175	1.58	26	41.08	27.9

Measurements were made during one week, the average values of irradiance according to time being presented in figure 4.

Variation of voltage and amperage were recorded to the solar panel terminal. These

variations according to time are presented in figure 5.

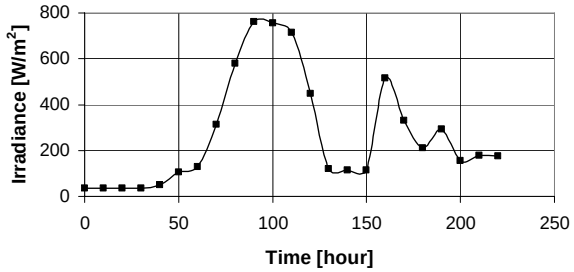

Figure 4. Variation of irradiance according to time during measurement

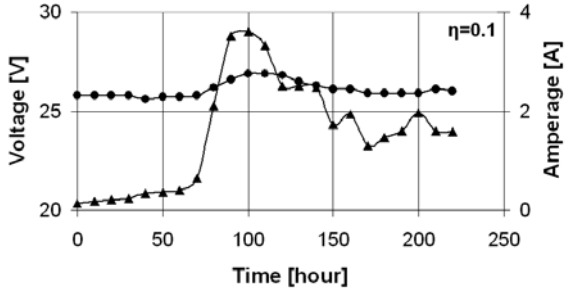

Figure 5. Variation of voltage and amperage according to time at solar panel terminal

5. Conclusions

When photovoltaic modules are sold they are rated with a peak power output. This is denoted as the power produced by the module under Standard Test Conditions 1000 W/m^{-2}, AM 1.5, 25ºC.

Experimentally it is shown that in real operation, the efficiency of commercial crystalline silicon modules is about 10 %, which is smaller than the indicated values by the manufacturer (between 12 and 15 %) under standard conditions.

6. Acknowledgement

By this way, the main author expresses his appreciations towards contract POSDRU/6/1.5/S/13 of ‘‘Politehnica’’ University of Timisoara and Norway Grants for RADO contract STVES 115266 for opportunity of participating in these programs.

References

1. G. L. Araujo, A. Marti, Absolute limiting efficiencies for photovoltaic energy conversion - Solar Energy Materials Solar Cells 33 (1994) pp. 213–240, ISBN 082475963X
2. M. D. Archer, R Hill, Clean Electricity From Photovoltaics, Ed. Imperial College Press, London, 2001, pp. 11-17, 91-149
3. C. Del Canizo, G. Del Coso, W. Sinke, Crystalline silicon solar module technology, Progressin Photovoltaics, Researchand Applications, Vol. 17 (2009), pp.199–209, ISSN 0957-0233
4. L Fara, E Tulcan-Paulescu, M Paulescu, Sisteme Fotovoltaice, Ed. MatrixROM, Bucureşti (2005) pp. 12-76
5. K. Yamamoto, A. Nakajima, M. Yoshimi, T. Sawada, A high efficiency thin film silicon solar cell and module; Ed. Kaneka Corporation, 2-1-1, Hieitsuji, Otsu, Shiga 520-0104, Japan
6. C. Lungenschmied, G. Dennler, H. Neugebauer, S. N. Sariciftci, M. Glatthaar, T. Meyer, and A. Meyer, Solar Energy Materials Solar Cells 91, 2007, pp. 379, ISBN 082475963X
7. S. Sun, Advances in Solar Energy, Ed. by Y. Goswami, International Solar Energy Society, Freiburg, Germany, 2007, Vol. 17, Chapter 3, ISBN 9780849392849
8. A. Usami, Optical and electrical modeling of nanocrystalline solar cells - Nanostructured Materials for Solar Energy Conversion, Ed. by T. Soga, Elsevier Asmsterdam (2006), pp. 11-34

EFICIENȚA PANOURILOR FOTOVOLTAICE DE PRIMĂ GENERAȚIE

Rezumat

Industria fotovoltaicelor este una cu cea mai rapidă creştere în prezent. În ultimii cinci ani, producția de celule solare fotovoltaice a crescut constant de la o medie anuală de 40 %, determinată nu numai de progresul înregistrat în tehnologia materialelor, ci şi prin programe de introducere pe piață în țările din întreaga lume. Această creştere este, în principal atinsă de o îmbunătățire a capacităților de producție bazată pe tehnologia de dispozitive cristaline cu joncțiuni unice. În concordanță cu timpul necesar pentru orice schimbare majoră în infrastructura energetică, o altă perioadă de 20 - 30 ani de creştere economică durabilă şi activă va fi necesară pentru fotovoltaice pentru a înlocui o parte semnificativă din sursele convenționale de energie. Astfel sunt prezentate rezultate experimentale referitoare la eficiența modelelor comerciale şi sunt făcute aprecieri despre capabilitatea unui sistem fotovoltaic autonom de 180 W în alimentarea unor consumatori.

Scientific reviewers: Winfred Maria RUSS, Technical University of München, Germany
Peter STURM, Technical University of Graz, Austria

SCIENTIFIC BULLETIN OF
THE „POLITEHNICA" UNIVERSITY OF TIMISOARA, ROMANIA
TRANSACTIONS ON MECHANICS
BULETINUL ŞTIINŢIFIC AL
UNIVERSITĂŢII „POLITEHNICA" DIN TIMIŞOARA, ROMÂNIA
SERIA MECANICĂ
Tom 54 (68) **ISSN 1224 - 6077** **Fasc. 4, 2009**

MODELING OF MIDDLE EAR IN ORDER TO BUILD A PROSTHESIS

Cosmina VIGARU*, Antonius STANCIU*
Mechanical Faculty Engineering, Bv. Mihai Viteazu, No.1, 300222, Timisoara, Romania,
cosmina@cmpicsu.upt.ro, antonius@cs.upt.ro

Abstract. The goal of the study is to produce a computer model that can be used to simulate the ear function. The middle ear function is important for sound transmission to the cochlea. The modeling of middle ear is important in order to build middle ear prostheses. The aim of any prosthesis is to rehabilitate the damaged organ in order to improve its natural function. Based on a better understanding of the middle ear's sound transmission, prostheses' design could be optimized to produce transmission characteristics that are seen in the normal human ear. Partial ossicular reconstruction prostheses (PORP) are frequently used in practice to restore ossicular continuity when the incus is eroded or missing, and total ossicular reconstruction prostheses (TORP) are used when the arch of stapes are absent or the malleus is missing or eroded.

Keywords: middle ear, prosthesis, model, hearing aid

1. Introduction

The mechanism of hearing involves conduction of mechanical vibrations along the ossicular chain to the inner ear.

When the tympanic-ossicular system is affected, a diminution of aerial transmission of sound from tympanic membrane to the oval window is resulting.

The most important sources of ossicular chain interruption are: congenital, traumatically and inflammatory. In cronic middle ear disorders the damaged ossicular chain is replaced through middle ear prostheses.

When both the incus and malleus are eroded or absent, the ossicular chain is reconstructed with a partial ossicular replacement prosthesis (PORP).

In case when the incus and arch of the stapes are eroded, or the malleus, incus and arch of the stapes are absent, the ossicular chain is reconstructed with a total ossicular replacement prosthesis (TORP).

The literature reveals that the implants used today for total or partial ossicular chain replacement only address limited aspects of functional ossiculoplasty [2], [3], [6].

There are many studies regarding the modeling of middle ear (figure 1) [5], [4]. The modeling methods are useful for numerical analysis based on the theory of finite element method.

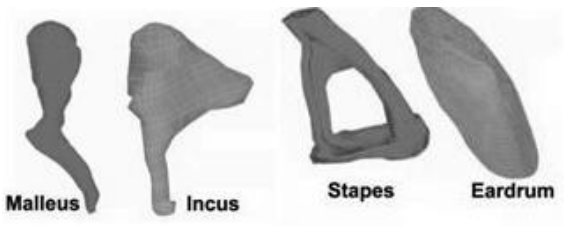

Figure 1 Components of the middle ear model

2. Functional anatomy of the ear

The auditory analyzer is a complex structure with an amazing sensibility. The auditory analyzer has three important parts: external ear, middle ear and inner ear.

The external ear is the external portion of the ear, which consists of the pinna, concha, and auditory meatus. From the pinna, the sound pressure waves move into the ear canal (a tube running through the middle ear) [4]. This tube leads inward from the bottom of the auricula and conducts the vibrations to the tympanic cavity, concentrating frequencies in the range of 3 KHz to 12 KHz.

The middle ear is the portion between ear drum and cochlea, naturally filled with air. The middle ear's cavity is (15x5x2) mm. It consists of three little bones (called malleus, incus, and stapes), five ligaments and two muscles (tensor tympani and stapedius muscle) [4].

The inner ear includes both the organ of hearing (the cochlea) and a sense organ that is attuned to the effects of both gravity and motion (labyrinth or vestibular apparatus).

3. Ossicular chain and tympanic membrane model

Based on the medical atlas [4], the geometry of small bones of the middle ear (malleus, incus and stapes) and the eardrum were achieved. The solid modelling software used was SolidWorks.

The tympanic membrane (figure 2) separates the tympanic cavity from the external acoustic meatus. Its function is to transmit sound from the air to the ossicles inside the middle ear. The malleus bone bridges the gap between the eardrum and the other ossicles. Rupture or perforation of the eardrum can lead to conductive hearing loss.

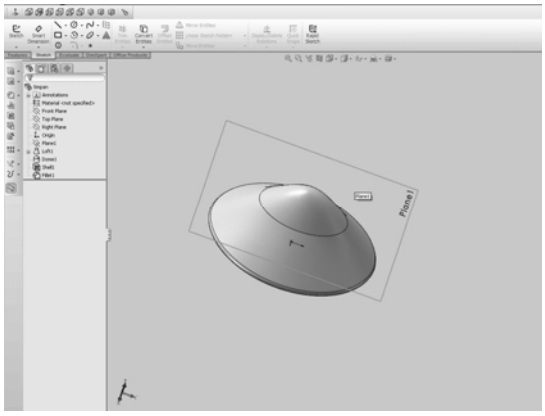

Figure 2 Tympanic membrane

The malleus has two main parts: the manubrium, which adheres to the tympanic membrane, and the head, which articulates with the incus. The malleus is the longer bone from middle ear, 7-9 mm and its motion is synchronous with the tympanic membrane.

Starting from the anatomy of the malleus (figure 3) [4], a simplified model was realized (figure 4).

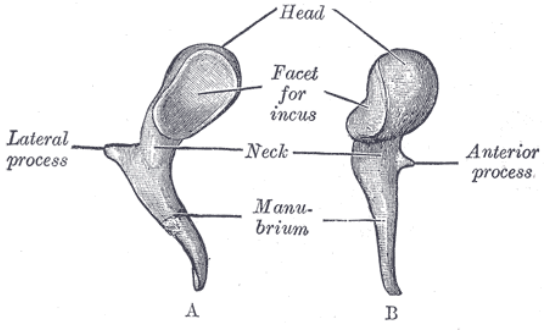

Figure 3 Anatomy of the malleus with detailed description.

The simplified model was built by eliminating the lateral process of the malleus. This simplified model is easy to manufacture and is not influencing the normal functionality of the middle ear.

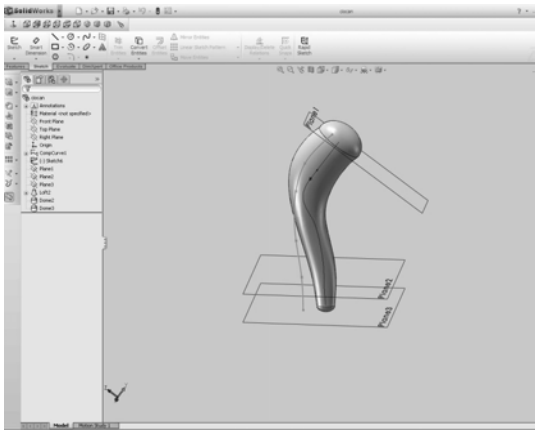

Figure 4 Simplified model of the malleus

The incus, which is articulated with the malleus, is the biggest bone of the middle ear, but without having a great physiological function, other than relaying the sound towards the cochlea. The incus is divided into three principal parts: a body and two processes (named short and long, respectively). The head of the incus articulates with the head of the malleus.

Also, starting from the anatomy of the incus (figure 5), [4] we realized a simplified model (figure 6). By eliminating the short crus of the

incus (which has no influence on the sound transmission) the simplified model was built.

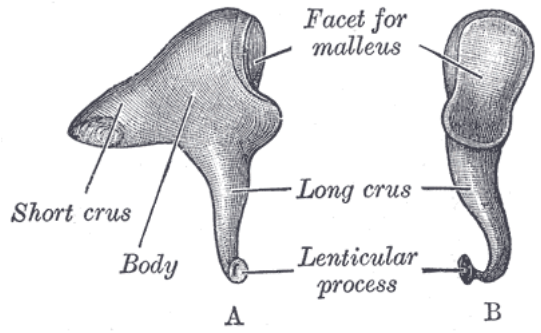

Figure 5 Anatomy of the incus with detailed description

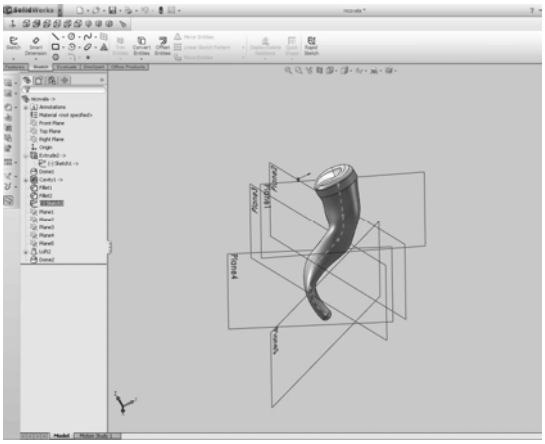

Figure 6 Simplified model of the incus

The stapes is the smallest bone in the human body and looks like a stirrup. The stapes transmits the sound vibrations from the incus to the inner ear through the oval window. The stapes has the following parts: head, neck, two limbs and a base.

The simplified model of the stapes (figure 8), [4] is the most similar to the anatomical model.

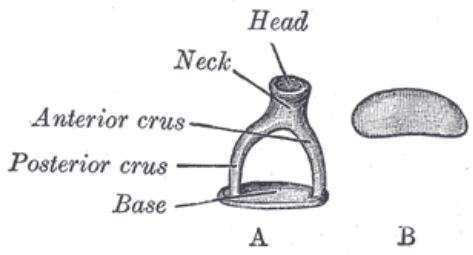

Figure 7 Anatomy of the stapes with detailed description.

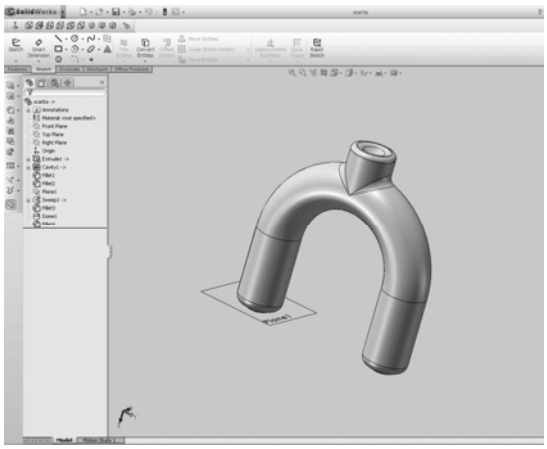

Figure 8 The simplified model of the stapes

The model of middle ear was realized in Assembly module, after constructing all the parts (figure 9). Using this model, we can simulate the movement of middle ear, taking into account the existing joints between all the components of the osscicular chain.

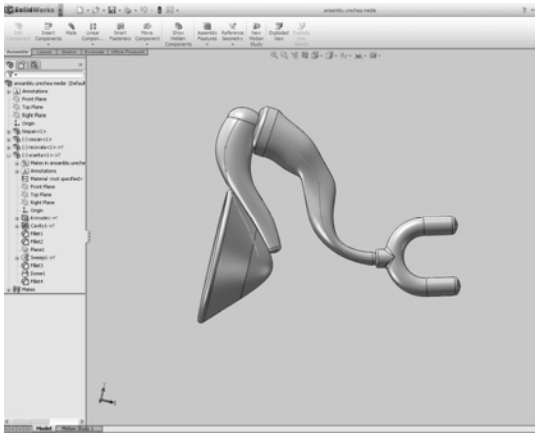

Figure 9 Model of middle ear

In future researches we intend to realize a finite element analysis in order to improve the model.

4. Conclusion

The proposed model represents just a preliminary model of the bone components. This virtual model of the ossicular chain, described here, can be further used to make a real model using a prototyping machine.

Our bone model of the middle ear is based on the anatomy of auditory system. Results from the model of middle ear bones was in reasonable agreement with the anatomical bones.

In future works we intend to realize a model from a high resolution CAT scanning of the middle ear, which could be performed using

the CAT scan machine existing in" CMPICSU" Medical Imaging Laboratory from Politehnica University of Timişoara.

References

1. M. Ferrazzini, A dynamic mathematical model based on the finite element method, PhD thesis. Swiss Federal Institute of Technology, Switzerland, 2003
2. C.F. Lee, P. R. Chen, E.J. Lee, J. H. Chen, T.C. Liu, Computer aided three-dimensional Reconstruction and modeling of middle ear Biomechanics by high-resolution computed Tomography and finite element analysis, Biomedical Engineering: Applications, Basis and Communications (BME), Volume: 18, Issue: 5 October 25, 2006, pp. 214-221, ISSN 1016-2372, Taipei, Taiwan
3. H. Mojallal, M. C. Stieve, I. Krueger, N. Witteck B. Süß, Functional evaluation of Middle ear prosthesis, World Congress on Medical Physics and Biomedical Engineering 2006 August 27 – September 1, 2006 COEX Seoul, Korea, ISBN 978-3-540-36839-7
4. S. Standing: Gray's Anatomy. The Anatomical Basis of Clinical Practice, 2005, Elsevier Churchill Livingstone, ISBN 0443066752
5. Q. Sun, R. Z. Gan, K.-H. Chang, K. J. Dormer, Computer-integrated finite element modeling of human middle ear, Biomechanics and Modeling in Mechanobiology Journal, Vol.1, No.2, October 2002, pp.109-122, Springer Berlin/Heidelberg, ISSN 1617-7959
6. R. Vincent, N. M. Sperling, J. Oates, J. Osborne, Ossiculoplasty with Intact Stapes and Absent Malleus: The Silastic Banding Technique, Otology & Neurotology, Vol. 26, No. 5, 2005, pp.846-852, ISSN 1531-7129

MODELAREA URECHII MEDII ÎN VEDEREA PROTEZARII

Rezumat

Scopul acestei lucrari este de a realiza un model care să simuleze funcționarea urechii medii. Funcționarea urechii medii este importantă pentru transmiterea sunetului către cohlee. Modelarea urechii medii este importantă în scopul realizării ulterioare a unei proteze. Protezele de ureche medie au ca obiectiv principal reabilitarea părții anatomice, deteriorate în scopul îmbunătățirii auzului.

O înțelegere bună a modului de funcționare a organului auditiv şi a modului de transmitere a sunetului conduce la o optimizare a protezelor, astfel încât transmiterea suntului să se realizeze ca şi în cazul urechii umane. Protezele osiculare parțiale (PORP) sunt utilizate frecvent în pactică pentru a reface continuitatea osiculară atunci când nicovala lipsește sau când este deteriorată. Protezele osiculare totale (TORP) se utilizează atunci când cele două brațe ale scăriței sunt rupte sau lipsesc, respectiv când ciocanul este deteriorat.

Scientific reviewers: **Liviu BERETEU, "Politehnica" University Timişoara, Romania**
Ion DUMITRU, "Politehnica" University Timişoara, Romania

SCIENTIFIC BULLETIN OF
THE „POLITEHNICA" UNIVERSITY OF TIMISOARA, ROMANIA
TRANSACTIONS ON MECHANICS
BULETINUL ŞTIINŢIFIC AL
UNIVERSITĂŢII „POLITEHNICA" DIN TIMIŞOARA, ROMÂNIA
SERIA MECANICĂ
Tom 54 (68) **ISSN 1224 - 6077** **Fasc. 4, 2009**

DYNAMIC ANALYSIS OF A SIMPLIFIED MODEL OF LOWER LIMB PROSTHESIS

Lucian RUSU
Mechanical Faculty of Engineering, Bv. Mihai Viteazu no. 1, 300222, Timişoara, Romania, luck@cmpicsu.upt.ro

Abstract. The lower limb prosthesis has to perfectly fit to human body and also to accomplish the human locomotion. There are many types of lower limb prosthesis. In this paper is presented a simplified model of lower limb prosthesis. The proposed model is analyzed from the dynamical point of view. The dynamical analysis takes into account the anatomical human motion. Velocity, acceleration, material properties and mechanical design of the prosthesis are the giving data and the variation in time of the joint reactions and torques are the output data. Based on the obtained results, a constructive design of the lower limb prosthesis will be possible to generate.

Keywords: prosthesis, human motion, dynamic model, walking step.

1. Introduction

For the lower limb prosthesis the most solicited parts during the gait cycle are the joints. Using the dynamic model is possible to determinate the reactions and torques in the joints during walking.

The aims of this paper are: to obtained a simplified model of the lower limb prosthesis and to perform a dynamical analysis of it.

2. Geometrical model of the lower limb prosthesis

The simplified model of the prosthesis consists of the following major components[1]:

- femoral part;
- tibial part;
- foot part.

The joints connecting the three components of the proposed model allow only rotations between the femoral and tibial parts respectively between the tibial and foot parts[2]. The nut and the bush have a cylindrical profile witch blocks there its own rotation. The role of the screw is to determinate the rotation axis and to assure the joint lock.

The geometrical model of the lower limb prosthesis (figure 1) was designed using the Solid Edge V19 software.

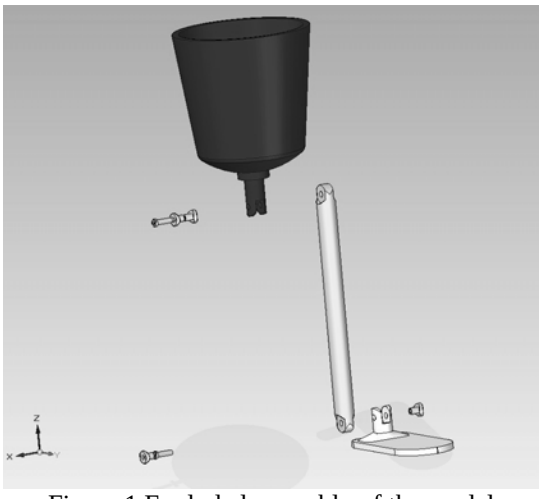

Figure 1 Exploded assembly of the model of the lower limb prosthesis

Using this nut-bush-screw system only the rotation is allowed in joints.

The nut-bush-screw system is geometrical locked so it can be considered together with the femoral part in the knee case (figure 2) and together with the tibial part in the case of ankle joint (figure 3).

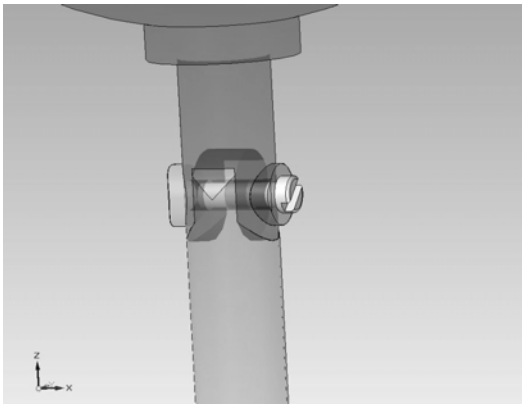

Figure 2 Knee joint

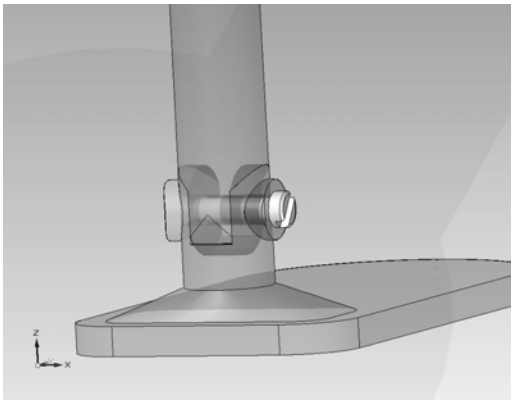

Figure 3 Ankle joint

3. Dynamical analysis of the simplified model

The dynamic analysis of the prosthesis model during the gait cycle was realized using the Dynamic Designer - Motion Professional software witch is an add-on to the Solid Edge V19 software.

The average duration of a stride is generally considered at 1.8 seconds in healthy gait[3]. In the performed analysis the time interval was considered to have 2 seconds for a stride. For the dynamical analysis of the prosthesis model, the walking step was divided into several sequences. First sequence is the extension, from position A (maximum angle in knee for flexion - figure 4) to position B (maximum angle in knee for extension - figure 5). The second sequence is flexion and it is exactly the opposite way from the first sequence[5,6].

The configurations of the two positions are:

- position A: α=-90˚, β=-80˚;
- position B: α=90˚, β=-5˚,

where α is the angle in the knee joint and β is the angle in the ankle joint.

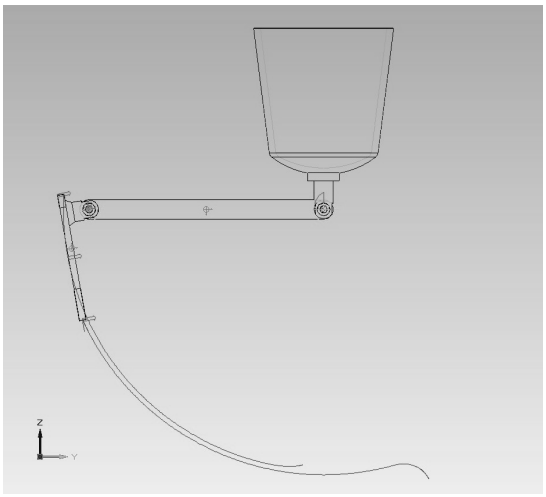

Figure 4 Position A - flexion

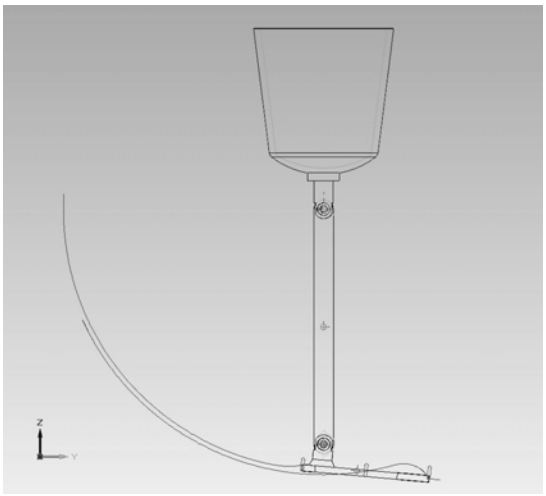

Figure 5 Position B – extension

The weight of the prosthesis model must be comparative with the weight of the amputated part of the lower limb[4]. For the used model were selected the following materials:

- polyethylene for the femoral part;
- stainless steel for the tibial part and joints components;
- aluminium alloy for the foot.

Using these materials, the resulted weight of the prosthesis model was 4,365Kg.

During the extension sequence, the resulted maximum angular velocity was of 1.35 deg/sec into the knee joint, and the resulted maximum angular velocity reached in the ankle joint was of 1.12 deg/sec. The maximum angular accelerations in knee and ankle joints resulted of 0.053 deg/sec^2, respectively 0,22 deg/sec^2.

During the flexion sequence the distributions of angular velocity and acceleration are different but the maximum values were the

same because there is no reaction force from the ground.

At the contact between the foot and ground it appears a reaction force. This reaction force is simulated by three forces placed in heel, foot and toe. The value of the normal reaction force is calculated for a person having 80 Kg weight.

The reaction force at hell contact (figure 6) reaches a maximum value of 400 N because during the heel contact corresponds to double support phase. The reaction forces at foot contact (figure 7) and toe-off contact (figure 8) with the ground reach a maximum value of 800 N corresponding to the single support phase.

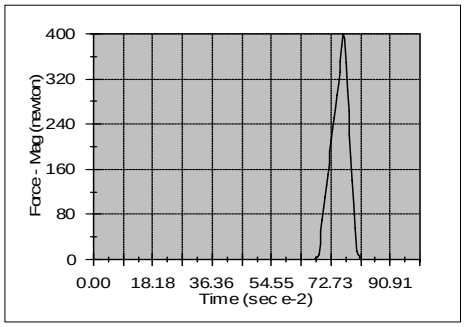

Figure 6 Normal reaction force at heel contact

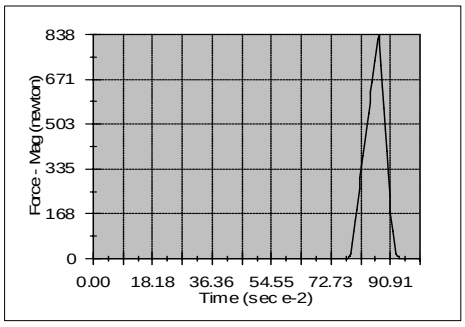

Figure 7 Normal reaction force at foot contact

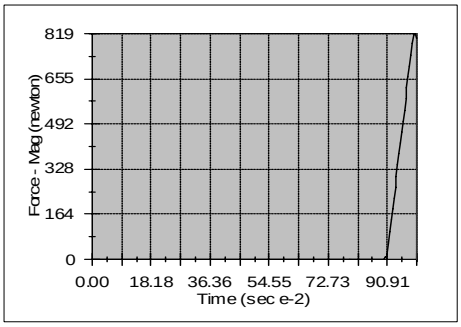

Figure 8 Normal reaction force at toe contact

During the gait cycle the switch between normal reactions is not happened suddenly. In order to simulate this, the applied forces are overlapping for a short time interval.

4. Results and conclusions

In the extension sequence it can be observed a higher reaction force that appears in the ankle joint (832 N - figure 9) then the one that appears in the knee joint (812 N – figure 10). This difference is induced because the ankle joint is closer to the contact area than the knee joint. But the equivalent torque in the knee joint (6357 N*mm – figure 11) is higher that the one in the ankle joint (6241 N*mm – figure 12) because the force arm is greater for the knee joint.

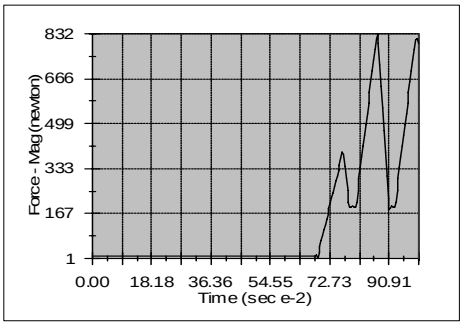

Figure 9 Reaction force in the ankle joint - extension

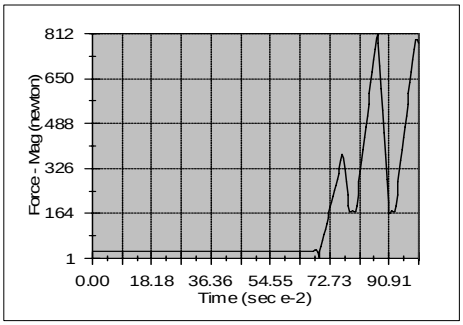

Figure 10 Reaction force in the knee joint - extension

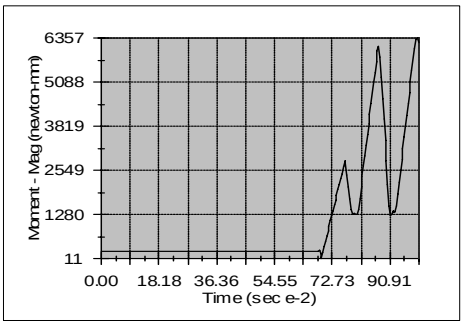

Figure 11 Torque in the knee joint - extension

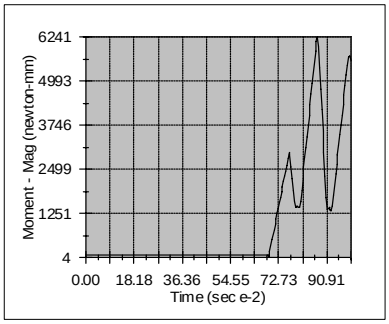

Figure 12 Torque in the ankle joint - extension

In the flexion sequence it can be observed that the reaction force and the equivalent torque are higher in the knee joint (26,19 N – figure 13; 196,36 N*mm – figure 14) than in the ankle joint (6,27 N – figure 15; 47,20 N*mm – figure 16) because there is no normal reaction force from the ground.

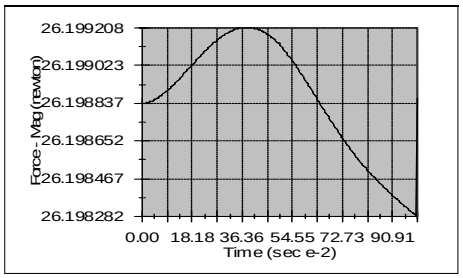

Figure 13 Reaction force in the knee joint - flexion

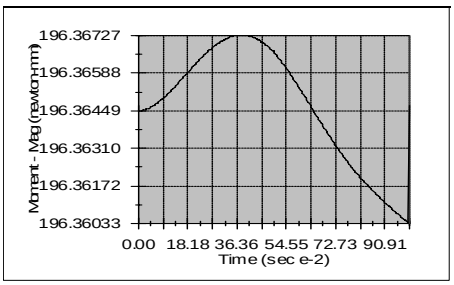

Figure 14 Torque in the knee joint - flexion

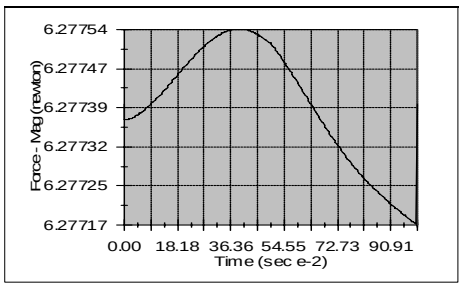

Figure 15 Reaction force in the ankle joint - flexion

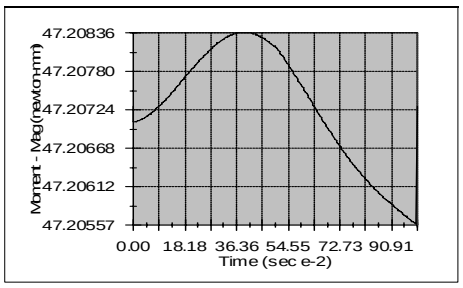

Figure 16 Torque in the ankle joint – flexion

Taking into account the material properties, the reaction forces and torques acting in joints it can be concluded that this simplified model that was presented in this paper can be used as a start-up for a constructive solution of lower limb prosthesis.

References

1. O. Atsuo, O. Goro, H. Kazunori, D. Ashish, N. Miyoshi, Design of lower limb prosthesis with contact pressure adjustment by MR fluid, Engineering in Medicine and Biology Society, 2008. EMBS 2008, 30th Annual International Conference of the IEEE, 20-25 Aug. 2008, pp. 330-333, ISSN 1557-170X, ISBN 978-1-4244-1814-5
2. Y. Isobe, T. Takeuchi, K. Furuya, K. Hosoda, A Japanese lower limb prosthesis with a fore-joint foot and turntable, International Orthopaedics, Vol. 6, No. 1, June, 1982, pp. 49-54, ISSN 1432-5195
3. C. Kirtley, Clinical Gait Analysis, Theory and Practice, Elsevier Churchill Livingstone, 2006, ISBN 0 4431 0009 8
4. S. R. Rozbruch, S. Ilizarov, Limb lengthening and reconstruction surgery, Informa Healthcare USA, Inc., 2007, ISBN-10 0-8493-4051-9, ISBN-13 978-0-8493-4051-2
5. A. Tözeren, Human Body Dynamics: Classical Mechanics and Human Movement, Springer-Verlag New York, Inc., 2000, ISBN 0-387-98801-7
6. J. Xiaohong, Z. Ming, C. Winson, C. Lee, Load Transfer Mechanics Between Trans-Tibial Prosthetic Socket and Residual Limb — Dynamic Effects, Journal of Biomechanics 37(9) Jan 2003, pp.1371-1377, ISSN 0021-9290.

ANALIZA DINAMICĂ A UNEI PROTEZE SIMPLIFICATE DE MEMBRU INFERIOR

Rezumat

Proteza de membru inferior trebuie să se potrivească corpului uman şi de asemenea să îndeplinească rolul funcțional. Există mai multe tipuri de proteze pentru membrul inferior. In această lucrare se prezintă un model simplificat pentru o proteză de membru inferior. Acest model a fost analizat din punct de vedere dinamic, ținându-se cont de caracteristicile locomoției umane. Ca date de intrare au fost considerate vitezele, accelerațiile şi proprietățile de material, torsorul din articulații fiind rezultatul urmărit. Pe baza rezultatelor obținute în urma analizei dinamice se va putea concepe o solutie constructivă care să aibă la bază modelul simplificat prezentat în lucrare.

Scientific reviewers: **Nicolae FAUR, "Politehnica" University of Timişoara, Romania**
Liviu BERETEU , "Politehnica" University of Timişoara, Romania

SCIENTIFIC BULLETIN OF
THE „POLITEHNICA" UNIVERSITY OF TIMISOARA, ROMANIA
TRANSACTIONS ON MECHANICS
BULETINUL ŞTIINŢIFIC AL
UNIVERSITĂŢII „POLITEHNICA" DIN TIMIŞOARA, ROMÂNIA
SERIA MECANICĂ
Tom 54 (68) **ISSN 1224 - 6077** **Fasc. 4, 2009**

INVESTIGATIONS OF FAILURE FOR A CHASSIS COMPONENT

Aurel RĂDUŢĂ*, Carmen OPRIŞ*, Ibolyka BRAN*
*Mechanical Engineering Faculty Timişoara, No 1, M. Viteazul Bvd, 300222, Romania
e-mail: aurel.raduta@eng.upt.ro , copris@eng.upt.ro, ibi.bran@yahoo.com

Abstract. This paper investigates the causes of failure of the support which is mounted on the chassis of the cistern cars, playing an essential role in fixing them. After welding and than during operation, cracking occurred on these components in the welded area. In order to determine the causes of failure, the quality of materials used to manufacture the parts was investigated.

Keywords: chassis, cistern car, weld, material quality, heat treatment

1. Introduction

For the welded constructions at railway rolling stock fine grain steels are used, presenting low risk of brittleness in the welded area. For special railroad cars, in the composition of the chassis there are elements obtained by casting. In these conditions, it is imperative that the cast steel ensures good dynamic and fatigue loading characteristics and to have a good welding behavior [1].

This paper investigates the causes of failure of the support which is mounted on the chassis of the cistern cars, playing an essential role in fixing them. The support is fixed to the chassis by welding, and then the clamps that sustain the tank are fixed on it (figure 1). After welding and than during operation, cracking occurred on these components in the welded area.

Since on the production flow there were many cars that already had the support welded on them, it was necessary to conduct some analysis in order to appreciate if these elements may be used or the possibility of improving their mechanical properties by heat treatments applied before and after welding [2].

In order to determine the causes of failure, the quality of materials used to manufacture the parts was investigated. In this purpose, measurements were made investigating the hardness and chemical composition of the material for the support [3].

2. Experimental research

2.1. Testing of chemical composition and hardness

The chemical composition of the parts was determined in the first stage of experimental tests using the spectral method, for the support made of a steel type G18 CrMnMo 5-5; results are presented in table 1. These were then compared with the specific steel melt. The values for the chemical composition specific the steel melt and aberrations admitted on the product are presented in table 2.

The chemical analysis conducted found that the values obtained fall in the range of specific

compositions for the melt steel, according to standard values and deviations permitted on products, except the contents of S and P, which have double the concentration limit.

Hardness measurements showed that hardness is higher than that recommended, being around 320 HV5 (HB 300). Excessive hardness could be one of the causes of failures reported in these parts. Therefore it was attempted to apply heat treatments with different parameters, in order to modify the structure of the material, thereby decreasing its hardness, and avoiding damage to products.

Figure 1 Fixing form of the support on the chassis

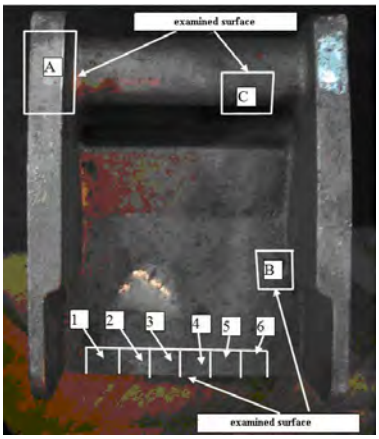

Figure 2 Sampling mode

Table 1 Chemical composition determined experimentally

Element	Percent (%)	Uncertainty (%)	Element	Percent (%)	Uncertainty (%)
Fe	95.90	±0.1033	Mo	0.36	±0.0155
C	0.15	±0.0112	Cu	0.12	±0.0066
Si	0.47	±0.0089	Al	0.02	±0.0144
Mn	1.23	±0.0376	Ti	0.00	-
P	0.04	±0.0049	V	0.01	±0.0020
S	0.03	±0.0060	Co	0.01	±0.0052
Cr	1.45	±0.0428	Nb	0.00	-
Ni	0.10	±0.0502	W	0.03	±0.0563

Table 2 Chemical composition of the analyzed steel, according to the standards

Element	Percent (%)	Aberration on the product (%)
C	0,15 – 0,21	±0,02
Si max	0,60	+0,1
Mn	1,2 – 1,6	±0,1
P max	0,02	+0,005
S max	0.015	+0,002
Cr	1,2 – 1,5	+0,1

2.2. Sampling mode

Several samples were analyzed, taken according to figure 2:

- Sample A - cylindrical journal, lateral side, untreated
- Sample B - lower corner, untreated
- Sample C - section through the cylindrical journal, treated with flame
- Samples 1 ... 6 taken from the inferior area of the bearing, as shown in figure 2 for the simulation of heat treatments cycles.

The mechanical characteristics of materials determined before the heat treatments are presented in table 3.

Table 3 Mechanical characteristics of materials before the heat treatments

Property	Measured value
Yield, N/mm^2	min. 600
Tensile strength, N/mm^2	730-880
Elongation at break, %	12
Resilience, J	min. 27 at 30^{o}C

Mechanical characteristics of samples A, B and C after the heat treatments are presented in table 4.

Samples taken as shown in figure 1 were heat treated according to the following schemes (table 5).

Table 4 Mechanical characteristics of samples A, B and C after the heat treatments

Sample	Hardness HB	Parameters of the heat treatment					Properties after the heat treatments				
		Heating times, hours	Heating temperature, °C	Holding time, hours	Holding temperature, °C	Cooling	Yield, N/mm^2	Tensile strength, N/mm^2	Elongation at break, %	Resilience, J	Hardness HB
A	325	1,5	550	1,5	550	protected	923	975	8	8	283
B	330	1,5	530	0,5	530	protected	960	1000	10	10	264
C	305	1	620	3	620	protected	581	697	22,2	22	204

Table 5 Parameters of the heat treatments for samples 1-6

Sample	Heat treatment	Parameters of the heat treatments for samples		
		Temperature, °C	Duration, minutes	Cooling environment
1	untreated			
2	normalization	920	30	Furnace, 50 ºC/min
3	normalization + quenching	Quenching parameters		
		950	30	water
4	normalization + quenching	Quenching parameters		
		950	30	oil
5	normalization + water quenching + annealing	Annealing parameters		
		650	60	air
6	normalization + oil quenching + annealing	Annealing parameters		
		650	60	air

Control sample (sample 1) has not undergone any heat treatment and is in its original condition. Microscopic aspect of sample 1 before etching is shown in figure 3.

Microscopic aspect of sample 1 after etching is shown in figure 4. It is visible the presence of inclusions (sulfides and oxides), arranged after the casting dendrites. Material structure is acicular.

Sample 2 was submitted to a normalization treatment at 920ºC, holding time 30 minutes, cooling rate 50 ºC/min. Microscopic aspect of sample 2 after the normalization treatment before etching is presented in figure 5, and after etching in figure 6.

Non metallic inclusions are disposed uneven. After treatment, a polyhedral structure of ferrite and pearlite is obtained.

Sample 3 was submitted to a normalization treatment followed by quenching at 950ºC, holding time 30 minutes, cooling in water. Microscopic aspect of sample 3 before etching is presented in figure 7, and after etching in figure 8. The structure obtained is acicular.

Sample 4 was submitted to a normalization treatment followed by quenching at 950ºC, holding time 30 minutes, cooling in oil. Microscopic aspect of sample 4 before etching is presented in figure 10, and after etching in figure 10. The structure obtained is acicular.

Sample 5 was submitted to a normalization treatment followed by quenching in water and annealing at 650 ºC, holding time 60 minutes, cooling in air. Microscopic aspect of sample 5 before etching is presented in figure 11, and after etching in figure 12. In the sample not etched

there are visible micro shrinking holes at dendrite limits. The structure obtained after the heat treatment is acicular with carbides precipitations.

Sample 6 was submitted to a normalization treatment followed by quenching in oil and annealing at 650 ºC, holding time 60 minutes, cooling in air. Microscopic aspect of sample 6 before etching is presented in figure 13, and after etching in figure 14. In the sample not etched there are visible micro shrinking holes at dendrite limits. The structure obtained after the heat treatment is acicular with carbides precipitations.

a) area with less defects

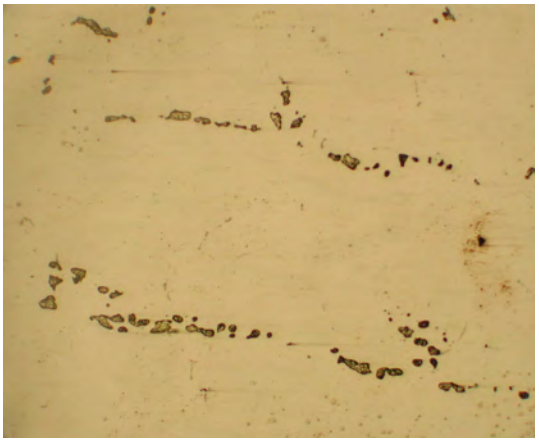

b) area with defects

Figure 3 Aspect of sample 1, not etched

b) OM 200x

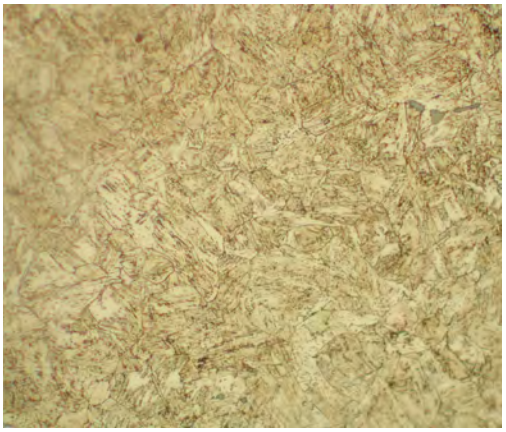

c) OM 500x

Figure 4 Microstructure of sample 1

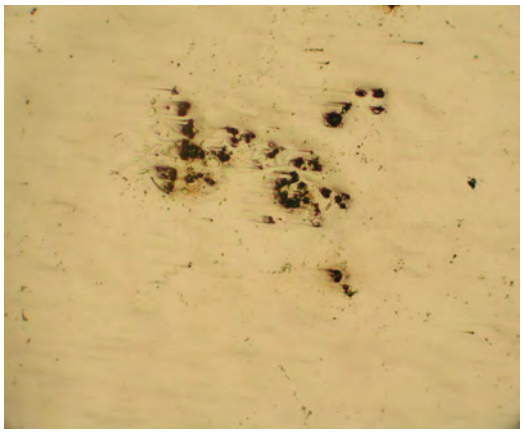

Figure 5 Aspect of sample 2 after the normalization treatment, area with defects, OM 100x, not etched

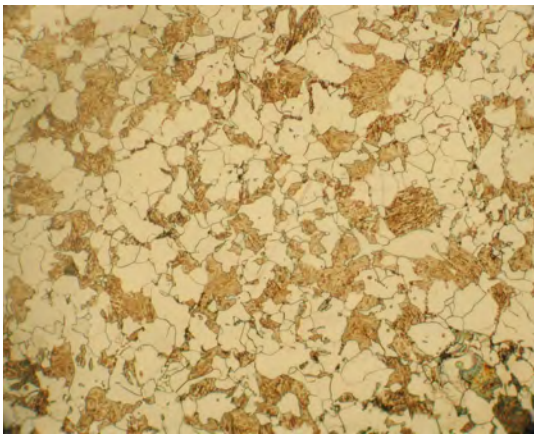

Figure 6 Microstructure of sample 2, OM 200x

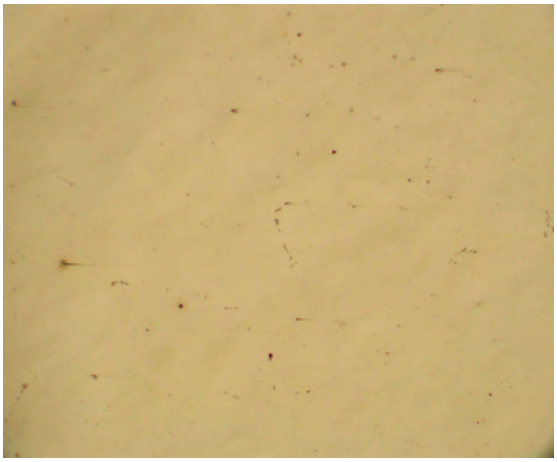

Figure 7 Aspect of sample 3, not etched, area with less defects, OM 100x

Figure 8 Microstructure of sample 3, OM 200x

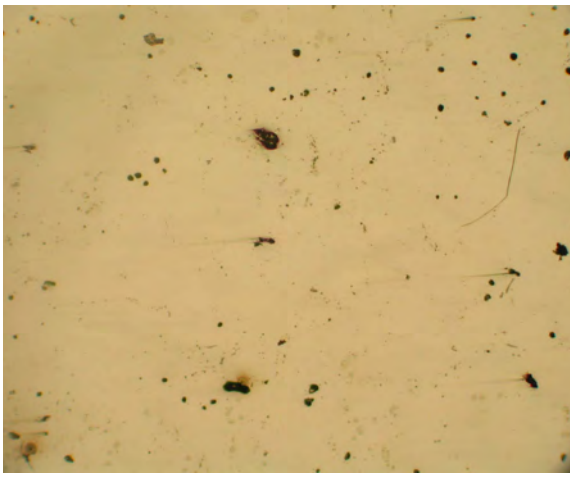

Figure 9 Aspect of sample 4, area with defects, OM 100x , not etched

Figure 10 Microstructure of sample 4, OM 200x

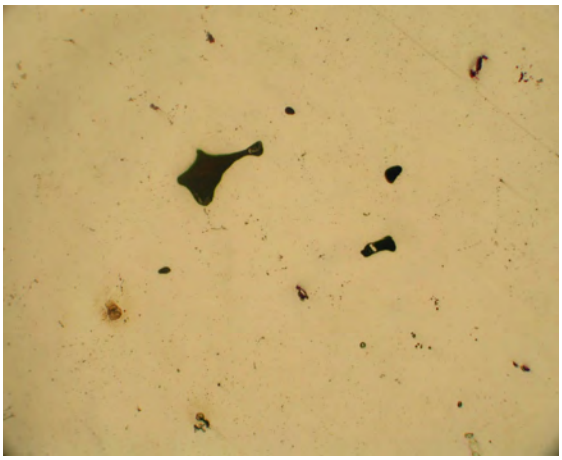

Figure 11 Aspect of sample 5, area with defects, OM 100x, not etched

Figure 12 Microstructure of sample 5, OM 200x

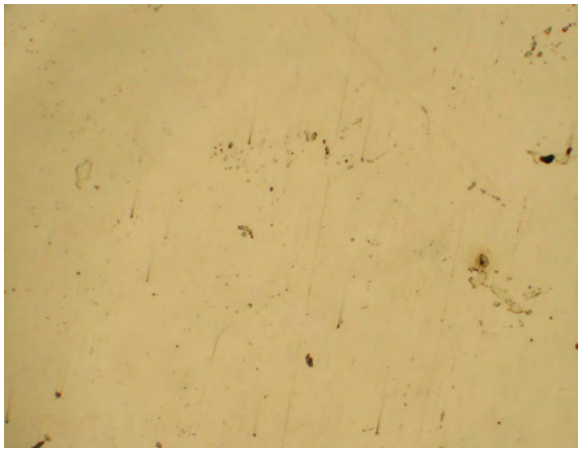

Figure 13 Aspect of sample 6, area with less defects, OM 100x (not etched)

Figure 14 Microstructure of sample 6, OM 200x

Nonmetallic inclusions in the most impure fields from the analyzed samples correspond to score 4.

Experimental hardness values measured on samples 1-6 are presented in table 6.

Table 6. Hardness measured values for samples 1-6

Sample number	Vickers hardness, HV 5	Brinell hardness, HB
1	320	300
2	238	222
3	429	405
4	418	400
5	251	235
6	248	234

3. Conclusions

The recommended heat treatment scheme is normalization followed by quenching in water and annealing at 650 ºC, holding time 60 minutes, cooling in air. It is also recommended that the heat treatment should be applied on the product prior to welding, and for the already welded pieces, it must be applied after that.

References

1. W.D., Callister Jr., *Materials Science and Engineering, An Introduction*,6th Edition, John Wiley and Sons, Inc., USA, 2003
2. A. Hazotte, (ed.): *Solid State Transformation and Heat Treatment*,Wiley-VCH, Weinheim 2004, ISBN-10: 352731007X, ISBN-13: 9783527310074
3. V.A., Şerban, A., Răduță: *Materials Science and Engineering*, Politehnica Publishing House, Timişoara, 2006, ISBN (13) 978-973-625-322-5

EXPERTIZAREA AVARIEI COMPONENTELOR DE TIP ŞASIU

Rezumat

Lucrarea de față investighează cauzele defectării reperului suport care se montează pe şasiul vagoanelor cisternă, jucând un rol esențial în fixarea acestora. După sudare şi respectiv în timpul exploatării, pe aceste componente au apărut fisuri în zona îmbinării. S-a impus efectuarea unor analize prin care să se poată aprecia dacă aceste elemente pot să fie folosite sau posibilitatea de îmbunătățire a proprietăților mecanice prin tratamente termice aplicate înainte şi după sudare.

Scientific reviewers: **Viorel-Aurel ŞERBAN, "Politehnica" University of Timişoara, Romania**
Mircea NICOARĂ, "Politehnica" University of Timişoara, Romania

SCIENTIFIC BULLETIN OF
THE „POLITEHNICA" UNIVERSITY OF TIMISOARA, ROMANIA
TRANSACTIONS ON MECHANICS
BULETINUL ŞTIINŢIFIC AL
UNIVERSITĂŢII „POLITEHNICA" DIN TIMIŞOARA, ROMÂNIA
SERIA MECANICĂ
Tom 54 (68) **ISSN 1224 - 6077** **Fasc. 4, 2009**

CAD MODELING AND NUMERICAL ANALYSIS OF THE LUMBAR SPINE UNIT

Cristian SĂFTESCU-JESCU*, Delia BUGARIU*, Liviu BERETEU*
* Mechanical Engineering Faculty, Bv. Mihai Viteazu No.1, Timişoara, Romania
cristi@cmpicsu.upt.ro, delia@cmpicsu.upt.ro, liviu.bereteu@mec.upt.ro

Abstract. The paper presents a study of modelling and FEM analysis of the lumbar spine unit, considering basic movement of the spine anatomical segment, either implanted or not. Firstly, both the 3D models of the lumbar spine and the appropriate implant are described, next following to endure stresses through a static structural simulation. The implant is designed for the intervertebral disc stabilization in case of spinal fusion. The working environments used are Solid Works 2007 for modeling and ANSYS 11.0 for FEM analysis.

Keywords: CAD software, 3D modeling, lumbar spine unit, FEM analysis

1. Introduction

The human spine, an element which influences our everyday life, both as a basic biomechanical component and as a metaphor of one's personality, has been the subject of various researches, due to the increasing rate of back pain, especially in the lumbar segment of the spine.

Statistics nowadays show that 75-85% of people suffer from spine disorders at some point in their lives, back pain representing the second most common reason for seeing any doctor, the third most common reason given for surgery and the fifth most frequent cause of hospitalization [1].

Creating a 3D model of the lumbar spine unit implies various methods, from CAD drawing software to image reconstruction, derived from CT, MRI or X-rays investigations, each one with their advantages and disadvantages.

There is no standard detailed shape of the human spine due to the specific characteristics of each individual, therefore the resulting models present either mean values of the components or personalized data obtain from a single person.

The contribution of the paper to the spine research domain consists in developing of a 3D model of the lumbar spine unit, five vertebra and four intervertebral discs, obtained with CAD software, followed by a finite element method structural analysis of the spine segment for basic movement and an analysis of an implanted lumbar unit with an intervertebral cage.

2. Modelling

In order to succeed in modeling a functional lumbar unit, the anatomy, structure of the components and biomechanical behavior of the spine have been studied [2].

The 3D models were obtained using a combination between the part design, drawing and assembly modules of SolidWorks 2007 environment.

The next figure presents a comparison between the initial modeling phase of the

vertebral body (figure 1.a) and the final 3D obtained model (figure 1.b).

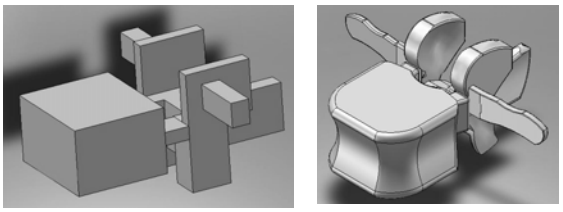

a. b.

Figure 1
a. Rough shaped design of lumbar vertebra;
b. Proper functional 3D model of a lumbar vertebra

Similar to vertebrae modeling was the design of the intervertebral discs. Prior defining the 3D model of the disc, the shape as well as the distinctive properties of the *annulus fibrosus* and the *nucleus pulposus* were taken into account (Figure 2).

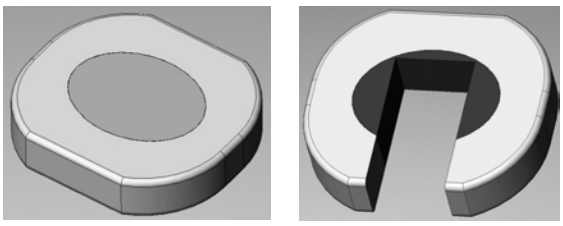

a. b.

Figure 2 a. Model of healthy intevertebral disc;
b. Intevertebral disc prepared for implantation

The dimensions were taken from scientific literature [3, 4]. Morphometric characteristics were obtained from 15 sets of lumbar vertebrae deriving from human bodies. The dry vertebra measurements were performed using Vernier calipers with a resolution of 0.1mm and standard goniometer with accuracy of 1°. The mean values of the width and height of the left and right pedicle are shown in Table 1.

Table 1 – Mean values of pedicle characteristics

Vertebra	Pedical Width [mm]		Pedicle Height [mm]	
	Left	Right	Left	Right
L1	6,40	6,50	13,60	13,70
L2	7,4	7,00	14,00	14,10
L3	9,3	9,00	13,90	13,90
L4	11,6	12,20	12,50	13,00
L5	17,5	17,70	12,30	12,70

Modeling the stabilization implant was the next step of the process. When dimmensioning the implant, the geometry of both the appropiate vertebra and the disc were taken into account. The shape of the intevertebral cage was considered as a truncated cone beacause in the implanted area, the mutual positioning of the vertebra sorrounding the implanted disc is deviated from the vertical plane, creating a different angle for each person (Figure 3).

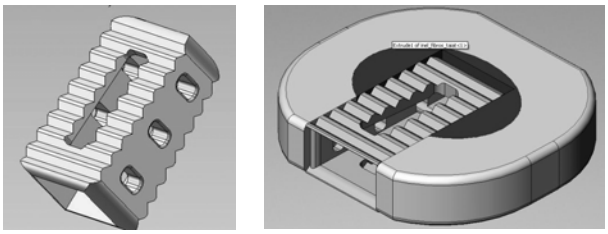

a. b.

Figure 3 Intevertebral implant (cage): a. Isometric view;
b. Intevertebral assembly.

The parallel threaded areas of the cage ease the implantation procedure, while the other bevel help creating a better accomodation. The cage orifices have a crucial role in bone fusion and osseointegration, the cage being filled with bone graft for lumbar stabilization.

Creating the 3D assembly of the lumbar unit was the final step in modeling. The mates contained pairs of coincidental planes and coincidental surfaces, leading to the model presented in Figure 4.

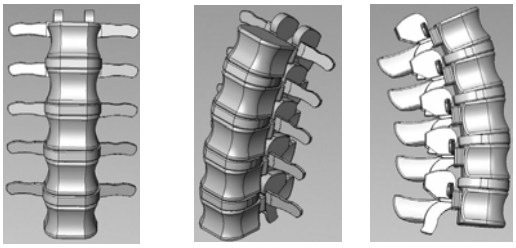

Figure 4 3D lumbar unit model:
a. Front view; b. Izometric view; c. Side view

3. FEM Analysis

Next to importing the 3D model from SolidWorks, simulations were developed in ANSYS Workbench 11.0 software which performs numerical analysis using the finite element method. The study considered the lumbar unit performing an extension movement with and without the intervertebral implant. The first phases of the FEM are the same for both situations: importing the 3D geometrical model, defining contacts between the elements, declaring constraints and forces.

3.1 Normal Lumbar Spine Analysis

The material used in the static structural simulation satisfies the mechanical properties of

the cortical bone, for the vertebral bodies, as well as for the anulus fribrosus and nucleus pulposus of the intevertebral disc (Table 2) [2].

Table 2 – Material properties used in simulation

Properties	Nucleus pulposus	Vertebral body	Annulus fibrosus
Young's Modulus [Mpa]	2,1	250	8000
Poisson's Ratio	0,499	0,35	0,34
Density [kg/mm³]	1,e-006	5,e-006	6,e-007

The contacts between the components were defined and the inferior surface of the bottom vertebral body was considered the fixed support (Figure 5).

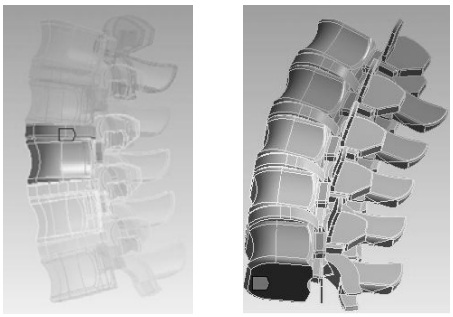

a. b.

Figure 5 a. Defining contacts; b. Fixed support

There were several forces taken into account. The weight of the individual load acts on the top of the vertebrae having the value of 500N, along a vertical direction, in the middle of the L1 superior lumbar facet (Figure 6.a).

The application point of the force is in the centre of L1 vertebra.

The extension force was displaced on the anterior side of the assembly, having a horizontal direction and 100N magnitude on the L1 vertebra and being executed voluntary (Figure 6.b).

Along the considered loads, the abdominal muscles influence the spine movement as well. Their functional anatomy determines the displacement of the muscle forces on both lateral sides of the all the vertebral bodies, as components on the X and Z axes, the magnitude of each resulting force being 20N (Figure 6.c) [5].

The analysis continues with meshing the lumbar unit and solving the model in the given conditions. The mesh generated 139267 nodes of 70303 elements, resulted from fourteen active bodies of an amount of a fourteen bodies totaly (Figure 7).

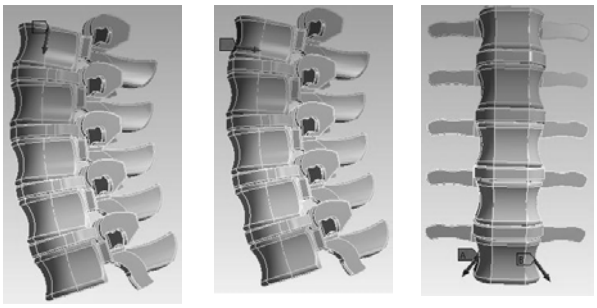

a. b.

Figure 6 Active forces: a.Weight; b. Extension force; c. Abdominal muscle force

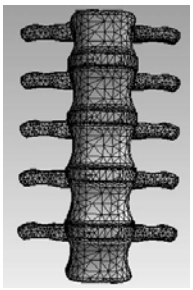

Statistics	
Bodies	14
Active Bodies	14
Nodes	139267
Elements	70303

a. b.

Figure 7 a. Meshing model b. Mesh statistics

3.2 Implanted Lumbar Spine Analysis

The analysis continues with the implanted lumbar spine testing. The intervertebral cage was placed into the fourth lumbar disc, between the L4 and L5 vertebrae, due to the great amount of load that it has to bare.

For the intervertebral implant Titan alloy *Ti6Al4V* was considered to be the best option, due to its mechanical properties (Table 3) and for the biocompatibility with the human body [6].

Table 3 – *Ti6Al4V* material properties

Young's Modulus [MPa]	96000
Poisson's Ratio	0,36
Density [kg/mm³]	4,62e-006
Thermal Expansion [1/°C]	9,4e-006
Tensile Yield Strength [MPa]	930
Compressive Yield Strength [MPa]	930
Tensile Ultimate Strength [MPa]	1070

After meshing (Figure 8.a) statistics shown there have resulted nineteen of ninteen active bodies, 163356 nodes and 78386 elements (Figure 8.b).

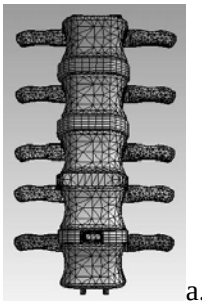

a.

Statistics	
Bodies	19
Active Bodies	19
Nodes	163356
Elements	78386

b.

Figure 8 a. Meshing model b. Mesh statistics

4. Results and Discussions

Solving both models in the given conditions offered information regarding the variation of stress, strains and displacements of the lumbar unit with and without the intervertebral implant (Table 4).

Table 4 – Extreme values of testing parameters

Results	Non-Implanted Lumbar Spine	Implanted Lumbar Spine
Equivalent Stress[MPa]	19, 53	61,34
Equivalent Elastic Strain [mm/mm]	0,03	0,01
Total Deformation[mm]	0,91	0.23

In both situations, the contact area between the articular processes of the L3 and L4 vertebrae present the highest value of equivalent stress. Considering the given hypothesis, in which the lumbar unit is bending and knowing its shape, it is natural to assume that the anterior side of the spinal segment is most affected, the extension movement increasing the curvature of the vertebrae. The implanted lumbar spine higher stress value appears due to the presence of the intervertebral cage. The *Ti6Al4V* implant restores the initial height of the disc however constraining its movement and also hardening it to the adjacent vertebrae.Total deformation reaches its highest value on the L1 vertebra, the place where the most load is found. The resulting displacement and equivalent elastic strain values are enclosed in the functional anatomic intervals [5].

Yet the equivalent stress values show a slightly exceed of normal stress values. In this situation, the geometry of the 3D components plays a decisive role, in that the analysis results and the accuracy of the components design are in direct ratio. All the lumbar unit vertebrae were considered to have the same constructional dimensions. The curvature of the spine segment was given by the L3/L4 and L4/L5 associated intervertebral discs. Future work will refine the analysing method results by obtaining the 3D models from CT images, thus the lumbar spine components obtained would behave closer to reality.

References

1. M.I. Creţan, M. Gafitanu, F. Munteanu, The geometrical parameters of the human intervertebral disc measured using CT and Autocad, 7th International Multidisciplinary Conference Baia Mare, Romania, May 17-18, 2007, Baia Mare, 17-18 May, 2007, ISSN-1224-3264
2. T.S. Hin, Engineering Materials for Biomedical Applications, World Scientific Publishing Co. Pte. Ltd, Singapore, 2004, pp. (1-6) - (1-8), ISBN 981-256-061-0
3. S. Kurtz, E. Avram, Spine Technology Handbook. Elsevier Academic Press, , London, 2006, pp. 35-44, ISBN-13: 978-0-12-369390-7, ISBN-10: 0-12-369390-X
4. B.S. Lien, N.H. Liou, S.S. Wu, Analysis of anatomic morphometry of the pedicles and the safe zone for through-pedicle procedures in the thoracic and lumbar spine, European Spine Journal, Vol 16, Number 8, Decembre 2006, pp. 1215-1222, Great Britain, ISSN 0940-6719
5. M.G. Morse, I.A.F. Stokes, J.O. Laible, Role of muscles in lumbar spine stability in maximum extension efforts. Journal of Orthopaedic Research, Vol.13, Issue 5, February 2005, pp. 802-808, ISSN 13802-808, Vermont, U.S.A.
6. A.D. Sculco, Spine Stats, The Spine Journal, Volume 1, Issue 2, March-April 2001, pp. 153, Norwich U.S.A., ISSN 1529-9430

MODELAREA CAD ŞI ANALIZA NUMERICĂ A UNEI UNITĂŢI DE COLOANĂ LOMBARĂ

Rezumat

Lucrarea prezintă modelarea şi analiza cu element finit a unităţii vertebrale lombare (cinci vertebre, patru discuri), luând în considerare mişcarea de extensie a coloanei vertebrale, cu şi fără implant. O primă etapă constă în realizarea şi prezentarea componentelor 3D ce alcătuiesc asamsamblul lombar, urmând a se studia şi evalua stările de tensiuni şi deformaţii ce apar în urma solicitării, prin utilizarea metodei elementului finit, într-o analiză structurală statică. Implantul este intervertebral, cu rolul de a stabiliza coloana, în cazul herniilor de disc. Mediile de lucru utilizate sunt SolidWorks 2007, la partea de proiectare, şi Ansys 11.0, la analiza cu element finit.

Scientific reviewers: **Viorel ŞERBAN, "Politehnica" University of Timişoara, Romania**
Dumitru ŢUCU, "Politehnica" University of Timişoara, Romania

SCIENTIFIC BULLETIN OF
THE „POLITEHNICA" UNIVERSITY OF TIMISOARA, ROMANIA
TRANSACTIONS ON MECHANICS
BULETINUL ŞTIINŢIFIC AL
UNIVERSITĂŢII „POLITEHNICA" DIN TIMIŞOARA, ROMÂNIA
SERIA MECANICĂ
Tom 54 (68) **ISSN 1224 - 6077** **Fasc.4, 2009**

USING FEM ANALYSIS IN ORDER TO CHOSE THE OPTIMAL HIP PROSTHESIS

Mihai Ovidiu GHIBA [*]
[*] Mechanical Engineering Faculty, Bv. Mihai Viteazu No. 1. 300222, Timişoara, Romania, ovidiu@cmpicsu.upt.ro

Abstract. Many studies have shown that femoral and pelvic geometry has a great influence on the distribution and amount of tensions and displacements related to it. This study was conducted on a three-dimensional model (3D) derived from computer tomography images (CT), of the coxofemoral joint of a patient requiring custom made hip endoprosthesis. The results confirmed that the tensions, displacements distributions and values are slightly different from those known in the literature due to the geometry and properties of the material used. Such results were used to run a FEM analysis of a set of three personalized endoprostheses in order to take a decision on the most suitable solution.

Keywords: hip joint, finite element analysis, customized implants, bone modeling

1. Introduction

It is necessary to design better hip endoprosthesis, since hip arthroplasty is one of the most common surgical procedures [4].

The bone rebuilds its structure continuously according to the direction of the loads exerted on it. The bone's stress reduction causes its adaptation to the new conditions manifested by the changing of the mass and of the bone density. The changing of the bone density is very dangerous because it can cause the loosening of the implant. In order to reduce this probability, it must be taken into consideration the behavior of the bone tissue that is in contact with the stem and remodeling the stem until this behavior presents an optimal distribution of stresses. This can be done by running FEM (Finite Element Method) analysis on the implanted femur [5].

To solve the problem of a geometrical mismatch between the anatomic shape of the femoral canal and conventional stems, and to achieve the best possible fit between vital bone tissue and stem surface, a set of three endoprostheses were developed, custom-fitted to the patient's anatomy. For the implantation of these endoprostheses uncemented method was adopted [5, 6].

By using a custom endoprosthesis it can be obtained contact all around the medial and lateral stem in the metaphysis and diaphysis of the femur and it can allow broad stress distribution. This should result in a very high initial stability [6].

The value and distribution of the forces that act upon the femoral head, since they also differ from person to person, were also considered [6].

By combining a custom hip stem with FEM analysis of the hip joint, the behavior of the surrounding bone can be predicted and can highlight the difference between natural and artificial joints. Following this FEM analysis the implant can be redesigned until it achieves optimal results [3, 6].

This paper exhibits the process of design of a real hip joint of one patient along with a set of three custom hip endoprosthesis.

The results of the FEM analysis of the hip joint model were compared with the FEM analysis of the custom hip endoprosthesis in order to decide upon the most suitable endoprosthesis for the patient.

2. Experimental part

2.1. Designing of a hip joint from CT images

CT measurements were performed on a patient in order to acquire coordinates of the points defining the joint shape. The CT images obtained were then processed to filter the required data and detect the joint shape.

The process of the joint shape generation is carried out, with Mimics software (Figure 1).

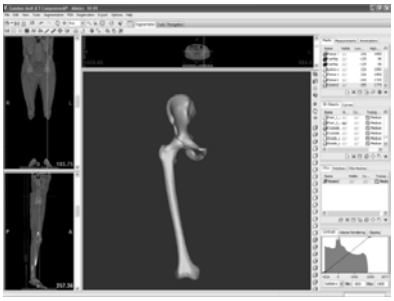

Figure1 The 3D model of the hip joint.

2.2. Designing the endoprostheses

In order to design a personalized hip endoprosthesis the CT data were used to determine its ideal dimensions.

The prosthesis stem design (figure2) consists in defining its contour by using the CAD model of the femur and taking into account the femoral canal. The contour sketches were defined on sections planes of the 3D femur model. A set of three hip endoprostheses were designed.

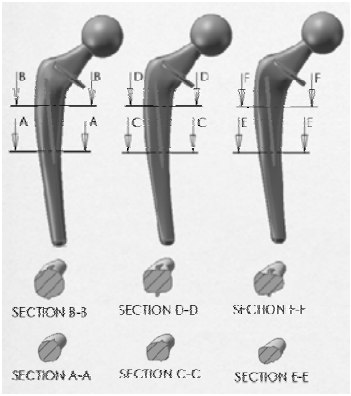

a b c

Figure2 The prostheses design. a) hip stem type 1, b) hip stem type 2, c) hip stem type 3.

2.3. The FEM analysis of the hip joint

The analyses were carried out using Ansys Workbench software.

The 3D hip joint model was divided in eight parts as shown in figure 3 as the trabecular and cortical bone has different properties on the entire length of the femur. By this division, it was possible to assign different material properties for each zone. Each region was assumed to be homogeneous, isotropic, and linearly elastic. The properties of the material of the various tissue regions of a normal hip joint are given in table 1.

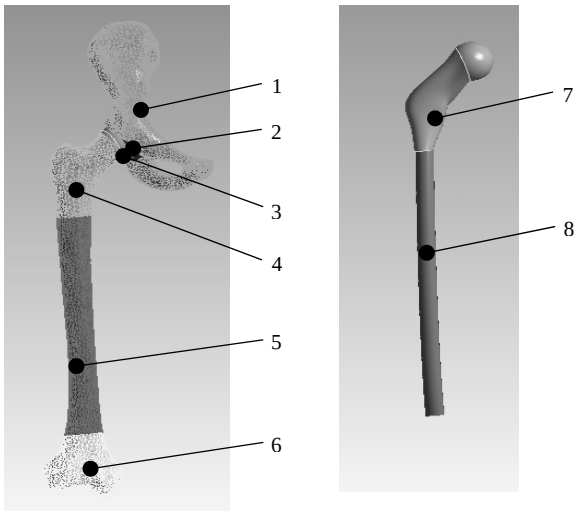

a b

Figure3 The 3D model used for FEM analysis: **a)** cortical bone, **b)** trabecular bone

Table 1. The properties of the materials used for the joint simulation (adapted from Cheng-Kung Cheng and all 2007 and Rusu L 2006) [3, 7].

Region	Young's modul [MPa]	Poisson	Density [kg/m^3]
1	8000	0.3	$1.8*10^{-6}$
4	2000	0.3	$1.8*10^{-6}$
5	1900	0.34	$6*10^{-6}$
6	1900	0.34	$6*10^{-6}$
7	600	0.3	$1*10^{-6}$
8	600	0.3	$1*10^{-6}$
2	15	0.45	$1*10^{-6}$
3	15	0.45	$1*10^{-6}$

The loads of 1840N body weight, 1300N abductor muscle force were loaded to the model on the y direction according to figure 4. Regarding the boundary conditions, the pelvis component was allowed to displace in the sagittal plane only, the distal end of the femur was fixed and the condition between the pelvis and femur cartilages was no separation. These conditions correspond to one leg stance phase of slow gait.

It was chosen this stage because according to Bergmann et all (2001) studies, during this

phase the loading force has the maximum value [1].

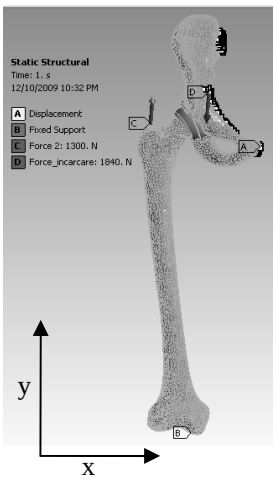

Figure4 The FEM analysis conditions.

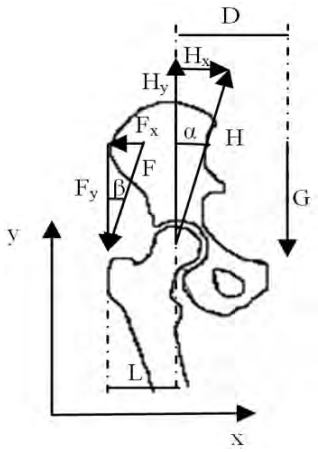

Figure5 Loading scheme of hip joint model according to Brinckmann et all.

The force values were calculated using formules 1, 2 and 3 adapted from *Brinckmann et all (2002*). The formulas below are for loading model from figure 5 [2].

$$G_y = 0.8 \times m \times g \quad (1)$$

$$H_y = -3 \times G_y \quad (2)$$

$$F_y = 2 \times G_y \quad (3)$$

$$F_y + G_y = H_y \quad (4)$$

m = body mass

g = gravitational acceleration

2.2. The FEM analyses of the endoprostheses

These simulations were made in order to predict bone activity after implantation.

The body weight load acting on the femur has the same value and orientation as in the analysis of the hip joint. Also the material properties for the bone are the same as in table 1 region 5 and for the prostheses stems it was used Ti6Al4V properties. These properties were chosen for the bone because it was considered that region 8 will be replaced by stem implant.

Regarding the boundary conditions, the femur was allowed to displace in the sagittal plane only, its distal end was fixed and the condition between the stem and bone was no separation (figure 6).

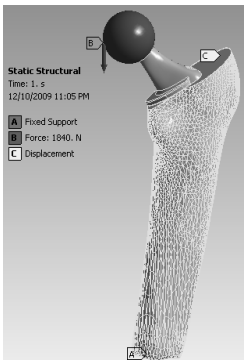

Figure6 Body weight load position.

3. Results

The results of the FEM analysis of the hip joint showed that the maximum equivalent stress was approx 23 MPa, the maximum total deformation 5 mm, the maximum pressure value was approximately 32 MPa for the femur cartilage and 2.4 MPa for the femoral head (Figure.6.a,b,c,d). These values are much lower than those determined experimentally by Bergmann et all (2001) and much higher than those estimated by Cheng-Kung Cheng et all 2007. From figure 6 it can be observed that the values of the equivalent stress and the total deformations for the one leg stance phase of slow gait are very high at the femoral neck level.

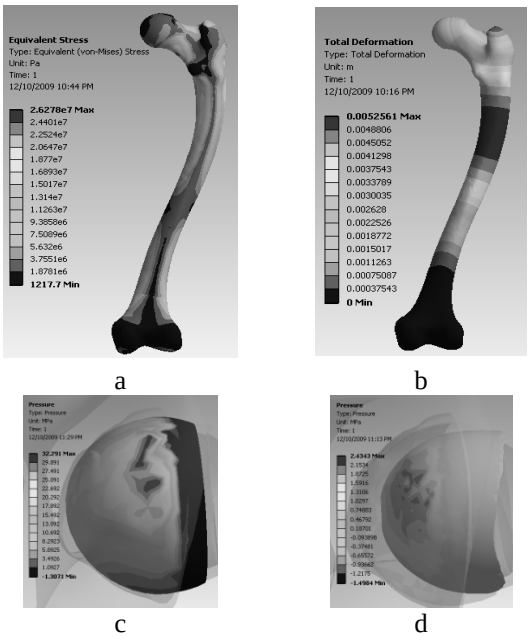

Figure7 Results: a) equivalent stress of the femur, b) total deformations of the femur, c) presure values on the cartilage, d) presure values on the femoral head, e) section view.

The results of the FEM analysis of the hip prostheses are presented as equivalent stress and maximum principal stress distributions in figure 7.

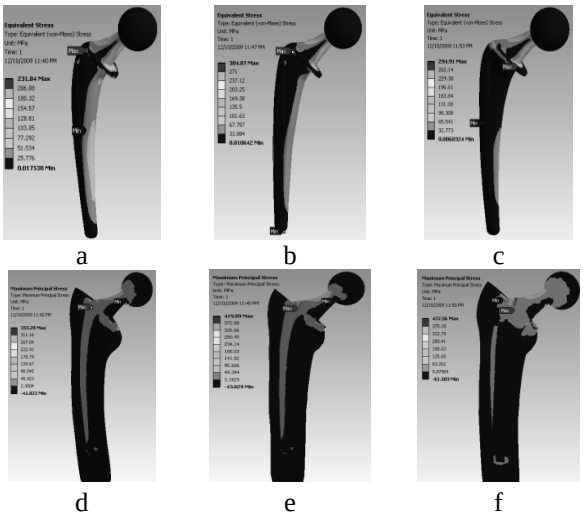

Figure8 Stress distribution. Equivalent stress :a) hip stem type 1, b) hip stem type 2, c) hip stem type 3. Maximum principal stress: d) hip stem type 1, e) hip stem type 2, f) hip stem type 3.

From figure 7 it can be clearly seen that the type 1 prosthesis has the lowest equivalent stress value but type 3 can cause the least bone resorption along the stem because it's maximum principal stress distribution. This distribution is due to the trapezoidal shape of the stem because it is the only factor that differs in the three analyses.

At the neck level of the stem the equivalent forces has a medium value of 210 MPa for hip stem type 1, 180 MPa for hip stem type 2 and 200 MPa for hip stem type 3. These values are very high compared with FEM analysis results of natural joint maybe because of the Ti6Al4V properties.

The results showed that FEM analyses of the hip joint can improve the doctor's decisions regarding the most suitable stem for the patient.

4. Conclusions

This paper presents some solutions regarding the 3D model drawing steps and FEM analyzes.

The FEM analyzes of the customized hip endoprosthesys helped us take better decisions regarding which endoprosthesys is more suitable for the patient.

The simulation was a very helpful and low cost method that helped drawing conclusions about the hip joint and the endoprosthesys.

Future plans regarding custom made implant are to manufacture the implant by using rapid prototyping Electron Beam Melting technology for quick and economical fabrication of custom implant components.

References

1. G. Bergmann, G. Deuretzbacher, M. Heller et. all, Hip contact forces and gait patterns from routine activities, Journal of Biomechanics, Vol.34, No 7, July 2001, pp. 859-871, ISSN 0021-9290, USA
2. P. Brinckmann, W. Frobin, G. Leivseth Musculoskeletal Biomechanics. New York, Ed.Thieme Stuttgart, 2002, pp. 69-75, ISBN 3131300515, 9783131300515
3. C.M. Dijk, R. Bimmel, F.S. Haddad, Surgical approaches in primary total hip arthroplasty, Orthopaedics and Trauma, Vol. 23, No. 1, February 2009, pp. 27-34**,** ISSN:1877-1327, USA
4. M.O. Ghiba, L. Rusu et al., Design process of custom-made femoral stem prosthesis, Annals of the Oradea University, pp. 658-663, ISSN 1583-0691, Romania, 05.2009, Editura Universității din Oradea, Romania
5. M. Pawlikowski, K. Skalski, M. Haraburda Process of hip joint prosthesis design including bone remodeling phenomenon, Computers and Structures, Vol.81, 2003, pp. 887–893, USA
6. L. Rusu, Surgical implants and research studies for approval, "Politehnica" University of Timişoara, Timişoara, Romania, 2006, pp. 41-42, ISBN (10): 973-625-375-9, ISBN (13) 978-973-625-375-1, ISSN 1842-4937 (Romania).

UTILIZAREA ANALIZEI FEM PENTRU ALEGEREA ENDOPROTEZEI OPTIME

Rezumat

Numeroase studii au demonstrat că geometria femurului şi a pelvisului influenţează distribuţia şi valoarea tensiunilor şi deplasărilor care apar la nivelul acesteia. Acest studiu a fost efectuat pe modelul tridimensional, realizat din imagini Computer Tomograf (CT), al articulaţiei coxo-femurale a unui pacient care necesită o endoproteză personalizată de şold. Rezultatele au confirmat faptul că distribuţiile şi valorile tensiunilor şi deplasărilor diferă putin de cele existente în literatură datorită geometriei şi proprietăţilor de material utilizate. Acestea au fost comparate cu cele ale analizei FEM a unui set de trei endoproteze personalizate in vederea luarii unei decizii asupra celei mai potrivite endoproteze pentru persoana respectivă.

Scientific reviewers: **Liviu BERETEU, "Politehnica" University Timişoara, Romania**
Ion DUMITRU, "Politehnica" University Timişoara, Romania

SCIENTIFIC BULLETIN OF
THE „POLITEHNICA" UNIVERSITY OF TIMISOARA, ROMANIA
TRANSACTIONS ON MECHANICS
BULETINUL ŞTIINŢIFIC AL
UNIVERSITĂŢII „POLITEHNICA" DIN TIMIŞOARA, ROMÂNIA
SERIA MECANICĂ
Tom 54 (68) **ISSN 1224 - 6077** **Fasc. 4, 2009**

BRAKE ENERGY RECOVERY TO ELECTRIC LOCOMOTIVES AND DIESEL ELECTRIC LOCOMOTIVES

Georgeta Emilia MOCUTA*, Alexandru POTOCEAN, Ioan Dănuţ DAN****
* Mechanical Engineering Faculty, Timisoara, Bv. Mihai Viteazul No.1, Romania 300222
e-mail: mocuta_ge@yahoo.com, a_potocean@yahoo.com, idd@yahoo.com
** SNTFM SA "CFR Marfă" Timişoara Branch, Str Gării No 1 Timişoara, Romania

Abstract. When a train with diesel-electric or electric locomotive is brake the kinetic energy decrease. This decrease of kinetic energy can be dissipated without being recovered. The challenging alternative is to use the braking energy on board transformed in another energy type. This energy can be either immediately reused or it is stored for later use. It presents new technologies for applying braking energy recovery both on board and at loconotivei fixed installations for electric locomotives.

Keywords: diesel electric locomotive, electric locomotive, brake, recuperative brake

1. Introduction

When a vehicle (diesel-electric or electric) is brake the kinetic energy decrease. This decrease of kinetic energy can be dissipated without being recovered.

The quantity of decrease energy in the braking time is expressed like lost power. So for any vehicles type this lost power during braking processes is 20-40% of mechanical tractate power. It is very important to apply a method of recovered this energy.

The challenging alternative is to use the braking energy on board transformed in another energy type. This energy can be either immediately reused or it is stored for later use (Table 1).

Electric and diesel-electric locomotives use electric traction motors attached to the axles to apply tractate force to the wheels. An electric motor can act as generator when a magnetic field is present and a rotational force is applied to the rotor.

During braking the rotors of the electric motors are allowed to rotate and produce electricity.

There are several commercially viable energy storage systems that are being developed.

The types of devices that hold the most promise to solve the energy storage problems are batteries, flywheels, and ultracapacitors.

Batteries (or accumulators) are electrochemical energy storage devices used for a wide variety of purposes. Compared to other storage devices batteries have very high energy densities, but low power density and therefore high charging times.

Some modern high performance batteries do however reach power densities that are promising for braking energy storage in automotive and (to a smaller extent) railway applications.

The fly-wheel is an electro-mechanical energy storage system based on rotating masses. It is a powerful storage technology which may be

used both for on-board and for stationary applications.

Double-layer capacitors (also named "supercapacitors" or "ultracapacitors") store energy in the electric field of an electrochemical double-layer.

The use of high surface-area electrodes results in an extremely large capacitance.

The power and energy densities make capacitors an option for brake energy storage in rail vehicles.

Table 1 Energy recovering in diesel electric and electric stock.

Manner of use from braking processes	Immediately use	Later use
Electric locomotive	The electrical energy generates in the brake process and recovered can either be transmitted trough overhead catenary's wire or an electrified third rail figure 1 [4]	The electricity generate in brake process is transmitted trough overhead catenary's and is stored in fixed installation each time a vehicle brakes and reduce it during acceleration. Later is used by follow stock in way [5] (figure 2)
		The electricity can be stored on board of the electric locomotive in an energy storage system and later used (figure 4)
Diesel electric locomotive	The energy recovered in brake process do supplies the auxiliary installations on board.	The electricity generate in brake process is stored on board in an energy storage system. The structure of the storage system is with one of the elements a) Supercapacitors b) Batteries c) Flywheels d) Hybrid storage Characteristic for various energy storage devices is Plot of energy versus power

2. Energy saving potential in railway transport

Electrodynamics braking is the main braking technique used for modern electrically - driven locomotives. High accuracy of braking force regulation helps decrease longitudinal dynamic forces developed in stepwise pneumatic braking.

When locomotives use regenerative braking of high-speed trains under the conditions of heavy railway traffic allows 25–40 % of electric power to be returned to the power system.

The required braking forces can be obtained in a wide range, with regeneration braking used in a high-speed range and rheostat braking, in a low-speed range.

Mechanical braking, commonly used now, should be kept in reserve as a technique duplicating the main braking method and used to completely stop a locomotive when its speed is 5–2 km/h.

In upgrading the infrastructure and technical equipment of railways, the influence of electrodynamics braking of the elements of infrastructure should be taken into account.

The demand peaks are cut down by the use of a storage system.

This saves energy costs, not only due to a reduced energy demand but due to a price effect as well [1, 2].

The energy price is determined by electricity suppliers in a way that basic demand is much cheaper than peak demands.

Therefore, a smoothened power demand substantially reduces the price per kWh.

The electricity generate in the brake process recovered transmitted trough overhead catenary's (figure 1) [3, 4]

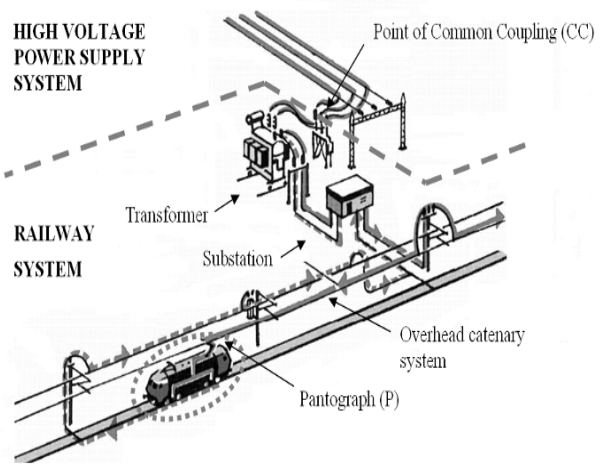

Figure 1: Sketch of system boundaries

The electricity generate in brake process is transmitted trough overhead catenary's and is stored in fixed installation each time a vehicle brakes and reduce it during acceleration. Later is used by follow stock in way (figure 2).

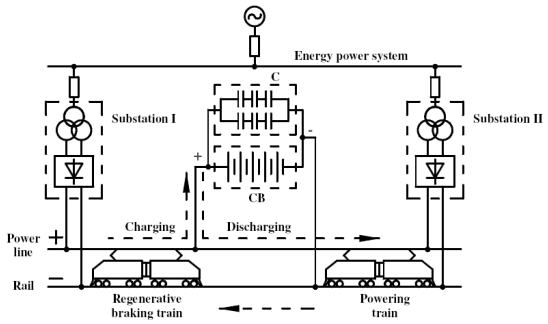

A circuit diagram of using regenerative braking returning energy: C – capacitors; CB – conventional batteries

Figure 2 The electricity generate in brake process stored in fixed installation [5]

3. Recovering braking energy and storage on-board of the stock

Conventional diesel locomotives that are by powered electrical transmission cannot use brake energy. The main energy losses in such a system are essentially due to two elements.

The first one is the thermal engine itself, as the conversion of chemical energy to mechanical energy leads to efficiency near of 40%.

Moreover, as the thermal engine has to work in a very large range of power, strong speed/torque variations lead to difficulties in having a thermal engine able to work on its maximal efficiency point, and at its lowest pollutant emissions level [3, 5].

In railways transport for recovering braking energy and storage on-board of the stock (diesel-electric and electric) DC link will be a supply for energy storage device (figure 3 and 4).

Especially in DC system, where energy losses in the distribution network are high, this could be an interesting alternative to feeding back energy into the supply system [9, 10, 11]. Furthermore reduced peak load is beneficial for system capacity, voltage stability and energy costs.

Even if losses due to elements in the energy transfer chain cannot be neglected (mechanical losses, losses into the various power converters), the second main "losses generator" is the braking system. A part of these losses are due to conventional mechanical brakes, but most of the losses are operated into braking resistors. Note that this last property consists in converting mechanical energy of the train in electrical energy again, and then in warm.

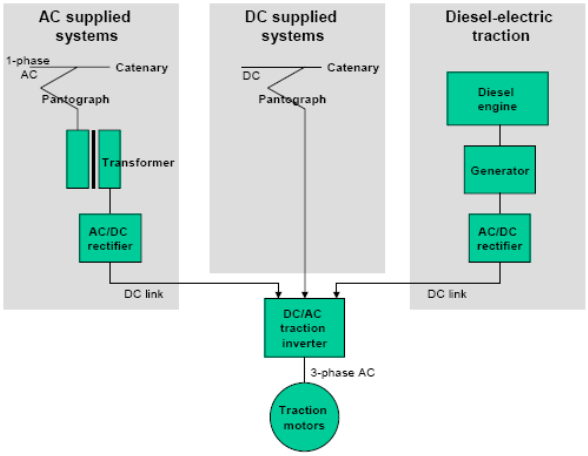

Figure 3 Principle of (electric or diesel electric) vehicles with electric traction motor without energy storage device

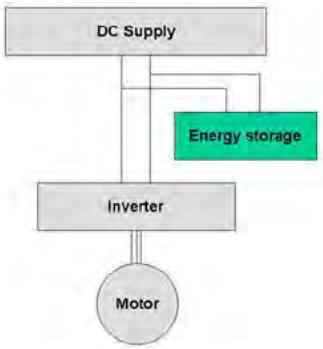

Figure 4 Energy storage devices on board of vehicle

In order to increase the efficiency of diesel-electric trains, a first approach consists in the analysis of a direct mean that allows saving of energy. As the DC-DC converters that supply the electric motors of the train are generally reversible, the solution that consists in replacing braking resistors by any storage system appears to be the most evident. In this case, the system should be adapted.

Replacing braking resistors with storage devices compared to the initial solution braking resistors have been replaced by storage elements.

As energy should be stored during braking, and restored during the acceleration of the vehicle, energy flows must be bidirectional between the DC bus and the storage tank. This is the reason why the initial nonreversible DC-DC converter must be replaced with a reversible one. In this case, it is obvious that power constraints on the diesel engine can be minimized during accelerations, as the needed power can be partially provided by the storage system.

Regarding the choice of storage elements, various properties should be matched. The storage system has to be power compatible, especially regarding the instantaneous power needed for railway traction application.

Power compatible means a high efficiency during charges and discharges. In extreme cases, the peak power that the storage should assume must correspond to the maximum power needed for the traction, when the diesel engine is switched off.

For better energy efficiency it use brake energy with energy storage devices battery, super-capacitors, flywheels, hybrid storage, etc.

It supposes an efficient energy management on board of diesel-electric locomotive [5, 7].

During braking phases the kinetic energy of the vehicle is transformed into another form of energy (e.g. electrostatic energy in the case of a capacitor) and stored in the storage device. When the vehicle stands still the energy storage device should be fully charged to be able to deliver energy during the subsequent acceleration phase.

The power supply during acceleration is supported by the stored energy. The energy management system should be designed in such a way that the external energy supply never needs to deliver the full accelerating power - important condition to down size energy supply.

When driving at maximum speed the storage device should be completely discharged.

Regarding energy storage technologies, batteries are not good candidate as their lifetime and number of cycles are strongly reduced compared to the general lifetime of railways applications.

4. New technologies for energy storage device

Storage elements must have the properties like:

- can store the entire amount of braking energy
- the storage system must be power compatible to the energy needs for railway traction application (train stops, speed limitations, start up).
- is desirable to have high efficiency during charges and discharges.
- the storage device should have the volume adequate on board of diesel electric locomotive including electronic device.(it is an important restriction in many cases) .
- The energy storage system is considered as an energy buffer, dedicated for smoothing power constraints on the resized diesel engine.

Two technologies appear to be energy and power compatible with such an application, supercapacitors and flywheels [8, 9, 10, 1, 12]. Both of these two technologies offer also the largest lifetime.

However, flywheel technology needs strong mechanical developments and maintenance, while supercapacitors manufacturers are able to propose complete storage system including the components themselves and the electronics needed for the symetrization and the monitoring.

Moreover, the number of cycle and the lifetime of supercapacitors seem to be compatible with traction applications.

In [6] it is compare the standard diesel-electric unit (Altaria) with the trains were built by Patentes Talgo, Spain (coaches) and Alsthom-Macosa, Spain (locomotives T26TW licensed by General Motors). The comparison between supercapacitors (SC) and batteries in this case will only be valid for the chosen itinerary Albacete-Cartagena. Obviously, the same simulation method can be applied to analyze other railway lines. Table 2 presents the main characteristics of supercapacitor and battery energy storage systems used in this study case[1].

Table 2 Caracteristics of battery and supercapacitors [6]

Parameter	Battery	Supercapacitors
Energy [Wh/kg]	10-600	1-10
Number of cycles	1000	500 000

It is interesting to focus on hybrid dieselel-ectric train with battery and supercapacitors [7, 8].
Recently appeared the hybrid locomotive that has 2 sources of power (one source can be a diesel engine and the other can be electric motor supply from battery, capacitors etc.)

5. Conclusions

New technologies for the recovery of braking energy are evolving mainly because inducing a primary energy saving and thus protects the environment.

References

1. L. Accardo, Ansaldobreda, On board Efficient Energy Management, Energy Efficiency Days 2009, in Tours/France
2. E, AGENJOS, S, VALERO, U. M,l Hernandez, A, GABALDON, M, ORTIZ F, G. FRANCO, R, MOLINA, R, J.

[1] The batteries considered are lead acid, NiCd, and gel technologies from the manufacturer SEC Industrial Battery, (UK). The supercapacitors chosen for that application were BCAXX form Maxwell Technologies, USA.

GABALDON, "Energy Efficiency In Railways: Energy Storage And Electric Generation In Diesel Electric Locomotives "20th International Conference on Electricity Distribution Prague, 8-11 June 2009
3. Ph. Barrade, A. Rufer, "High-Power Fast Energy Exchange between Storage Systems: Supercapacitors as energy buffer in transportation systems", EVS-18: The 18th International Vehicle Symposium, 20-24 October 2009, International Congress Centre (ICC), Berlin, Germany
4. Ph. Barrade, A. Rufer, Current capability and power density of supercapacitors: considerations on energy efficiency, EPE 2003 : European Conference on Power Electronics and Applications, 2-4 September, Toulouse, France
5. M. Bergendorff – Macroplan, Railenergy - Energy Efficiency Days 2009. in Tours/France
6. J.N. Buurgaard, H.P. (Huib) van Essen, L.C. (Eelco) den Boer, Tracks for saving energy, Energy saving options for NS Reizigers Delft, CE, July 2005 (Publication number: 05.4878.30 CE-publications are available from www.ce.nl)
7. L. LIUDVINAVICIUS, L. P. LINGAITIS, "New Technical Solutions of Using Rolling Stock Electrodynamical Braking", Transport Problems (Problemy Transportu) 2009, Volume 4 Issue 2 pp. 23-35
8. S. Pay, Y. Baghzouz, Effectiveness of Battery-Supercapacitor Combination in Electric Vehicles, IEEE Bologna, Power Tech Conference, June 23th – 26th, 2003
9. A. Schnewly, R. Gallay, "Properties and applications of supercapacitors – From the state-of-the-art to future trends", PCIM2000 Power Quality, Nürnberg, Germany
10. M. Steiner, J. Scholten, Energy Storage on Board of DC Fed Railway Vehicles, 35th IEEE PESC Conference, 21-24 June 2004, Aachen, Germany
11. D. Vastel, SNCF Energy Saving Program, Energy Efficiency Days, sept 24th 2009, in Tours/France
12. *** UIC CODE 345R Environmental specifications for new rolling stock, 2006, 1st edition, pp.21-22.

RECUPERAREA ENERGIEI DE FRÂNARE LA LOCOMOTIVELE ELECTRICE ŞI LA LOCOMOTIVELE DIESEL-ELECTRICE

Rezumat

Atunci când un tren cu locomotivă diesel-electrică sau electrică este de frânat, o dată cu scăderea vitezei apare şi scăderea energiei cinetice. Această scădere a energiei cinetice poate fi disipată fără a fi recuperată. O alternativă este aceea de a recupera şi utiliza energia de frânare care la bordul trenului este transformată într-un alt tip de energie. Această energie poate fi fie reutilizată imediat, fie stocată pentru o utilizare ulterioară.

Se prezintă noile tehnologii de aplicare a recuperării energiei de frânare atât la bordul loconotivei cât şi la nivelul instalaţiilor fixe în cazul locomotivelor electrice.

Scientific reviewers: **Ioana IONEL, "POLITEHNICA" University of Timişoara, Romania**
Inocenţiu MANIU, "POLITEHNICA" University of Timişoara, Romania

SCIENTIFIC BULLETIN OF
THE „POLITEHNICA" UNIVERSITY OF TIMISOARA, ROMANIA
TRANSACTIONS ON MECHANICS
BULETINUL ŞTIINŢIFIC AL
UNIVERSITĂŢII „POLITEHNICA" DIN TIMIŞOARA, ROMÂNIA
SERIA MECANICĂ
Tom 54 (68) **ISSN 1224 - 6077** **Fasc. 4, 2009**

GENERAL PRINCIPLES OF ERGONOMICS WITH DIRECT APPLICATION IN WELDING ENGINEERING

Mihaela POPESCU*, Ionuț Marius DANCIU*, Cosmin CODREAN*, Ionuț Dragoş UȚU*
*Mechanical Engineering Faculty, No 1, M. Viteazul Bvd, 300222, Timişoara, Romania
e-mail: mihaela.popescu@mec.upt.ro, imdanciu@yahoo.com, cosmin.codrean@mec.upt.ro, dutu@eng.upt.ro

Abstract. Ergonomics as a science describes the reaction possibility, but also the limit of the operating personnel in its activity, the optimum adaptability of the operating personnel to the working conditions during the service. The welding operation is a demanding profession which imposes a sure hand, total concentration to the working object, and experience in the work, reflected in a lot of skill. The principles of ergonomics, applied in welding lead to the performance, economic efficiency, productivity and all these respecting the quality assurance and the environment protection.
The simple design adapted to logical adjustments, intelligent programs and extreme flexibility of welding equipment of the last generation are only some elements of applying the principles of ergonomics in the field of welding [1-13].

Keywords: ergonomics, welding, musculoskeletal, disorders

1. Introduction

Welding has a strong interdisciplinary impact in its studying and applying interfere numerous science and subjects. If generally the preoccupations are related to the technological side, recently, even representative companies offering welding equipment, accessories, clothes, shoes etc., on the market, insist on adapting them to apply the principles of ergonomics [1, 2, 3, 4, 7, 10, 13].

2. Ergonomics in Welding Industry

The trend towards mechanization and automation in the welding industry is, in part, based on ergonomic concerns. Designing an ergonomic work place is a profitable investment from the economic point of view. Developing preventive ergonomic action leads to improvements such as higher productivity, less absenteeism, and more self-satisfaction of the welders. Ergonomic investigations require a thorough knowledge in various fields, especially physiology, psychology, sociology, technology and economics [2, 4, 6, 3].

3. European Welding Federation

European Welding Federation, as international forum in the field of welding has constant preoccupations in ergonomics, which are illustrated in Table 1.

4. Ergonomics in the Welding Environment

Productivity or quality of work is the decisive factor in marketing ergonomics. Quality tools should be designed from the starting point of adjusting tasks and equipment to human possibilities and limitations. Companies should consider an investment in ergonomic equipment as a profitable addition to indispensable productive machinery.
Ergonomics is also called human factors engineering (HFE). It involves making the workplace fit the needs of workers [13].
Ergonomics focuses on chaining things - tools, equipment, facilities etc. but not chaining people (figure1).

Table 1 Risk levels – Accidental events – EWF SMS

Material Management						
Material manipulation	Musculo-skeletal overloading	Musculoskeletal disease	low	low	tolerable	Maintaining the current safety system
	Falling of heavy objects from the working table	Body injury	low	medium	moderate	Provide the adequate fixing of heavy objects
	Dangerous objects and materials	General or local wounds	medium	low	moderate	Informing the personnel and maintaining the equipment
Gas cylinders management and storage	Leeks, fire, explosions	Internal and external injury of the body	low	high	moderate	Periodical monitoring change all cylinders
Gaseous/ liquid fuel management and storage	Leeks, fire, explosions	Internal and external injury of the body, skin burning	low	high	elevated	Production stop and secure containers system
Material preparation						
Preparation of the joint by electric arc cutting process	Body contact with high temperature objects	Second degree burnings	low	medium	moderate	Assure the working zone with adequate signals in order to wear the safety equipment (for example gloves)
	Non ionized radiation	Damage on eyes and skin	low	medium	moderate	Increase the number of protection screens to increase the protection degree of the working area.
Preparation of the joint and mechanical processing	Moving components (rotors, grinders, cutting tools, etc.)	Body injury	low	medium	moderate	Use of personal protection equipment; assure maintenance equipment
	Noise	Loss of hearing (total or partial, temporary or permanently	medium	low	moderate	Assure the information of the personnel; use of personal protection equipment

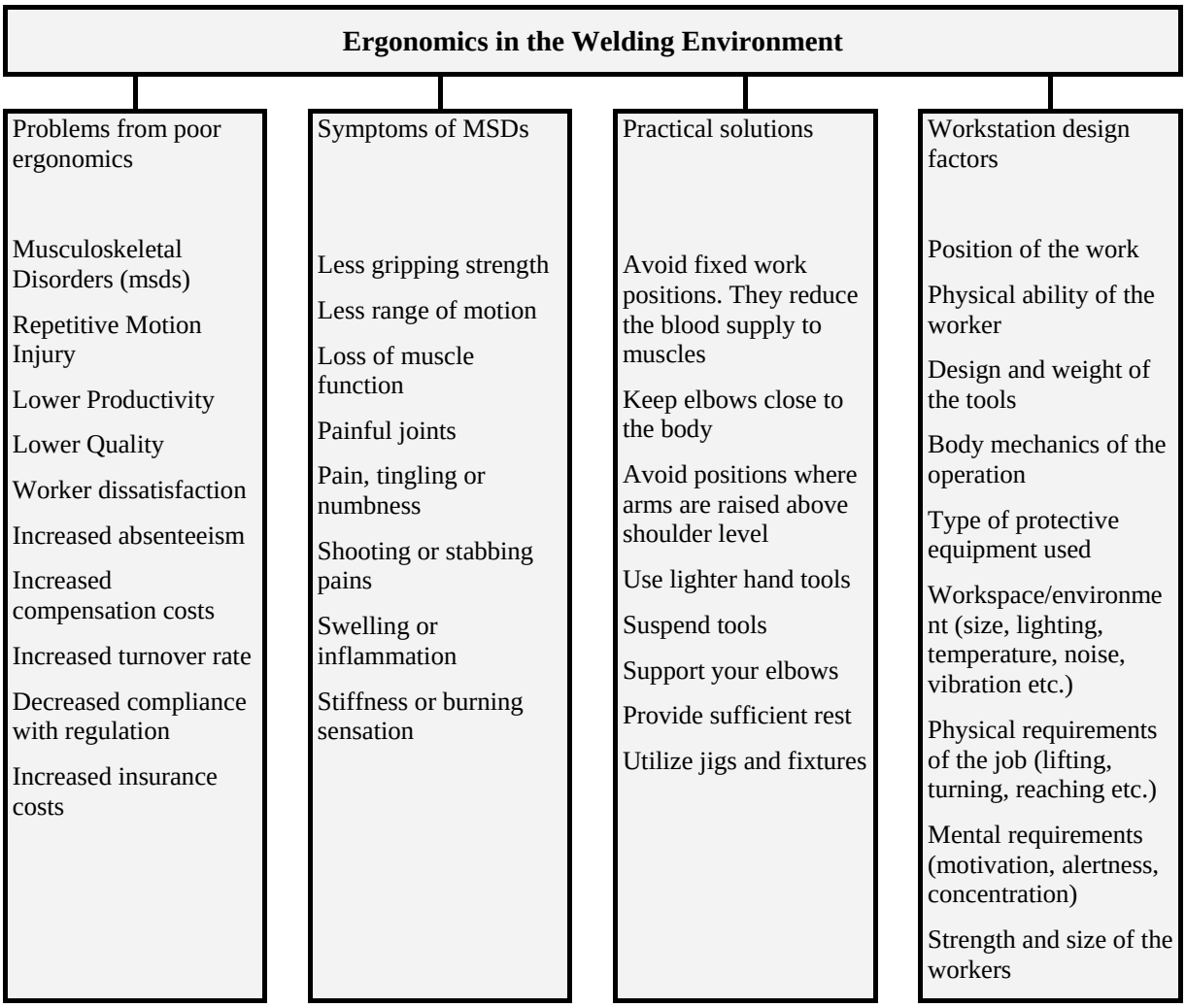

Figure 1 Ergonomics focuses

5. Action Plans to Implement Solutions coming out by Applying Ergonomic Principles

The research developed in the field of ergonomics knows a special dynamic, but a general priority element is noted, namely there is a preoccupation to minimize risks and professional illness, by conceiving secure, comfortable products, processes and systems, therefore adapted to the human operator, his skills, but also his limits. Adapting the welding operators to the environment conditions is an essential real problem, which join biological, psychological and social aspects.

Welding processes in their development, have as preoccupation and objective the correct location of welding equipment (in the technological flux) as they interfere, as distinct stages, in the technological itinerary, at the corresponding height for the operators, due to the static positions in prolonged periods, repeatability of some operation-actions, in order to avoid musculoskeletal disorders, correct ventilation of the working places, corresponding lightening at the desired level and from the right direction etc.

Diseases related to work that affect so many welders due to the working positions they have to adopt and difficulties they face to access the working place (figure 2).

Applying action plans consists in:

- Looking for activities indicators, by observing welding activities, risk factors, the moment the fatigue state of welding operators appears, the implications it has on welders, changes in the used tools, the moment the absenteeism at the working place appears with implications on the production cut, of the discontinuities it creates etc.
- Forming of action and designation "Ergonomic groups" and "Ergonomic contact point".
- Use of assessment instruments.
- Draw up lists of risk factors and their periodical checking etc.
- Improving the working place conditions

which had to become an absolute priority.

- Considering the frequency and severity of risk factors, the frequency and severity of "complaints", of potential injuries, of proposals and ideas coming out from those working in direct production, of difficulties in making improvements.
- Operation of improvements and improvement as regards the correlation between the working place requirements and their capabilities.
- Discussing with the employees, on different stages of professional hierarchy, contacting other industries, using INTERNET resources, consulting experts in ergonomics.
- Watching, IF each improvement brought reductions as regards the risk factors, fatigue of operators, discomfort or injuries symptoms, IF each improvement was accepted by the personnel, IF eventually some improvements created new risks or other problems, IF some improvements had an impact on production or on quality, IF improvements were implemented by training etc.

6. Possible Ergonomic Improvements

As regards the possible ergonomic improvements the following are to be imposed

- Measures to lift weights: manipulators, lighter welding equipment, with reduced rigidity or welding cables on transmission wheels/pulleys, use of cable supporting devices (balance levels); use of lifting and rotating tables.
- In order to avoid impossible positions: working position between waist and shoulder is to be used when possible, use of lifting tables and monitored positioning devices, rotating chairs.
- Use of equipments to pre-assemble and manipulation of materials, which help in reducing not necessary lifting or of any kind of material, for example rotating hooks for pipes.
- Robot automation is such a feasible solution for repetitive movements, with arms and hands. So, the fume exposure of operators is also reduced.

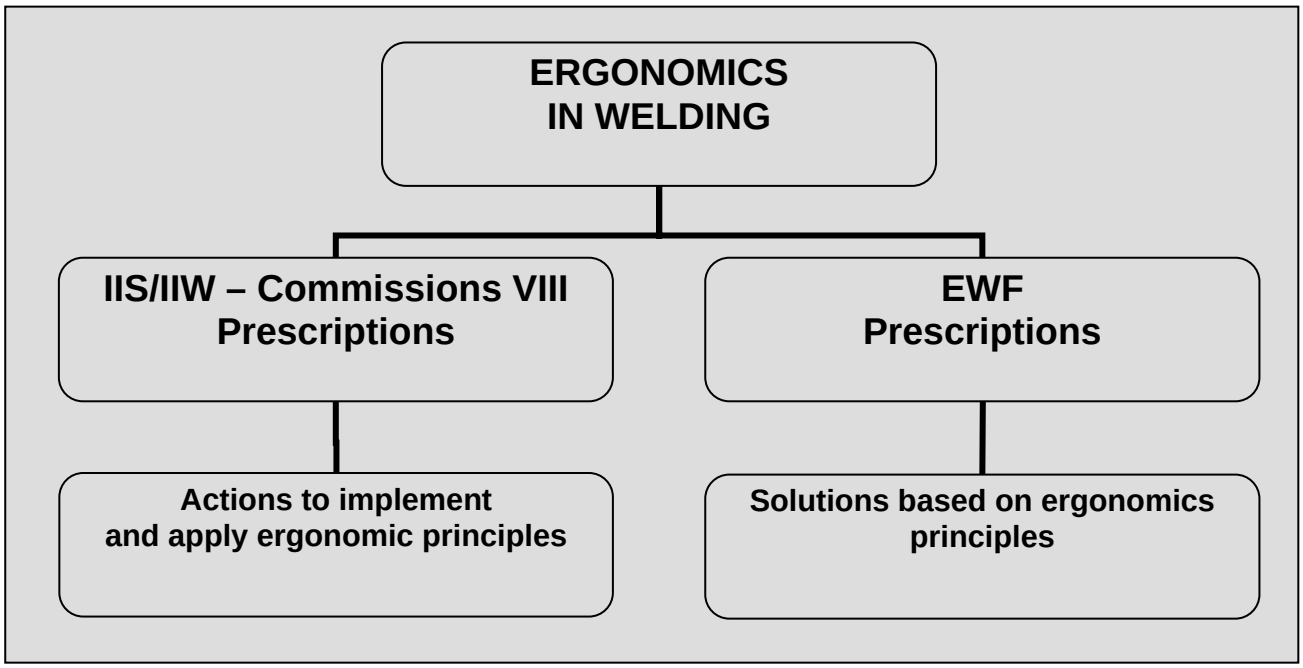

Figure 2. Actions – Solutions in ergonomics welding

7. Conclusions

The preoccupations of the International Institute of Welding (IIS/IIW) and of the European Welding Federation (EWF) are presented, preoccupations existing in the field of standardization: ergonomics – welding, respectively.

A key element, in implementing ergonomic

solutions in welding, is the training in the field, too for all interested factors, in exploitation, from manager, supervisors, professional staff at different levels, to the welding operator, from designers to welding equipment producers, accessories, devices, clothes, helmets etc.

Current hot topics include the need for effecting ergonomic changes to improve efficiency whilst preventing the work-related musculoskeletal disorders which affect so many welders because of the work positions they have to adopt and difficulties they face in achieving access and regress, e.g. in the double bottom of ships [1÷13].

References

1. F. Colombo, Ergonomia e organizzazione del lavoro, Rivista Italiana Saldatura, 2006, No. 6, novembre/decembre, pp. 817-822, ISSN 0035-6794
2. A.Draghici, Ergonomie, volI, Noi abordări teoretice şi aplicative, Editura Politehnica, Timişoara, 2006, ISBN 973-625-270-1
3. L. Gonnet, L., Toward An ergonomic design of welding stations, DOC IIW/IIS-K101-95
4. L. Gonnet, Vers une conception ergonomique du poste de soudage, Soudage et Techniques Connexes, 1994, vol. 48, No. 3-4, pp. 33-40, ISSN 0246-0963
5. G. Iosif, A.M Marhan, Ergonomie cognitivă şi interacţiune om –calculator, Editura Matrix Rom, Bucuresti, 2005, ISBN 973-685-923-1
6. P. Holstein, How to choose ergonomic hand tools, WELDING JOURNAL, 2009, vol.88, march, No.3, pp. 90-91, ISSN 0043-2296
7. R. Jastrzebski, M.Godniak, T. Skakug, A. Stencel, A Trojnack, L'application de la psychologie cognitive et de la mécanique des mouvements musculaires à l'entrainement des soudeurs, Soudage et Techniques Connexes, 2001, nov./dec., pp. 47-51, ISSN 0246-0963
8. M.R. Johnsen, Ergonomics: The Best Fit for Safety, Welding Journal, 1998, vol. 77, Oct., No. 10, pp. 45-48, ISSN 0043-2296
9. R. Kadefors, Ergonomic standardization and welding, DOC IIW/IIS-1995-05
10. R.Kadefors, Welding and ergonomics, Australasian Welding Journal, 2006, vol. 51, No. 1, pp. 22-23, ISSN 1093-0642
11. M.Pankratz, D. Dorn, Workplace safety: The human factor, Welding Journal, 2004, vol.49, september ,pp.32-35,ISSN:0043-2296
12. M. Parnianpour, L.M. Lai, A Shirazladl, Development of an interactive multimedia training tool for management of work related musculoskeletal disorders of shoulder in welding, Integrated Design and Process Technology, 1998, vol. 1, pp. 68-75, ISSN 1090-938
13. M. Popescu, C. Marta, C. Rădescu, I.M. Danciu, Welding and ergonomics. Case studyes, RADMI 2009 ,9-th International Conference "Research and Development in Mechanical Industry,16-19 Septembre 2009, Vrnjacka Banja, Serbia, ISSN 0354-6829

PRINCIPII GENERALE DE ERGONOMIE CU APLICABILITATE DIRECTĂ ÎN INGINERIA SUDĂRII

Rezumat

Ergonomia ca ştiinţă descrie posibilitatea de reacţie, dar şi limitele personalului operator în activitate, respectiv adaptabilitatea optimă a personalului operator la condiţiile de lucru din exploatare. Sudarea în sine este o profesie solicitantă care impune o mână sigură, concentrare totală la obiectul muncii, rutina şi experienţa în muncă, reflectată în multă îndemânare. Principiile ergonomice, aplicate în sudură, conduc la performanţă, eficienţă economică, productivitate şi toate acestea în condiţiile asigurării calităţii şi a protecţiei ambientale. Design-ul simplu şi adaptat cerinţelor, reglajele logice, programele inteligente şi extrema flexibilitate a echipamentelor de sudare de ultimă generaţie sunt doar câteva elemente ale aplicabilităţii principiilor ergonomiei în sudură.

Scientific reviewers: **Emilia Georgeta MOCUŢA, "Politehnica" University of Timişoara, Romania**
Aurel RĂDUŢĂ, "Politehnica" University of Timişoara, Romania

NEWS

The book **MACHINES AND ADVANCED PROCESSING SYSTEMS**, author Lecturer PhD Eng. ADRIAN BUT, appears within POLITEHNICA Publishing House from Timisoara.

It reunites two bases elements which are relatively distinct: the machine tool in the present case the CNC processing Centers and the processing system, underlying the close link between these by the scope it follows, namely the realization of a competitive product, respectively the obtaining of an efficient interaction of the process assembly – processing equipment. emphasizes on the necessity to automate processing procedures, a reference element in the integration development process. It can be done by using computer assistance in the processing subsystems, logistics and control, by a flexible fabrication system. It insists on the processing subsystem which is represented as a bases cell of advanced production systems.

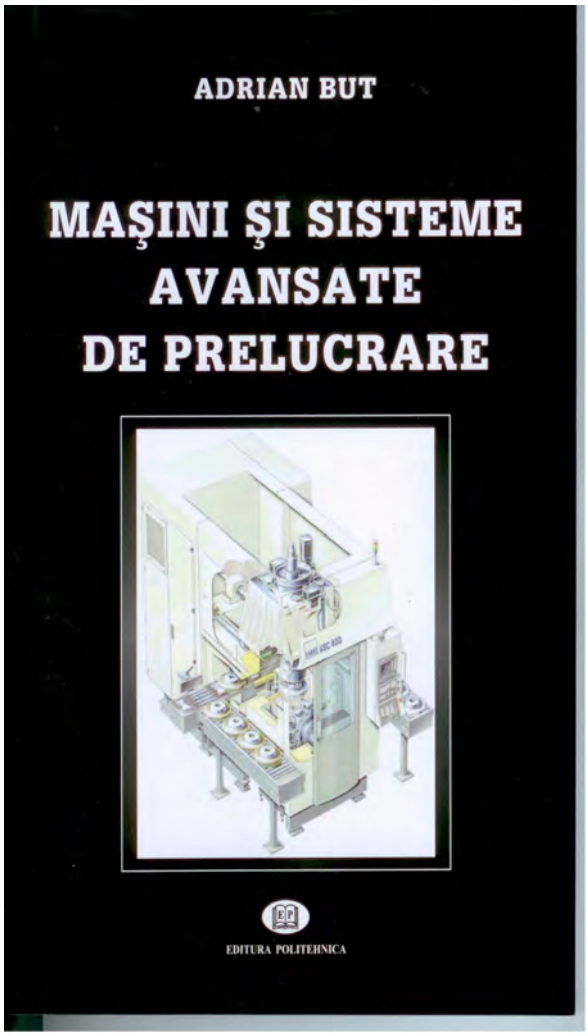

The book was structured on 8 Chapters as it follows:

1. Production process, the bases of advanced processing systems
2. Automated flexible production
3. Programmed control systems
4. Structure of advanced processing systems
5. Transport systems for components
6. Integrated systems
7. Flexible fabrication systems
8. Examples of advanced fabrication systems

The book addresses to technical staff directly interested in assuring competitive technological processes, but also to those that coordinate-organize, plan a modern, competitive production.

The book with the title **INTEGRATED MAINTENANCE OF MUNICIPAL WASTE**, authors Prof. PhD. Eng. CORNELIU UNGUREANU, Prof. Habil PhD. Eng. IOANA IONEL, Assoc. Prof. PhD Eng. PAUL DAN OPRISA STANESCU, Asist. PhD Eng. VASILE GRUESCU, appears within POLITEHNICA publishing House from Timişoara.

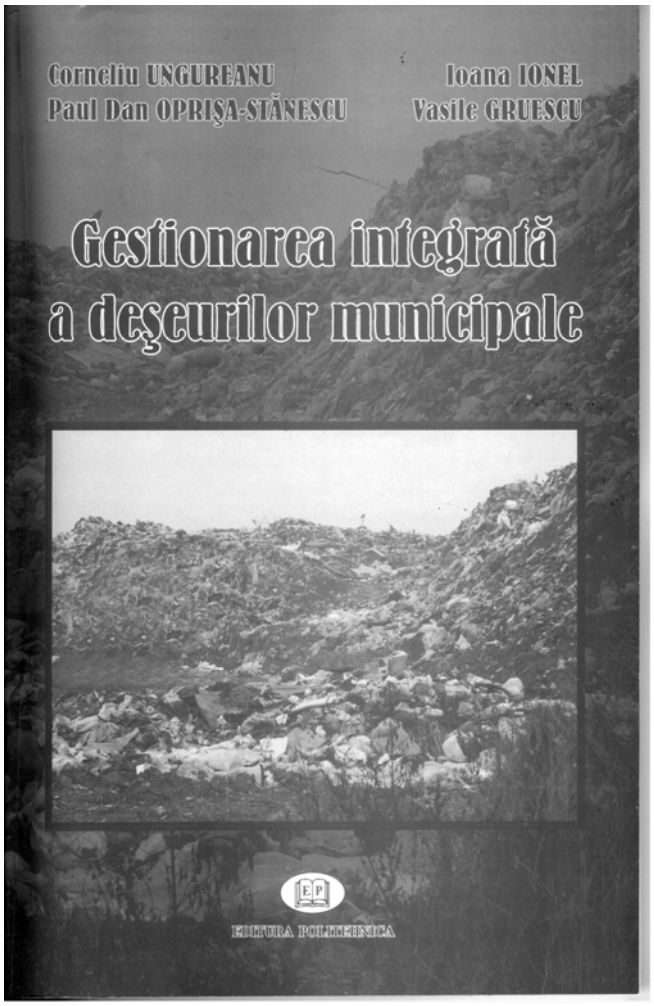

It addresses to those interested in protecting the environment, by a correct management of solid waste. It shows that it is more economic to prevent waste and then materialize them, before storing them ecologically. The use of waste, by recycling and as energetic resources, is extremely important and possible from technical point of view.

The book is structured on 9 chapters as it follows:

1. Introductive notions
2. Characteristics of municipal waste
3. Collecting and transport of municipal waste
4. Storing solid municipal waste
5. Punching
6. Incineration of solid municipal waste
7. Notions on thermal calculus of incinerators
8. Reduction of polluant emissions
9. Modelling gases treatment in the 100t/h owen

The book is conceived to be accessible, as technical information, and brings a novelty in the field, theoretically and classically, as well as from described applications. It consist legal information related to legislation, but also numerous technical applications, representing the state of the art in the field of durable development.

❖

This paper consists in theoretical and practical elements accumulated in design workshops and casting workshops. It addresses to students as well as engineers in the field.

The Scientific Bulletin of the Faculty of Mechanics within POLITEHNICA University of Timişoara, as it was in 1929. This is a copy of the cower who are existing in the archives of the Faculty of Mechanics.

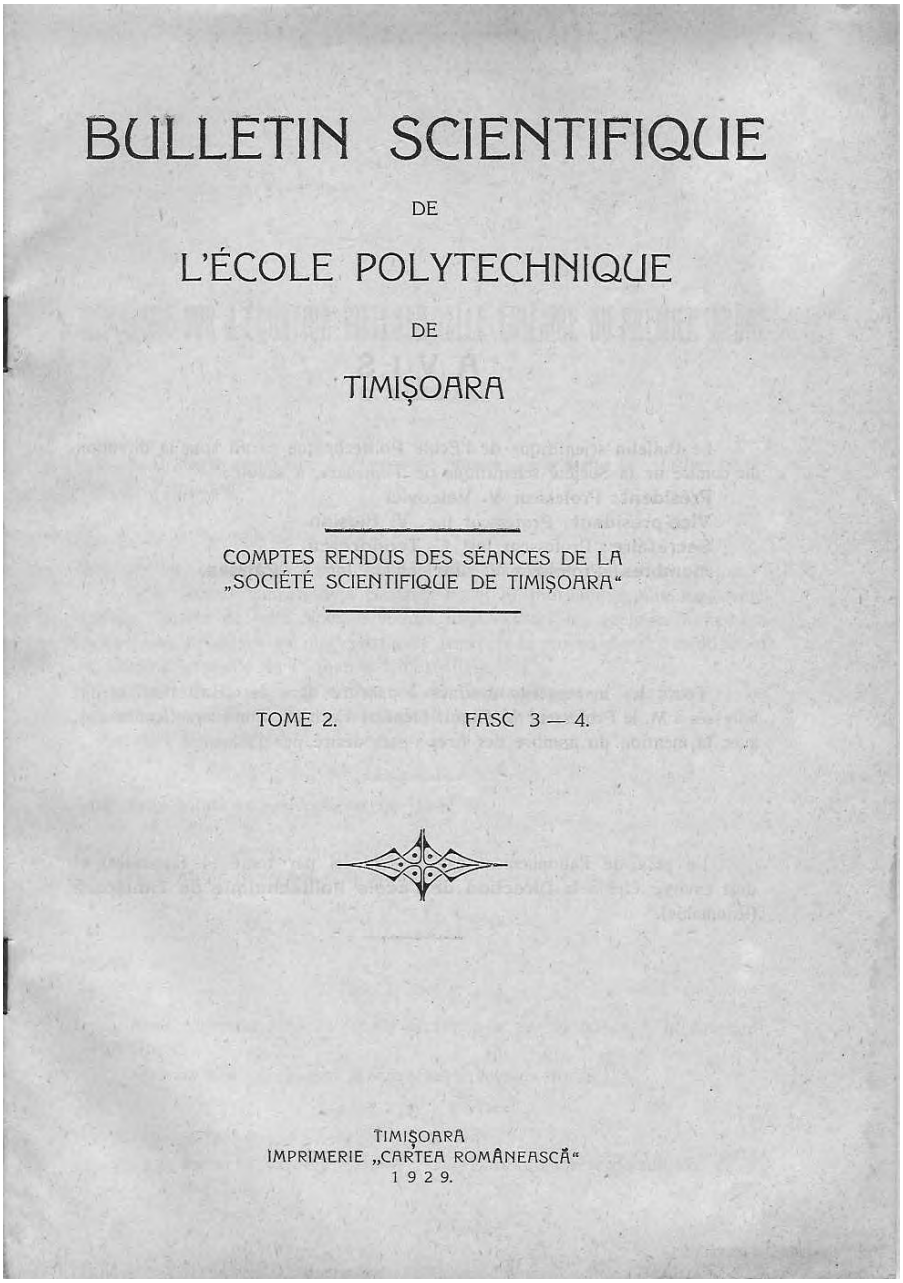

BULLETIN SCIENTIFIQUE

DE

L'ÉCOLE POLYTECHNIQUE

DE

TIMIŞOARA

COMPTES RENDUS DES SÉANCES DE LA
„SOCIÉTÉ SCIENTIFIQUE DE TIMIŞOARA"

TOME 2. FASC 3 — 4.

TIMIŞOARA
IMPRIMERIE „CARTEA ROMÂNEASCĂ"
1 9 2 9.

Buletinul Ştiinţific al Facultăţii de Mecanica din Universitatea POLITEHNICA din Timişoara, aşa cum se prezenta în anul 1929. Copia este a coperţii Buletinului din arhiva Facultăţii de Mecanică

A SHORT HISTORY OF THE JOURNAL

The history of this journal of "Politehnica" University of Timisoara is strongly related to its creation under the name Polytechnic School of Timisoara (Ecole Polytechnique de Timişoara). Due to the changes of names and development of new areas of specialization, the university journal has been adapted several times during its long history. These adaptations are presented below in a synthetic history.

Polytechnic School of Timisoara

1925 The first number in a single series for all areas of specialization in technical, mathematical, physical and chemical sciences

1925 and Bulletin Scientifique de l'Ecole Polytechnique de Timisoara

1928-1947 (Comptes Rendus des Seances de la Societe Scientifique de Timisoara)

1948 Bulletin de Science et Technique de la Polytechnique de Timisoara, ISSN 0563-5594

1949 - Change of name to Polytechnic Institute of Timisoara

1949 Buletinul de Stiinta si Tehnica al Institutului Politehnic din Timisoara (Bulletin for Science and Technique of Polytehnic Institute of Timisoara, Naucino-tehniceskij biuleten' Politehniceskogo Instituta Timisoara, Bulletin des Science et Technique de L'Institut Polytechnique de Timisoara)

1956-1969 Buletinul stiintific si tehnic al Institutului Politehnic Timisoara (Scientific and Technical Bulletin of Polytehnic Institute of Timisoara), New series ISSN 0373-4374

1970 Editing on areas of specialization (series) specific to the main engineering fields of the Institute

- Chemical Series, ISSN 0366-3701

- Civil Engineering Series, ISSN 1220-0573

- Mechanical Engineering Series, ISSN 0373-4390

- Mathematics-Physics-Theoretical and applied mechanics Series, ISSN 0366-3779

1970-1971 Buletinul stiintific si tehnic al Institutului Politehnic Timisoara, Seria Mecanica (Scientific and Technical Bulletin of Polytechnic Institute of Timisoara, Mechanical Engineering Series), ISSN 0373-4390

1972 - Change of name to "Traian Vuia" Polytechnic Institute of Timisoara

1972 - 1974 Buletinul stiintific si tehnic al Institutului Politehnic "Traian Vuia" Timisoara, Seria Mecanica (Scientific and Technical Bulletin of "Traian Vuia" Polytechnic Institute of Timisoara, Mechanical Engineering Series), ISSN 0253-2026

1975 - 1977 Buletinul stiintific si tehnic al Institutului Politehnic "Traian Vuia" Timisoara (Scientific and Technical Bulletin of "Traian Vuia" Polytechnic Institute of Timisoara) [Single series] Mathematics, Physics, Theoretical and applied mechanics, Electrical engineering, Civil engineering, Chemistry, ISSN 1220-0581

1978-1990 Buletinul stiintific si tehnic al Institutului Politehnic "Traian Vuia" Timisoara (Scientific and Technical Bulletin of "Traian Vuia" Polytechnic Institute of Timisoara, Mechanical Engineering Series), ISSN ISSN 0253-2026

1990 - Change of name to Technical University of Timisoara

1991-1994 Buletinul stiintific si tehnic al Universitatii Tehnice din Timisoara Scientific and Technical Bulletin of Technical University of Timisoara, Mechanical Engineering Series), ISSN

1995 Buletinul stiintific si tehnic al Universitatii Tehnice din Timisoara, Seria Mecanica (Scientific and Technical Bulletin of Technical University of Timisoara, Transactions on Mechanics), ISSN1224-6077

1996 - Change of name to "Politehnica" University of Timisoara

1996 - Today; Buletinul stiintific al Universitatii "Politehnica" din Timisoara. România, Seria Mecanica (Scientific Bulletin of "Politehnica" University of Timisoara, Romania, Transactions on Mechanics), ISSN 1224-6077

(Also see http://www.upt.ro/cercetare/publicatii_upt.php)